THE INFLUENCE OF NICKEL-NITROGEN RATIO ON THE DEFORMATION BEHAVIOUR OF AUSTENITIC STAINLESS STEELS

by

Otto Emil Schmid

A thesis submitted to the Faculty of Engineering, University of Cape Town in fulfilment of the degree of Master of Applied Science

Department of Materials Engineering
University of Cape Town

April 1992

ABSTRACT

This study examines the effect that a partial substitution of nickel with nitrogen has on the deformation behaviour of a metastable austenitic stainless steel, AISI 301. The effect on the tensile deformation behaviour is studied in detail at various temperatures, and the effect on impact behaviour at room temperature is given brief attention.

The uniform straining ability of a metastable austenitic stainless steel, such as AISI 301, which is used for stretch forming applications, is promoted by transformation-induced plasticity (TRIP), which depends on the manner in which deformation-induced martensite forms during straining. This includes both the rate of martensite formation, and the stage at which the martensite is formed. In particular, incipient necking is resisted when martensite forms gradually and selectively, preventing the formation and propagation of micronecks and microcracks.

The microstructures of ten alloys, each having a type 301 base composition, but systematically varying nickel-nitrogen ratios, were characterized before and after tensile deformation, using optical and electron microscopy as well as X-ray diffraction techniques. Tensile tests were performed on solution treated specimens at temperatures of 0, 20, 60 and 120°C. The martensite volume fraction present after a true tensile strain of 0.3 was measured, and the work-hardening behaviour of the alloys was characterized up to the point of maximum uniform elongation.

All the alloys considered, showed fully austenitic microstructures at the solution treatment temperature (1050°C), and the indications are that nitrogen is fully dissolved. The austenite stability of the alloys however, varies at room temperature. Alloys containing approximately 5 wt% nickel, with a maximum nitrogen content of 0.28 wt%, contain up to 97% retained austenite, whereas alloys with 3.4 wt% nickel and the same maximum nitrogen content, contain only up to 63% retained austenite.

The austenite stability is shown to affect the extent to which the TRIP behaviour occurs in the experimental alloys. In particular, the greatest ductility is provided by alloys containing approximately 5 wt% nickel and nitrogen contents in the range 0.14 - 0.16 wt%. This ductility is shown to be comparable to the AISI 301 alloy when deformed at 20, 60, and 120°C.

The addition of nitrogen results in much increased strength compared to AISI 301, due to the interstitial solution hardening effect of nitrogen in austenite, and to a greater extent in martensite. Furthermore, pronounced serrated flow is identified in the experimental alloys when deformed at 60°C, whereas the behaviour is absent in AISI 301. Both these factors need to be considered when taking into account the formability of the experimental alloys. This study illustrates the potential for obtaining much cheaper TRIP alloys relative to AISI 301, and at the same time indicates some of the limitations associated with alloying element substitution.

ACKNOWLEDGEMENTS

I would like to express my sincere appreciation to all who assisted me in this work, and in particular to:

Dr Robert D.Knutsen, my supervisor, for his encouragement, support and advice throughout this project (even from as far as Birmingham).

Miss Karien Botha, for her help in preparation of line drawings.

Mr Nick Dreze and Mr Glen Newins for their technical advice and assistance.

Mr Bernard Greeves and Mr James Petersen for the photographic work.

Mrs Jackie Sharland and Mrs Anne Ball for their administrative support.

Professor Les Erasmus (from the University of Canterbury, New Zealand) for the helpful discussions on statistical analysis.

My fiancè, Brenda for her general interest and support.

My sister Sabine, and my brother-in-law Chris for the use of their computer.

Mr Mark Kirby and Mr Gavin Doyle, for their assistance with X-ray diffraction.

The departmental staff and my fellow students for their encouragement and support.

The CSIR, FRD and Middelburg Steel and Alloys for their financial support.

Dedicated to Jesus

TABLE OF CONTENTS

INTRODUCTION

1.1 General

The development of austenitic stainless steels which are easily shaped and formed, started with the development of controlled-transformation (CT) stainless steels about thirty years ago[1]. These steels were developed to overcome fabrication difficulties encountered with previously used high strength steels. The alloy chemistry of the CT steels produced a fully austenitic structure, which was then easily deformed into the required shape. Thereafter, the finished product was either cooled to below the M_S temperature*, producing martensite, or aged at 700°C to precipitate carbides, and thus produce martensite by raising the M_S to above room temperature. At that time it was even more difficult to control the alloy composition accurately than it is nowadays, and the M_S temperature, which is especially sensitive to interstitial elements such as carbon and nitrogen, was consequently also difficult to control[2].

Ensuing research in the late 1960's, saw the development of metastable austenitic stainless steels, as well as transformation-induced plasticity (TRIP) steels. In these steels, strengthening due to martensite transformation occurs *during* rather than after deformation, eliminating the need for post-deformation strengthening processes. Moreover, under favourable conditions, the formation of martensite during deformation can enhance ductility, and elongations in excess of 100% have been achieved with some TRIP alloys[3]. In order to achieve elongations of such magnitude, the progression of martensite transformation must be carefully controlled (in as far as this is possible). This requires accurate steel-making procedures and an understanding of the effect which variations in temperature and alloy composition have on the martensite formation.

1.2 Aim of Research

Considerable work was carried out on the reduction of the nickel content in austenitic stainless steels during the mid 1950's to mid 1960's[4-7]. The primary reason for exploring alternative alloy compositions was, and remains, the relatively high cost of nickel as an alloying element, of which type AISI 304 and AISI 316 contain 8 - 12 wt%. In many instances, a combination of manganese and nitrogen as substitutes has been adopted, and much of this work has led to the development of the AISI 200 series alloys. A comprehensive study by Nijhawan *et.al.* has shown that nickel-free Cr-Mn-N steels, containing up to 15 wt% Mn and 0.6 wt% N, have comparable properties to AISI 304 and are successful for applications such as household utensils, motor car and railway fittings, hospital ware and dairy equipment[7]. Manganese, although classed as a very weak delta-ferrite former[6], stabilizes the austenite phase. Nitrogen

* M_S : Temperature below which martensite forms spontaneously on cooling

acts both as a potent austenite former (approximately 20 to 30 times the potency of nickel) and as an austenite stabilizer. It can therefore be expected that the various combinations of these elements have an influence on the stability of the austenite and on the overall mechanical properties of the steel.

The present study looks more closely at the consequences of modifying the nickel-to-nitrogen ratio of AISI 301, and of special interest is the effect on the transformation-induced plasticity (TRIP) phenomenon. A metastable austenitic stainless steel such as AISI 301 is used for products which require moderate strengths, and are produced by stretch forming processes, which rely on the attainment of good uniform straining ability (ductility). Type 301 alloys nominally contain 6 to 8 wt% nickel, and the objective of this study is to investigate the effects of the substitution of a limited amount of nickel content with nitrogen, on the microstructure-property relationships. In particular, this study has involved the microstructural investigation of some twenty alloy compositions from which ten were selected for the purposes of mechanical testing. The work involved a detailed study of the tensile deformation behaviour at various temperatures, and a brief study of the impact properties at room temperature.

The study contributes towards a better understanding of how a partial substitution of nickel with nitrogen affects the tensile deformation behaviour of a type 301 steel. The advantages as well as the limitations are discussed in the context of the development of metastable alloys which are more cost efficient than type 301 and achieve equivalent levels of ductility.

CHAPTER 2

LITERATURE REVIEW

2.1 DESCRIPTION OF AUSTENITIC STAINLESS STEELS

2.1.1 General

Austenitic stainless steels exhibit a good combination of mechanical properties as can be seen from the following table:

STEEL	YS (MPa)	UTS (MPa)	ELONG (%)
MILD	220	430	18-25
MARTENSITIC e.g.431	400-900	900-2000	10-20
FERRITIC e.g 430	280-450	450-580	20-35
AUSTENITIC e.g. 301	300-500	800-1300	45-65

Table 2.1 Comparison of mechanical tensile properties of mild, ferritic and austenitic steels[8,9].

Mild steels contain typically less than 1% total alloying additions (the balance being iron) and are relatively cheap. However, due to their low corrosion resistance they are increasingly being replaced by stainless steels which contain 12-26% chromium[10]. Martensitic and ferritic (Fe-Cr) stainless steels contain much less nickel (0-1%) than their austenitic counterparts and are therefore generally cheaper. However they generally have lower formability and toughness than the austenitics. For this reason, austenitic (Fe-Cr-Ni) stainless steels, are mostly used in applications which require good corrosion resistance and formability. Of the family of austenitic stainless steels, the AISI 300 series is perhaps the most widely used. The alloy compositions of some AISI 300 stainless steels are given in table 2.2.

STEELS	Cr	Ni	C *max.*	Mn *max.*	Si *max.*	Mo
301	16-18	6-8	.15	2.00	1.00	
302	17-19	8-10	.15	2.00	1.00	
304	18-20	8-12	.08	2.00	1.00	
310	24-26	19-22	.25	2.00	1.50	
316	16-18	10-14	.08	2.00	1.00	2-3

Table 2.2 Specified analysis (wt%) of the AISI 300 series austenitic stainless steels[11].

These are but a few examples of austenitic stainless steels which are utilized in petrochemical, food, medical and transport industries and owe their widespread application to their excellent combination of mechanical and physical properties.

2.1.2 Chemistry of Austenitic Stainless Steels

The formation of austenite at solution heat treatment temperatures is controlled by alloying elements, which lower the chemical free energy of the face-centred cubic austenite (γ) phase with respect to the body-centred cubic delta-ferrite (δ) phase. Alloying elements which promote this behaviour are referred to as austenite *forming* elements. The retention of austenite in the microstructure during cooling and during any degree of deformation is also controlled by alloying elements. Alloying elements which promote this behaviour are referred to as austenite *stabilizing* elements.

(a) Austenite formation

Nitrogen and carbon are the two most powerful austenite formers followed by nickel, which is approximately 25 to 30 times weaker in its austenite forming ability[1,2]. Thus, since nitrogen and carbon have such a pronounced effect, it is essential that they are closely controlled in steel-making. The addition of nickel to 18%Cr steels increases the austenite forming ability considerably[10]. A 18%Cr-8%Ni-0.1%C steel (type 304) has an M_s temperature (the temperature below which martensite starts to form) just below ambient and stable austenite is retained after cooling from the solution treatment temperature to room temperature. The composition of the steel is situated close to the austenite/ferrite boundary as shown in figure 2.1 and hence the steel may contain some δ-ferrite.

The relative effect of alloying additions is often expressed in terms of their nickel equivalent (Ni′) and chromium equivalent (Cr′) respectively:

$$[Ni']^{(10,11)} = [Ni] + [Co] + 0.5[Mn] + 30[C] + 25[N] + 0.3[Cu]$$

$$[Cr']^{(10,11)} = [Cr] + 2.0[Si] + 1.5[Mo] + 5[V] + 5.5[Al] + 1.75[Nb] + 1.5[Ti] + 0.75[W]$$

where [ ] = weight percent

The austenite forming elements contribute towards increasing the nickel equivalent and the ferrite forming elements towards increasing the chromium equivalent. The significant contribution of nitrogen and carbon towards increasing Ni′, can be seen in the magnitude of their coefficients. Considerable care must be taken in applying such equations if there is any undissolved carbide, particularly in steels containing titanium or niobium. However, it is possible to make adjustments for the effect of such undissolved carbides[10].

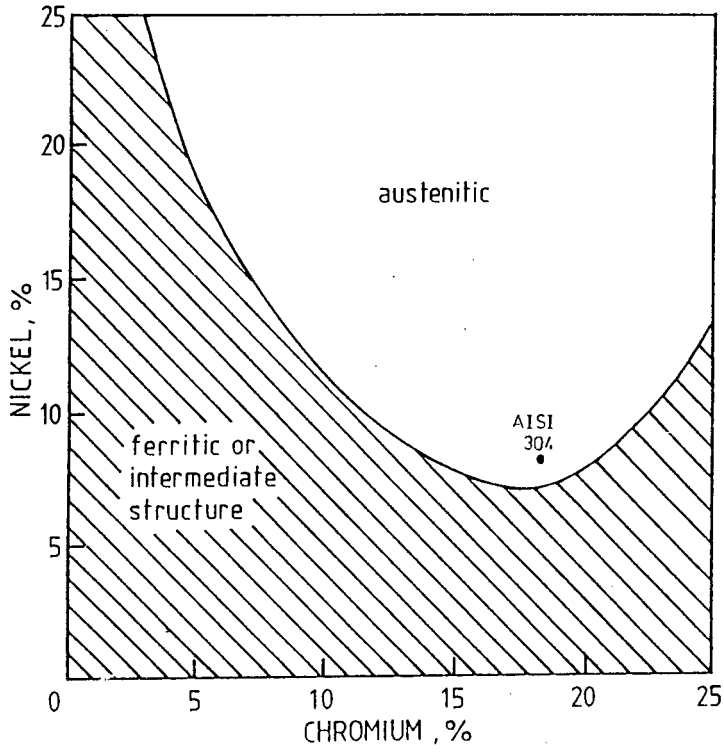

Figure 2.1 Effect of nickel and chromium on the constitution of 0.1%C steels at 900°C. At 18%Cr the amount of nickel required for an austenitic microstructure is a minimum and is approximately 8%[10].

(b) Austenite stabilization

The stability of the austenite phase depends on the combination of the alloy composition, temperature and deformation history of the material.

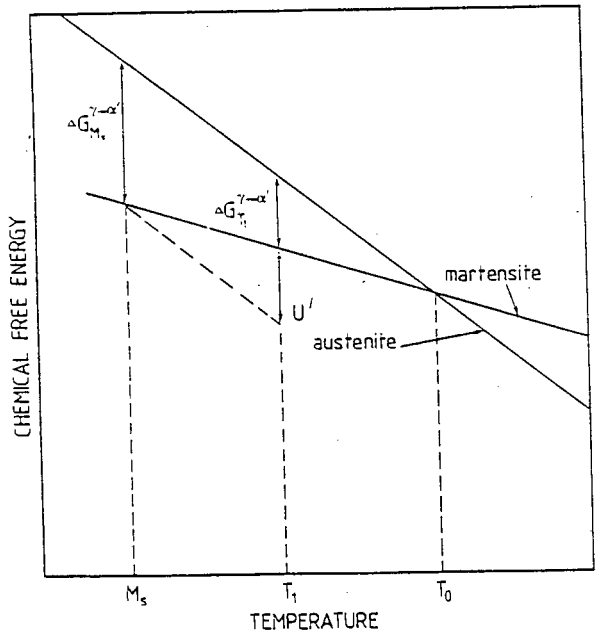

Figure 2.2 Schematic illustration showing chemical free energy of austenite and martensite as a function of temperature[12].

The chemical free energies of austenite and martensite vary with temperature as shown in figure 2.2. At T_O, the equilibrium temperature, the chemical free energies of the austenite and martensite phases are in equilibrium. For martensite to form, its free energy must be low enough so that the free energy change, of austenite on transforming to martensite, is large enough to enable the reaction to overcome the activation energy barrier between the austenitic and martensitic states[13]. It is due to this barrier that martensite does not form spontaneously at T_O, but only after a certain degree of undercooling, (usually about 200-300°C) at the M_s temperature. The difference of free energies between austenite and martensite $\Delta G(M_s)_{\gamma\rightarrow\alpha'}$ is the critical chemical driving force for the start of the martensitic transformation. When stress is applied to austenite at T_1 (between M_s and T_O), the mechanical driving force U' due to the stress, is added to the chemical driving force $\Delta G(T_1)_{\gamma\rightarrow\alpha'}$. Note that $\Delta G(M_s)_{\gamma\rightarrow\alpha'} = U' + \Delta G(T_1)_{\gamma\rightarrow\alpha'}$. The applied stress can be resolved into the shear stress and the normal stress components. Since the martensitic transformation proceeds by a shear mechanism[14], the applied resolved shear stress along a potential habit plane aids the transformation reaction. The reaction may however be aided or opposed by the resolved normal stress component, depending on wether it is tensile or compressive respectively[3,13]. The temperature above which no austenite to martensite transformation appeared to occur was termed the M_d temperature, corresponding to T_0 in figure 2.2[15]. However, it was found that this only applied at low strains, since at high strains martensite can be obtained well above this 'plastic critical temperature'. Hence Angel[13] suggested that the concept of a true 'plastic critical temperature' be replaced by that of a 'transition temperature' i.e. the temperature of transition from martensite formation, to slip in austenite as the primary mechanism of deformation.

It has long been recognized that slip in austenite competes as a deformation mode with transformation to martensite[16]. Angel thus introduced the M_{d30} temperature, which he defined arbitrarily as the characteristic temperature, at which 50% martensite is formed in tension after a true strain of 0.30. This temperature will vary with the method of deformation i.e. different values will be obtained for deformation by tension and by compression. Angel also derived a multiple regression equation by statistical methods, making two assumptions:

(1) The effect of alloying elements on the M_{d30} is additive i.e. there is no interaction between elements;
(2) The effect varies linearly with the weight per cent of the elements.

The M_d temperature-composition relationship derived by Angel is given by:

$$M_{d30}(°C) = 413 - 9.5[Ni] - 462[C+N] - 9.2[Si] - 8.1[Mn] - 13.7[Cr] - 18.5[Mo]$$

where [ ] = weight per cent

Angel points out that the equation was found to be statistically accurate for all alloying

elements except Mo, Si and Ni. He suggests that the equation can be further improved upon by taking into account possible interactions between elements and using a wider range for Mo, Si and Ni. One other formula for the M_{d30} temperature, which differs from Angel's equation in only two terms i.e. the constant term and the nickel term is given by[10]:

$$M_{d30}(°C) = 497 - 20[Ni] - 462[C+N] - 9.2[Si] - 8.1[Mn] - 13.7[Cr] - 18.5[Mo]$$

The reported M_s temperature-composition relationships differ widely and in general are only valid for the composition range for which they were derived[17]. Two equations which have been used most often in the literature are:

°C		[Ni]	[Cr]	[Mn]	[Si]	[C]	[N]	[Mo]	[Cu]
M_s[11]=	+1305	-61.1	-41.7	-33.3	-27.8	-1667	-1667	-	-
M_s[10]=	+502	-30	-12	-13	-	-810	-1230	-46	-54

where [ ] = wt per cent

Table 2.3 Equations for calculating M_s temperatures most often used in current literature.

Nitrogen and carbon reduce the M_s significantly as can be seen by the magnitude of their coefficients in table 2.3 and are 30 to 40 times more effective in doing so than nickel. Nickel is the only element which is capable of reducing the ferrite-forming tendency sufficiently without depressing the M_s too far[1]. Cr, Si and Mo stabilize austenite in the same way as Ni, Mn, C and N[13]. If the potency of nickel in reducing deformation-induced transformation is arbitrarily assigned the value 1.0 then the relative potencies of the other elements in solid solution are[18]:

ELEMENT	REL.POTENCY
C	21.6
N	17.1
Ni	1.0
Mn	0.683
Cr	0.515

Table 2.4 Relative austenite stabilizing potencies of alloying elements in solid solution.

At low carbon and nitrogen levels, the austenite stabilizing effect is outweighed by the strengthening of the martensite phase, so that an increase in either carbon and/or nitrogen increases the tensile strength. At high levels, the stabilizing effect is predominant and an increase in one and/or the other element results in a decrease in tensile strength. The yield strengthening effect of the alloying elements C, N, Ni, Mn,, and Cr is more pronounced in

martensite than in austenite as can be seen from table 2.5:

ELEMENT	Strengthening ability of 1% element in: austenite(MPa)	martensite(MPa)
C	+2450	+6700
N	+1670	+2660
Ni	-11	-10
Mn	+4	+150
Cr	+42	+260

Table 2.5 Yield strengthening ability of alloying elements[18].

2.2 DEFORMATION BEHAVIOUR OF AUSTENITIC STAINLESS STEELS

In a stable austenitic steel, martensite does not form during deformation and the ability of the austenite phase to deform uniformly determines the maximum uniform elongation. In contrast, the elongation of a metastable steel is determined by the formation of deformation-induced martensite, which can either enhance or impair the uniform straining ability.

2.2.1 Deformation of Stable Austenite

Stable austenite has a higher stacking fault energy (SFE) than metastable austenite. The Fe-Cr-Ni austenitic steels have stacking fault energies in the range 5 - 60 mJm^{-2}[19]. Nickel raises the SFE, while nitrogen, carbon and manganese tend to lower the SFE of austenite[20]. The work-hardening rate depends on the stacking fault energy, and raising the SFE lowers the work-hardening rate[21]. During deformation of a stable steel the work-hardening rate decreases continuously, giving rise to the parabolic stress-strain curve typical of polycrystalline face-centred cubic metals[22]. In general, a decrease in the work-hardening rate will lower the maximum uniform elongation and be detrimental to stretch-forming characteristics unless there is a corresponding decrease in the level of the flow stress[10]. The latter can be achieved by lowering the initial proof stress value, by coarsening of the grain size and the addition of alloying elements which increase the SFE but have as small a solid-solution strengthening as possible.

2.2.2 Deformation of Metastable Austenite

The SFE of metastable austenite is lower than that of stable austenite and hence the work-hardening rates are higher in the former due to the formation of martensite during deformation. The amount of deformation-induced martensite with increasing strain tends asymptotically towards a particular value, which varies according to deformation temperature as shown in figure 2.3.

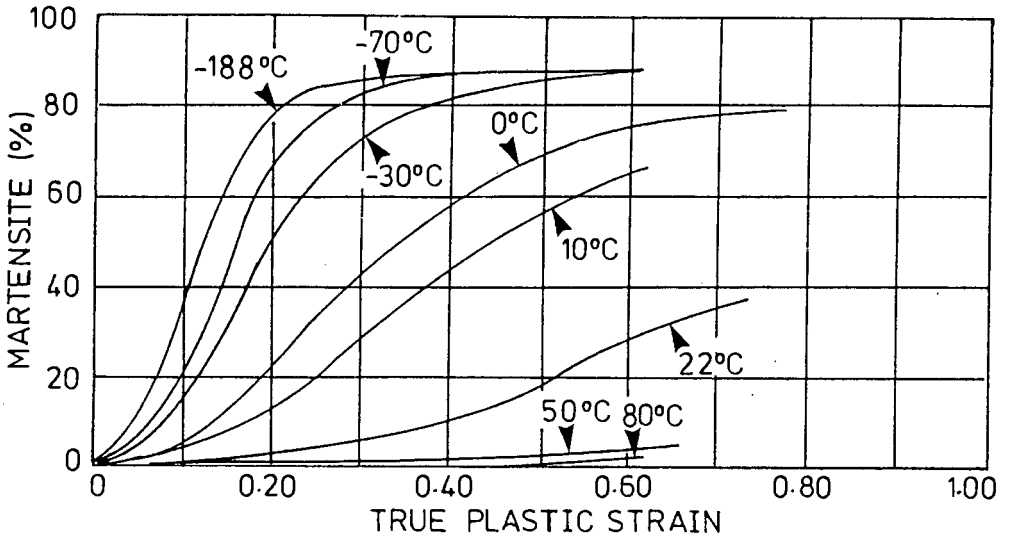

Figure 2.3 Formation of martensite by plastic tensile strain at various deformation temperatures[13].

From this figure it can be seen that the maximum amount of deformation-induced martensite decreases as the deformation temperature increases. In the beginning stages martensite formation is stimulated but as deformation progresses, this stimulating effect becomes a stabilizing one instead. Generally transformation does not start until a certain stress threshold is reached and this threshold value is generally higher, the higher the temperature and the higher the austenite stability[13].

Barclay studied the deformation mechanisms and associated microstructures with increasing strain in type 301[23]. Table 2.7 summarizes his observations at particular strain intervals :

TRUE STRAIN	OBSERVATION
.08-.10	Dislocation tangles form into dense cells Appearance of stacking faults Increase in stacking fault density
.20	Heavy dislocation density in austenite Deformation twins of lenticular shape form
.30	Martensite plates form
.60	Martensite volume fraction increases Twinned austenite volume fraction increases Austenite dislocation density is very heavy
>.60	Twin-like martensite structure forms

Table 2.7 Course of martensite formation as a function of true strain in a type 301 stainless steel[23]

At low strains (0.08-0.10) the work-hardening rate of the steel is low. As the stacking fault density increases, martensite starts to form and the work-hardening rate increases . As more and more martensite is formed during continued straining and because this martensite is strong, the flow stress rapidly increases as the martensite itself starts to participate in the deformation[10]. During straining a transformation strain is produced, which augments the applied strain. This results in high uniform elongations and thus type 301 steel is very suitable for stretch-forming operations. This plastic deformation behaviour is dealt with in more detail in the next section.

2.2.3 Transformation-Induced Plasticity (TRIP)

The enhancement of the ductility of an alloy due to the onset of deformation-induced martensite transformation is known as 'transformation-induced plasticity' (TRIP)[14]. This acronym refers to the phenomenon as well as the alloys themselves which were first developed by Zackay and co-workers (a typical composition being Fe-9.4%Cr-7.7%Ni-3.0%Mn-2.8%Si-3.9%Mo-0.28%C)[3]. The elongation was found to increase significantly when the transformation was gradual and occurred primarily at regions of incipient necking. High strength TRIP steels have been examined for some time, so as to understand the influence of transformation on various mechanical properties.

Huang *et.al.*[24] found that for type 304 steel the work-hardening rate goes through a minimum at low strains and then increases to a maximum at intermediate strains. At strains just prior to the minimum in work-hardening, it has been shown that the deformation-induced martensite transformation begins[25,26]. Hence at strains beyond those which produce a minimum in work-hardening rate, the transformation rate and correspondingly the volume fraction of

martensite increases, resulting in an increase in strength by the continual refinement of the martensite and austenite mixture. As a result, measured work-hardening rate values increase significantly with strain. As the martensite volume fraction increases to near saturation for a particular test temperature, the composite microstructure deforms and dynamic recovery results in a decrease in work-hardening rate with strain. At higher temperatures, the extent of the transformation at a given strain is lower and the magnitude of the peak in work-hardening rate decreases. At temperatures where martensite formation is insignificant, the work-hardening rate decreases continuously with an increase in strain (i.e. above the M_d).

Huang *et.al.* propose that maximum uniform elongations are produced when the increase in flow stress due to martensite formation becomes less pronounced together with a more gradual decrease in work-hardening rate at high strains[24]. They found that above the M_d, the induced martensite transformation did not occur and hence the resultant work-hardening rate was low at high strains, producing low uniform elongations. Also the uniform elongation decreased as test temperature increased above the M_d. Rosen *et.al.*[27] found that type 301 has a distinct strain peak on the elongation vs. test temperature curve as can be seen in figure 2.4. Type 304 also exhibits a peak but it is less pronounced.

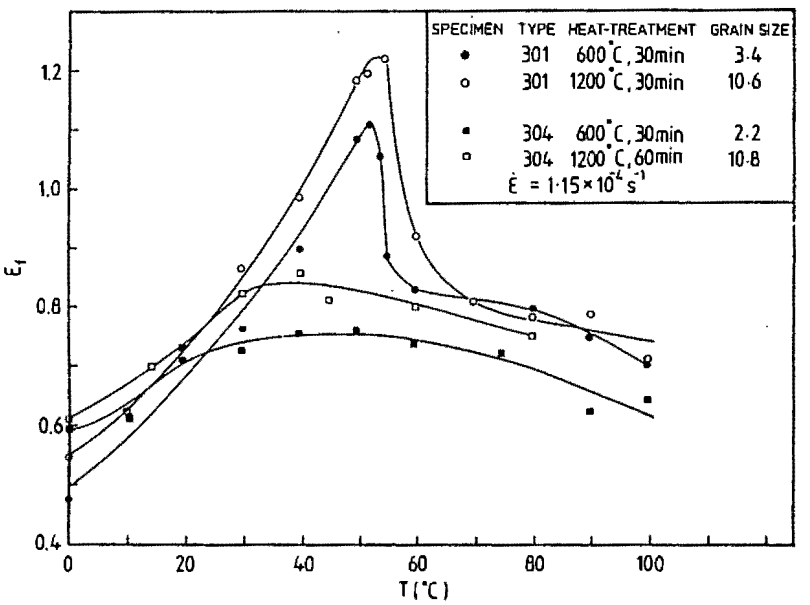

Figure 2.4 Elongation to failure versus testing temperature for type 301 and 304 steels for different heat-treatments.[27]

The test temperature at which the uniform elongation (or elongation to failure) of an alloy is at its maximum, is known as the maximum elongation temperature (MET). It has been shown that the MET for metastable steels lies between the M_s and M_d[16,24,27,28,29,30] . At the MET the (optimum) rate of martensite formation leads to an optimum work-hardening rate and thus to maximum elongation[16]. Martensite is formed little by little during deformation up to fracture. Tamura *et.al.*[31] propose two mechanisms by which transformation-induced plasticity is achieved:

(1) *Suppression of necking:* At regions of micronecking more martensite is induced than in the unnecked adjacent regions. Hence the necked regions are hardened more than the adjacent ones, so that the micronecks cease to grow. Deformation then occurs preferentially in the regions adjacent to the micronecks.

(2) *Suppression of initiation and propagation of microcracks:* Stress localizations in austenite may be relaxed by the formation of martensite at the regions, where the stress is concentrated during deformation. In this way the initiation of microcracks is suppressed. In the case of microcracks already having been initiated, their propagation will be suppressed as the stress is concentrated at the crack tip, so that martensite is induced ahead of the crack. This relaxes the crack tip stress concentration and counteracts crack propagation.

Above the M_d, where no deformation-induced martensite is formed, work-hardening of the austenite is too low to prevent failure at the site of incipient necking. Regions developing micronecks are not strengthened because no martensite is formed, so that the micronecks grow unchecked. Microcrack initiation and propagation occurs easily. Close to the M_s, ductility is also low since martensite, the inherent ductility of which is low, forms rapidly and the martensite saturation level is reached at low strains. Plasticity is impaired rather than enhanced by transformation and the resultant elongation is low, as is characteristic of martensitic stainless steels.

Type 301 has been reported to have the following maximum elongation temperatures in uniaxial tension:

AUTHOR	MET(°C)
Bressanelli & Moskowitz[32]	50
Fukase *et.al.*[33]	52
Rosen *et.al.*[27]	55

Table 2.8 Maximum elongation temperatures of type 301 steel as quoted by various authors.

Type 301 decarburized steel has an MET of 85°C, whereas type 304 has an MET between 40-45°C. The elongation vs temperature peak of type 304 is broader; hence the larger MET range. It has been reported that no martensite is formed before a certain strain is reached in type 304 and 301[27]. This effect was more pronounced in type 304 than type 301 and was attributed to the presence of finely dispersed inclusions, which were not present in type 301. These second phase particles were thought to set up stress concentrations, which in turn trigger the formation of martensite plates uniformly throughout the specimen.

A common feature of the elongation to failure vs test temperature curve is its asymmetry i.e. a

sharp drop in fracture strain values occurs above the MET, compared with a more moderate decline below this temperature[12,27]. (Type 301 curve in figure 2.4). At test temperatures close to the MET, the difference in the amount of martensite in the neck and adjacent zone (undergoing uniform elongation) is large, suggesting a large increase in the rate of formation of martensite late in the deformation process[28]. The necked region in type 304 was found to contain up to 70% martensite, whereas the adjacent zone contained typically 30-40%[24]. At temperatures further removed from the MET, the difference is less and most of the martensite is formed too generally and at too small a strain to increase stability at an incipient neck (at temperatures *below* MET), or insufficient martensite is formed (at temperatures *above* the MET). It is important to note that the occurrence of a large amount of martensite in the uniformly elongated zone has not necessarily coincided with what was previously found to be the MET. What is required is a large amount of martensite late in the deformation process[28], at strategic co-ordinates of potential necking[27].

The effect of a change in alloy composition on the austenite stability is shown in figure 2.5, which shows the effect of increasing the nickel content from 8 to 16% in a 9%Cr-2%Mn steel. Austenite in the steel containing 8% nickel transforms to martensite at a rate faster than the optimum (which is equivalent to deformation below the MET), while the one containing 16% nickel undergoes no transformation (which is equivalent to deformation above the M_d). The steel containing 12% nickel undergoes transformation at the optimum rate (which is equivalent to deformation at the MET) and consequently has a high uniform elongation.

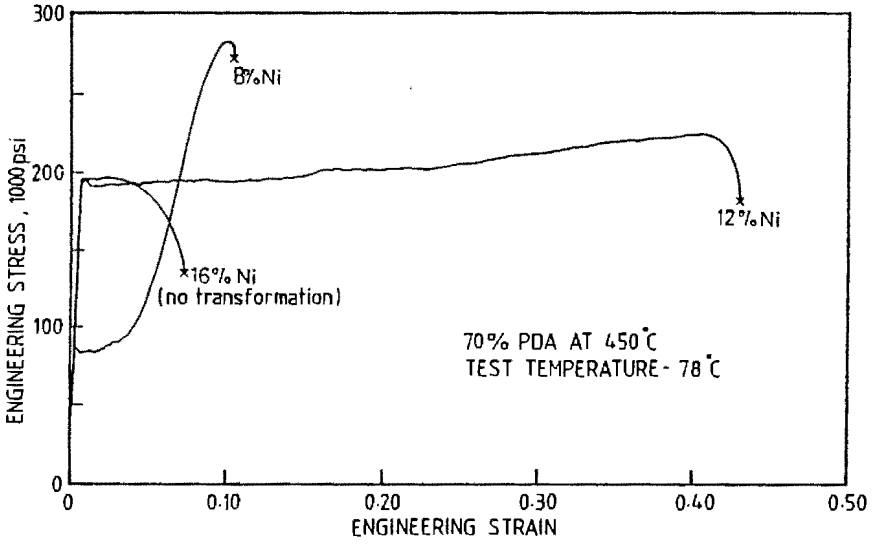

Figure 2.5 Engineering stress-strain curves for three steels containing 9%Cr, 2%Mn and different nickel contents (i.e 8%Ni, 12%Ni and 16%Ni) deformed 70% at 450°C and tested at -78°C.[34]

From the above it is evident that it is not so much the total amount of martensite formed that determines the ductility but rather the *stage* at which it is formed. It has been found that mechanical instability is promoted when transformation occurs mainly during the early stages of deformation[35], but if transformation is delayed in the straining sequence, concomitant

work-hardening will result in enhanced ductility. The martensite formation is *autocatalytic*, which means that the formation of a certain amount of martensite is able to act as a catalyst in accelerating the formation of additional martensite[18]. The autocatalytic nature of the martensite formation arises due to the dilational and coherency strains produced in the surrounding structure and it follows that the sooner the first martensite is formed, the more pronounced will be the autocatalytic effect. Furthermore, bursts of martensite have been observed to occur at early stages of deformation which resulted in low elongations[31]. Thus the conditions for obtaining the optimum uniform elongation are:

(1) The first martensite which forms, must not form too early or too late during the deformation process;
(2) The martensite formation must be gradual;
(3) The martensite must form selectively i.e. at points of potential instability.

2.2.4 Stress-Assisted and Strain-Induced Martensite

A variety of terms have been used to describe the martensite transformation as it occurs during mechanical straining. Commonly 'strain-induced martensite' is used to distinguish between martensite formed spontaneously during cooling and martensite formed during deformation with no specific implication about the role of stress or strain in its formation[18,24,25,36]. Some authors use more precise definitions of 'stress-induced' and 'strain-induced' martensite to distinguish between that martensite that forms either before or after plastic yielding respectively[16,34]. However, such operational definition of these terms ignores any difference in the martensite morphology or between mechanisms for martensite formation. Strictly speaking, one should differentiate between the two, because strain-induced martensite has a morphology, distribution and temperature dependence which are quite different from that martensite which is stress-induced. In many cases the two types of martensite do not form simultaneously and one type of martensite may form to the exclusion of the other.

The terms 'strain-induced' and 'stress-assisted' have been used to avoid confusion and are defined as follows:

Stress-assisted: Platelike martensite that forms in the presence of an applied stress by essentially the same nucleation and growth process that results in the spontaneous formation of the martensite which forms during the cooling of unstressed and unstrained austenite. Stress-assisted martensite can form above as well as below the spontaneous, unstressed M_S temperature; it can also form in plastically deformed austenite even after considerable plastic strain[37]. The formation of stress-assisted martensite *precedes* slip in austenite and hence the

condition for its formation is that $\sigma_{\gamma\to\alpha'} < \sigma_{YIELD\ \gamma}$[16].

Strain-induced: Lath-like martensite which is that transformation product which forms as direct consequence of plastic deformation and which apparently occurs by a mechanism distinctly different from that of stress-assisted martensite, and its morphology, distribution and temperature dependence and other characteristics are quite different[37]. The formation of strain-induced martensite occurs *as a consequence* of slip in austenite and hence the condition necessary for its formation is that $\sigma_{\gamma\to\alpha'} > \sigma_{YIELD\ \gamma}$[16].

Seetharaman[14] defines the temperature M_s^σ as the temperature below which stress-assisted nucleation of martensite occurs and above which strain-induced nucleation occurs (Figure 2.6). Hence stress-assisted martensite forms close to the M_s while strain-induced martensite forms close to the M_d[34].

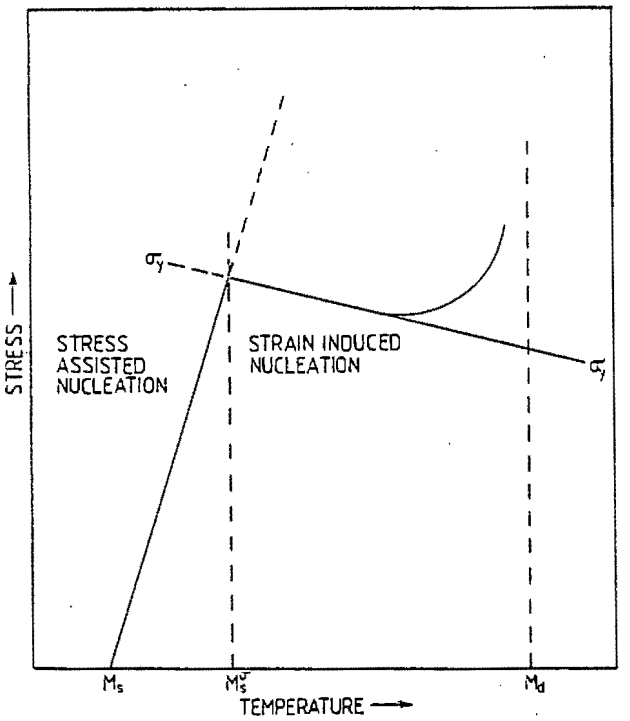

Figure 2.6 Variation of critical stress required for the onset of the transformation at different temperatures.[14]

The critical applied stress for martensite formation shows a linear dependence only between M_s and M_s^σ. Beyond M_s^σ the stress required would exceed the flow stress of the parent phase and thus cause plastic deformation of this phase.

The role of plastic deformation has been a subject of controversy. Olson and Cohen[38,39] firmly believe that the intersection of slip bands produced as result of plastic deformation acts as a nucleation site for martensite. In contrast Tamura[12] has expressed the opinion that local

stress concentration near the grain boundaries due to the pile-up of dislocations would raise the applied stress to values obtained by the extrapolation of the straight line in figure 2.6 well beyond that corresponding to M_s^σ. In addition he suggested that the transformation kinetics should be based on stress rather than strain since the martensitic transformation is promoted essentially by the shearing stress. Angel[13] in turn suggested that the conclusion that the formation of martensite is a function of stress alone is true only to a limited extent. He argues that in a polycrystalline material, the applied external stress is only a measure of the *average* stress in the material over the cross-section of the test specimen. Owing to the plastic straining of the material, *local* stress peaks which exceed the average stress level are set up in the lattice. Some of these peaks may be high enough to nucleate some martensite before the average stress level has reached the level necessary for martensite formation. Through the work-hardening action of the strain, the stress may thus be brought up to the critical stress level in some places. It may then be said that strain has as important a rôle as has stress. However Angel also points out that strain is only a consequence of the martensitic mode of deformation, taking place simultaneously and independently. There is indeed a complex interplay between cause and effect but the applications of energy considerations does clarify the picture somewhat.

It has been suggested that the maximum elongation cannot be obtained whenever the austenite stability is such that initial plastic deformation is due to the formation of stress-assisted martensite[16]. Work hardening rates will always be higher than the optimum in such a case. Thus the condition set forth for strain-induced martensite formation must be met for the optimum work-hardening rate[37].

2.2.5 Serrations In The Stress-Strain Curve

Serrations or jerky flow resulting from either discontinuous yielding or discontinuous stress drops during straining have been attributed to at least four different phenomena[3]:

(1) adiabatic heating;
(2) dislocation-impurity interaction;
(3) twinning;
(4) transformations.

Serrations have been observed to occur in a number of metastable stainless steel alloys[3,12,29,34]. Most of the authors attributed their occurrence to the effect of transformations during straining. Fahr[16] attributed serrations occurring in TRIP type steels to the competition of martensite formation and slip in the austenite as opposing modes of deformation. Particularly large serrations were observed by Goldberg *et.al.*[3] in a TRIP steel.

It was proposed that these were caused by the phase transition volume change. (The volumetric expansion of austenite undergoing martensite transformation is about 4% and this gives a linear increase of 1.3% for isotropic expansion). They also considered the effect of adiabatic heating and calculated a temperature rise of 92°C for complete transformation to martensite. This is not unreasonable since similar temperature rises have been observed, especially near the centre of the gauge length[28,40].

One of the most common causes of serrations, which authors have proposed, is the formation of stress-assisted and strain-induced martensite. Some report the presence of both types of martensite concomitant with serrations[3], while others have observed that the two types of martensite affect the serration phenomenon in different ways[12,16]. Fahr[16] proposed that stress-assisted martensite does not cause serrations whereas Tamura[12] associated it with the presence of large serrations. The picture is further complicated by the results of Goldberg *et.al.*[29]. They discovered that tensile tests from 0 to -30°C gave rise to extensive serrations (which were associated with stress-assisted martensite). However tests at -40 and -50°C did not show serrations in spite of the formation of stress-assisted martensite. The authors proposed that the presence of large amounts of stress-assisted martensite in the specimen at the onset of plastic flow prevents serrations during subsequent deformation even though a considerable amount of stress-assisted martensite forms.

Thus it appears, that serrations cannot simply be attributed to either the formation of stress-assisted or strain-induced martensite. Rather the presence of serrations is an indication that one or the other is likely to have formed depending on tensile test temperature. If the test temperature is close to the M_s they will more likely than not be due to stress-assisted martensite, since this is intrinsically the temperature regime of its formation. If the tensile test temperature is closer towards the M_d, serrations will most likely be caused by strain-induced martensite formation as has been demonstrated in TRIP steels[34].

2.2.6 Effect of Strain Rate

A number of authors have investigated the effect of strain rate on the austenite to martensite transformation[3,12,24,27,28,32,33,40,41]. The tendency for the work-hardening rate to increase more slowly at high strain rates is undoubtedly related to the adiabatic heating from the deformation[3]. It appears that the adiabatic heating phenomenon is the main topic of discussion but there may be other factors of importance as yet not properly investigated[12].

Adiabatic heating increases with an increase in strain rate; the temperature increase in turn reduces the amount of martensite formed during testing. When specimens are deformed in air, adiabatic heat is not readily dissipated and the transformation decreases. When they are

submerged in a liquid, adiabatic heating is reduced considerably[12,32,33]. Generally adiabatic heating has been reported to decrease the elongation and hence ductility[27,28]. However, adiabatic heating can also result in increased ductility in the case of low austenite stability, so that the rate of martensite formation is lowered toward the optimum rate. Decreased ductility is observed, when adiabatic heating occurs close to the M_d, since the specimen temperature is increased above the M_d. It has been observed that a fifty fold increase in strain rate of type 301 results in a 78°C increase in specimen temperature[32]. At very low test temperature, transformation is reported to be relatively independent of strain rate. However, the amount of transformation close to the M_d decreases markedly with an increase in strain rate.

Kumar *et.al.*[40] measured the increase in specimen temperature along the gauge length tested at low (10^{-3} s^{-1}) and high (10^{3} s^{-1}) strain rates. Figure 2.7 and 2.8 show the pronounced increase in specimen temperature at high strain rate and also that the centre becomes hotter than the ends of the gauge length.

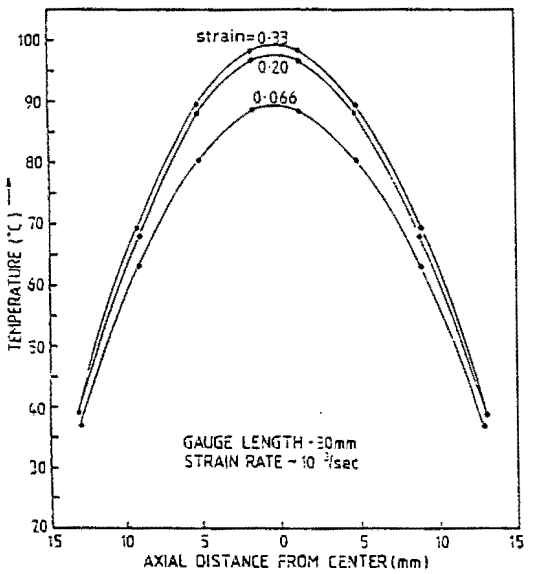

Figure 2.7 Effect of high strain rate on axial temperature distribution[40].

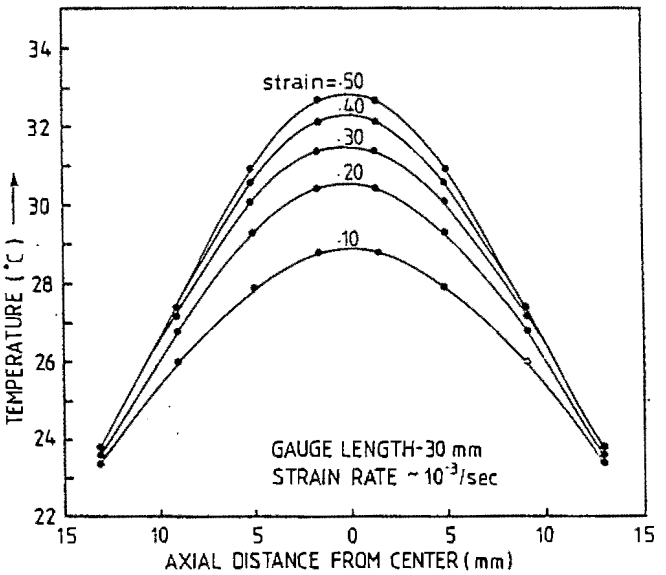

Figure 2.8 Effect of low strain rate on axial temperature distribution[40].

STRAIN RATE (s^{-1})	TEMP INCREASE(°C)	
	GL Centre	GL ENDS
10^{-3} (low)	11	2
10^{3} (high)	77	17

GL = gauge length

Table 2.9 Effect of strain rate on adiabatic heating in type 304 steel[40].

The reason for the differences in the centre and ends of the gauge length temperature

increases, is that non-homogeneous deformation takes place in the specimen. The true plastic strain is maximum at the centre of the specimen and it decreases from the gauge length centre to its ends as well as from the centre to the surface. As the elongation increases, the contour of maximum strain tends to be confined near the specimen centre. The non-homogeneous distribution of plastic strain, effective strain and variation in temperature along the gauge length is accompanied by a corresponding variation in the martensite volume fraction along the gauge length. Due to its intrinsic nature, the non-homogeneous deformation effect cannot easily be minimized but when precautions are taken in order to do so, the strain effect was found to be minimal[32]. Moreover, in metastable austenitic structures, the martensite volume fraction formed under *isothermal* conditions (i.e. adiabatic heat is removed at an equal rate to its formation) increases with increasing strain rate as shown in figure 2.9. This increase in martensite volume fraction due to increase in strain rate may increase overall strength by two mechanisms:

(1) A higher dislocation density may be introduced into the austenite to accommodate the martensite volume expansion;
(2) Load in the austenite-martensite composite is re-distributed due to the increase in volume fraction of higher strength martensite.

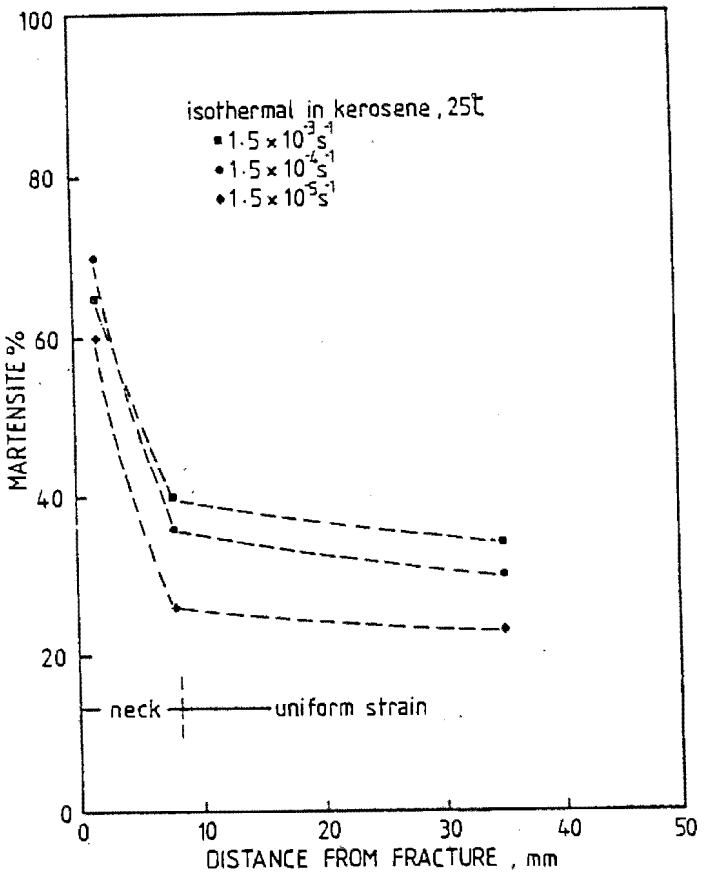

Figure 2.9 Increasing the strain rate under isothermal conditions increases the amount of deformation-induced martensite.[24]

2.3. NITROGEN IN AUSTENITIC (Fe-Cr-Ni) STEEL

Nitrogen is an essential, important and inexpensive alloying addition and a full appreciation of its many effects leads to the ability to optimize its use and capitalize on its undoubted beneficial effects[42]. The argon-oxygen decarburization (AOD) process makes it possible to control nitrogen concentration with greater precision without extra cost. A process model for nitrogen pick-up or removal in AOD when N_2-O_2 or Ar-O_2 gas mixtures are used has been developed, and can be used to predict accurately the switch point from N_2 to Ar for the optimum processes[43]. Thus the use of nitrogen alloyed austenitic stainless steels is steadily increasing[44].

In the formable mild steels, nitrogen is well known for its ability to segregate to dislocations and dislocation sources, thereby introducing discontinuous yielding and more specifically strain ageing. Strain ageing is detrimental to formability as it leads to stretcher strains. Other detrimental effects of nitrogen are often associated with embrittlement. For austenitic stainless steels in particular it is generally agreed that nitrogen must be in solution in order to avoid the deleterious effects that arise due to the precipitation of nitrides[45,46,47]. For example, nitride precipitation in solution treated stainless steel wire containing up to 0.7 wt% nitrogen before drawing, greatly reduces ductility and only a minor improvement in strength is obtained[45]. Also the precipitation of nitrides or carbo-nitrides reduces the resistance to stress-corrosion cracking[48].

Nitrogen in solid solution, increases the yield and tensile strength[46,47,48,49,50,51], corrosion and pitting resistance[44,45,46], and even the stress-corrosion cracking resistance[46] of austenitic stainless steels. The main part of the section below examines the strengthening effect in more detail. The other properties will be briefly discussed.

2.3.1 Strengthening Effects

The total yield strength contribution from nitrogen is composed of two separate parts[46,49]:

(1) Solid solution hardening (thermal)
(2) Grain boundary strengthening (athermal)

A third component, the matrix strengthening (athermal) is small compared to (1) and (2). The yield strength (YS) for Fe-Cr-Ni alloys containing nitrogen can be written as the sum of the matrix strengthening (ΔYS_{ma}), solid solution hardening (ΔYS_{sh}) and grain boundary strengthening (ΔYS_{gh})[46]:

$$YS = [\,(\Delta YS_{ma})^2 + (\Delta YS_{sh})^2\,]^{1/2} + \Delta YS_{gh})$$

where : $\Delta YS_{ma} = 68 + 230\,\{1 - (T/823)^{2/3}\}^{3/2}$ [MPa]

$\Delta YS_{gh} = \{8 + 75[1 - (T/823)^{2/3}]^{3/2}(\%N)\}\, D^{-1/2}$ [MPa]

$\Delta YS_{sh}(T=0K) = 1.77GX_N^{1/2}f_o^{3/2}$ [MPa]

T = temperature in Kelvin ($4 < T < 293$)
%N = nitrogen content in weight per cent
D = grain size in mm
G = shear modulus
X_N = concentration of nitrogen atoms in solution
f_o = interaction parameter between dislocations and solute atoms.

Below a certain transition temperature (TT), the solution hardening effect dominates and above TT the grain boundary strengthening effect becomes the dominant one. TT is dependent on composition and has been observed to occur in the following temperature range:

$$130^{(46)} < TT(°C) < 230^{(50)}$$

There are a number of theories of solid solution hardening which can be divided into two categories. The first category is concerned with dislocation locking, where the dislocation is at rest, and the other category with the frictional resistance of solute atoms to the movement of dislocations. Cottrell[52] and Suzuki's[53] locking theories can be criticized on the grounds that dissociated dislocations to which segregation takes place in the stacking fault, will not break free when stress is applied; rather new dislocations will be generated, and the stress to move these dislocations is the solution hardening stress[54]. Mott and Nabarro[55] developed a theory which assumed that solid solution strengthening arose from the interaction of randomly distributed solute atoms with moving dislocations. To date it appears that the biggest contribution to the flow stress of solid solutions arises not from the locking of dislocations, but from resistance to their movement, a frictional force, the magnitude of which is sensitive to both atomic size differences and differences in elastic properties between solute and solvent[54]. Valency differences are also likely to be significant.

The grain boundary strengthening effect at temperatures just above TT is due to dislocations moving in planar arrays. Planar dislocation arrays are further promoted when nitrogen is increased since wavy slip changes to planar slip on raising the nitrogen content. This suppresses dislocation climb and cross-slip and thus increases the work-hardening rate[50]. Dislocation dissociation does not occur since the stacking fault energy is too high for partial dislocations to be separated by stacking faults. At temperatures far above the TT, the grain boundary strengthening effect is thought to be due to lowering of the stacking fault energy, since planar arrays are unlikely to occur at elevated temperatures[49]. This lowering of the

stacking fault energy enhances twin formation on annealing and increases the efficiency of the grain boundaries to act as dislocation obstacles[48]. The most plausible explanation of both planar slip and nitrogen strengthening in austenitic alloys is the existence of some form of short-range atomic ordering but the exact nature of the ordering is unclear. A model of nitrogen strengthening is proposed, based on the effective ordering due to a strong chemical interaction between nitrogen and chromium. The essential feature of this model is disordering by the passage of a dislocation through a chemically ordered structure[50].

2.3.2 Impact Toughness And Corrosion Resistance

The significant strengthening effect is not accompanied by a loss of fracture toughness, at least up to 0.7 wt% nitrogen in austenitic steels with up to 20 wt% Cr, 20 wt% Mn and 10 wt% Ni[47]. Impact toughness of type 304 and 316 steels with 0.2 wt% nitrogen is still excellent at -196°C with no ductile to brittle transition occurring[51]. These two types of steel are already being used for applications requiring a good combination of strength, toughness and corrosion resistance. Despite the involvement of nitrogen in the precipitation of $M_{23}(CN)_6$ and Cr_2N, the presence of 0.2 wt% nitrogen in type 304 and 316 produces no adverse effect on sensitization[51]. Nevertheless, the general corrosion resistance of nitrogen-containing austenitics can be lowered in certain unfavourable environments[42].

From the preceding discussion it becomes evident, that nitrogen has been predominantly used for strengthening purposes in stable austenitics. Yield strengths as high as 2000 MPa have been obtained in cold-worked low carbon Fe-18Cr-18Mn-0.58N steels[47]. In contrast the use of nitrogen in metastable austenitics appears to be far less common. This could well be attributed to the careful chemistry control required to achieve a M_s and M_d temperature just below and just above ambient respectively.

2.4. NITROGEN SOLUBILITY AND NITRIDE PRECIPITATION

The nitrogen solubility in austenitic stainless steels has not been extensively investigated, in spite of its importance[44]. Figure 2.10 shows that Mo, Mn, Si, Cr and V increase the nitrogen solubility in liquid iron at 1600°C, whereas Ni, P and C decrease it.

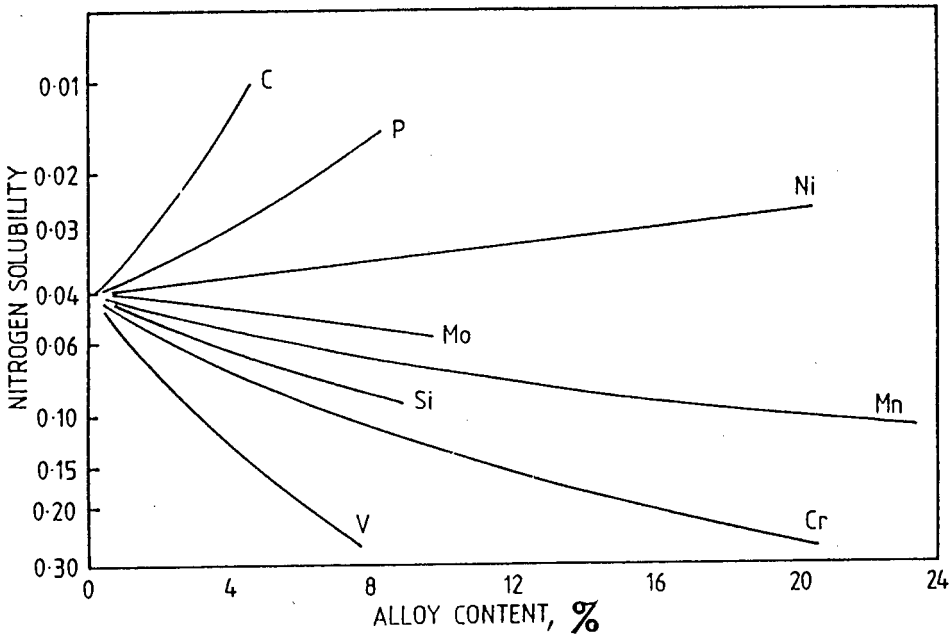

Figure 2.10 Effect of alloying elements on solubility of nitrogen in liquid iron at 1600°C.[42]

Nitrogen solubility is also a function of the solution treatment temperature. The equilibrium diagram for the Fe-18Cr-Ni-N system at 900°C is shown in figure 2.11. If the steel contains no nickel, the nitrogen solubility of Fe-18Cr steels is only about 0.07% but increases to above 0.25% on raising the nickel content to 3%. As nickel increase above 3%, the nitrogen solubility decreases.

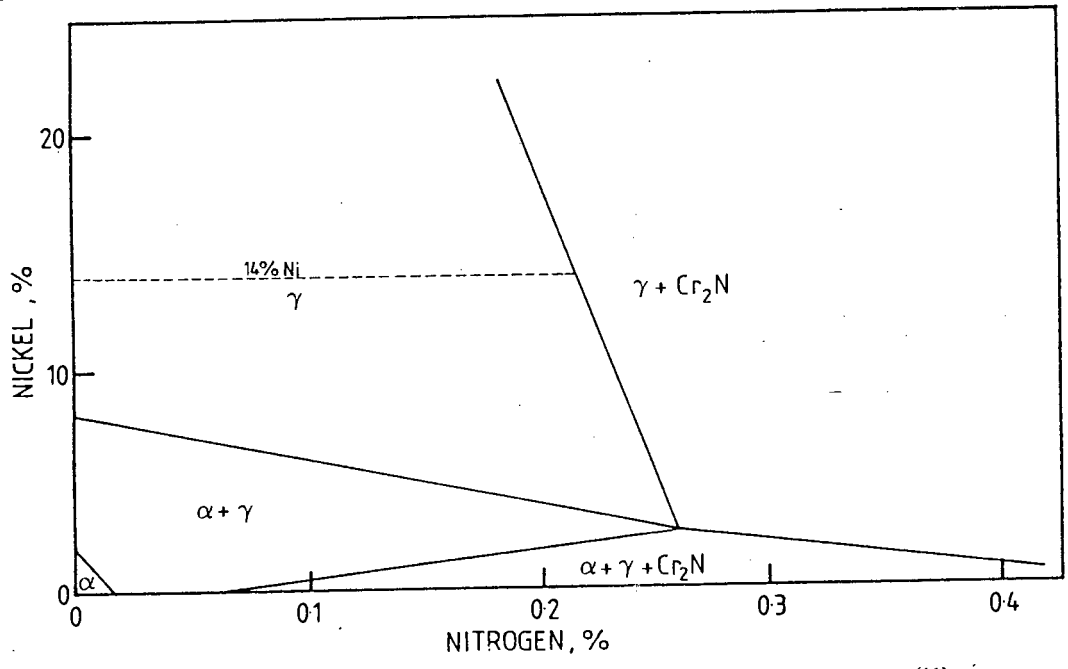

Figure 2.11 Equilibrium diagram for Fe-18Cr-Ni-N system at 900°C.[11]

If the solution treatment temperature is raised to 1050°C, the nitrogen solubility in Fe-18Cr steels is well in excess of 0.3%, since Fe-12Cr steels already have a nitrogen solubility in excess of 0.3%[17]. Hence by increasing the solution temperature the nitrogen solubility is markedly improved. It has for example been reported that type 304 (8-12% Ni) and 316 (10-14% Ni) solution treated at 1050°C can comfortably retain more than 0.2% nitrogen[51].

The solubility of nitrides (Cr_2N) in 18Cr-8Ni and 25Cr-20Ni steels, is greater than that of carbides ($C_{r23}C_6$) as shown in figure 2.12.

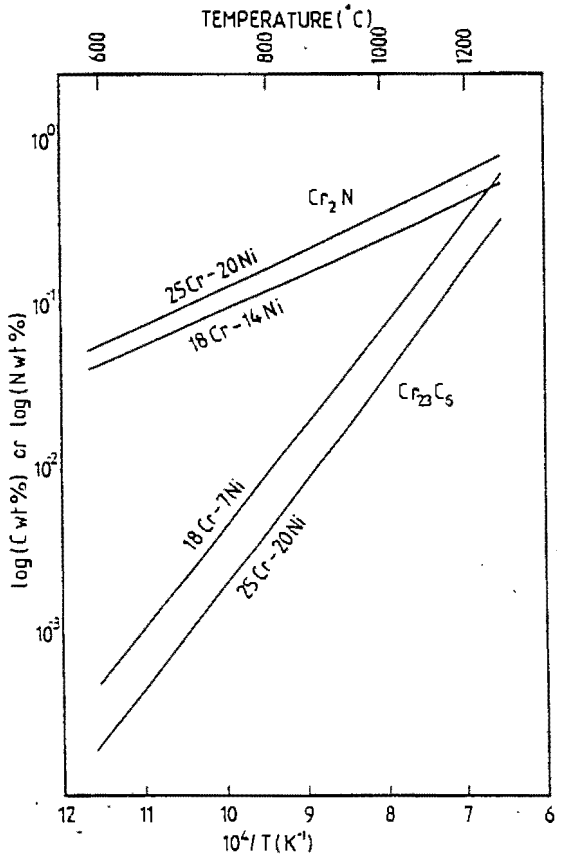

Figure 2.12 Solubility of nitrides compared to that of carbides in 18Cr-8Ni and 25Cr-20Ni alloys.[44]

This may lead not only to a larger concentration of solid solution nitrogen but also to a slower precipitation rate[44]. The latter is beneficial in reducing the sensitivity to intergranular corrosion of nitrogen alloyed austenitic stainless steels. This is one of the main reasons for using nitrogen in preference to carbon, for strengthening and austenite stabilization.

In nitrogen alloyed Fe-18Cr-(4-10%)Ni-(1-9%)Mn steels with less than 0.05%C, precipitation of Cr_2N takes place predominantly at grain boundaries and at the coherent and incoherent twin boundaries. For higher carbon steels (0.1%) continuous precipitation of Cr_2N occurs in the matrix[56]. Cellular precipitation of Cr_2N commonly occurs but with higher ageing time and temperature a type of 'nitrogen pearlite' can be obtained in high (0.7%) nitrogen steels. This nitrogen pearlite has a lamellar structure, comprising lamellae of austenite and Cr_2N[45].

CHAPTER 3

EXPERIMENTAL TECHNIQUES

3.1 EXPERIMENTAL MATERIALS

Twenty experimental alloy compositions were prepared by Middelburg Steel and Alloys research laboratory, based on the composition of AISI 301 (Cr = 17 - 18 wt%; Mn(max) = 2.00 wt%; Si(max) = 1.00 wt%; C(max) = 0.15 wt%) with nickel contents ranging from 3.2 - 5.2 wt% and nitrogen contents ranging from 0.087 - 0.276 wt%. Each experimental alloy was cast into a 5 kg ingot (50 mm thickness) and hot rolled to 10 mm plate gauge. A portion of this plate was further hot rolled to a sheet thickness of 4 mm. The twenty experimental alloys were examined using optical microscopy and X-ray diffraction (XRD). Ten of these alloys were selected for tensile and impact testing. The chemical compositions of the ten alloys selected for mechanical tests are given in table 3.1 - 3.3 and the rest are given in Appendix 1. In order to make it easier to associate an alloy designation with its nickel and nitrogen contents, alloys are given a four digit code. The first two digits represent the nickel content and the last two the nitrogen content. Thus alloy 5109 contains 5.1 wt% nickel and 0.09 wt% nitrogen, alloy 4711 contains 4.7 wt% nickel and 0.11 wt% nitrogen etc. The original heat numbers supplied by the Middelburg Steels and Alloys research laboratory are given in brackets.

	ALLOY			
ELEMENT	5109 (901891)	5113 (901911)	5216 (902121)	5028 (902131)
C	.084	.087	.075	.071
Mn	1.62	1.61	1.55	1.48
Si	.65	.65	.48	.44
V	.08	.08	.06	.06
Cu	.08	.08	.08	.08
Co	.02	.02	.02	.02
Mo	.03	.03	.05	.05
Cr	17.2	17.5	17.9	17.9
Ni	5.12	5.09	5.17	5.03
N	.087	.129	.163	.276

Table 3.1 Chemical composition of four of the selected experimental alloys containing 5.0 - 5.2 wt% nickel.

	ALLOY			
ELEMENT	4711 (901971)	4714 (901981)	4716 (901991)	4718 (902001)
C	.092	.090	.101	.087
Mn	1.78	1.69	1.60	1.29
Si	.71	.66	.63	.63
V	.08	.08	.08	.08
Cu	.10	.10	.10	.10
Co	.03	.02	.02	.02
Mo	.03	.03	.03	.03
Cr	18.1	18.2	18.4	18.5
Ni	4.73	4.69	4.66	4.74
N	.114	.138	.157	.179

Table 3.2 Chemical compositions of four of the selected experimental alloys containing 4.7 wt% nickel.

	ALLOY		
ELEMENT	3419 (902101)	3428 (902111)	AISI 301
C	.078	.070	.029
Mn	1.51	1.53	1.52
Si	.43	.43	.44
V	.07	.06	.05
Cu	.06	.06	.10
Co	.02	.02	.03
Mo	.05	.05	.20
Cr	18.0	18.0	17.7
Ni	3.41	3.36	7.48
N	.185	.275	.074

Table 3.3 Chemical compositions of two of the selected experimental alloys containing 3.4 wt% nickel and of AISI 301.

The alloys in tables 3.1 - 3.3 are grouped into sets according to their nickel content as shown in table 3.4. Thus the code of an alloy set corresponds to the first two digits of the alloys contained in that particular set, with the exception of alloys 5216 and 5028.

5.1% Nickel (SET 51)	4.7% Nickel (SET 47)	3.4% Nickel (SET 34)
5109	4711	3419
5113	4714	3428
5216	4716	
5028	4718	

Table 3.4 Grouping of selected alloys into three sets to facilitate easy identification.

3.2 HEAT TREATMENT

Specimens were ceramic-coated and given a solution treatment in air at 1050°C for 30 minutes, followed by an oil quench. This heat treatment was used for the tensile as well as the impact specimens.

3.3 TENSILE TESTS

Each tensile test (to fracture) was repeated three times to ensure reasonable statistical accuracy of the result. The result of a tensile test which differed notably from that of the other two tests performed under the same test conditions, was not included in the analysis, and due to a limited amount of specimens being available, some results represent the average of only two tests.

3.3.1 Specimen Geometry

For the purposes of general tensile property evaluation, Hounsfield-type tensile specimens were machined from the 10 mm plate with the dimensions shown in figure 3.1.

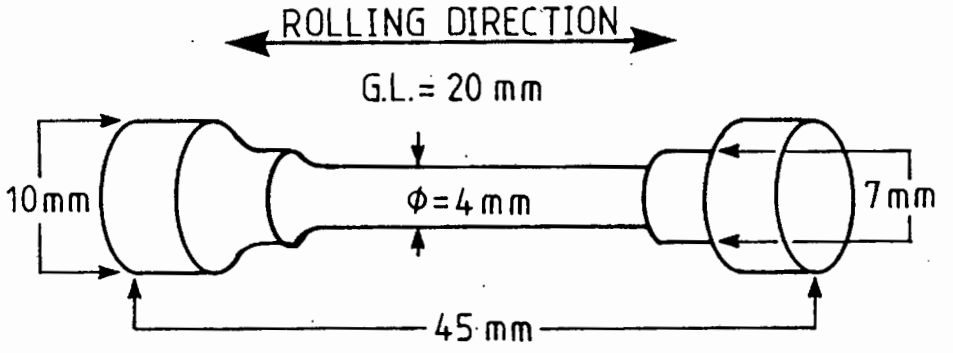

Figure 3.1 Hounsfield-type tensile specimen for general tensile property evaluation.

3.3.2 Test Apparatus

Tensile tests were performed using a computer-interfaced Zwick 1484 materials tester, which facilitated the capture of force (in Newtons) and gauge length elongation (in mm) on computer file (figure 3.2(a)). The test set-up incorporated a temperature bath (1), regulated by a Eurotherm temperature controller (2) to within 2°C. The temperature controller was connected to a chromel-alumel thermocouple (3), the tip of which was positioned in close

proximity of the specimen gauge length. Tensile fracture tests were performed at 20, 60 and 120°C, while tests terminating at 0.3 true strain were performed at the same temperatures, as well as 0°C. All experiments were carried out at an initial strain rate equivalent to 10^{-3} per second.

Figure 3.2 (a) Computer-interfaced Zwick 1484 materials tester, with test rig mounted underneath cross-head (XH), showing 200 kN load cell (LC) and temperature controller (2).
(b) Close-up view of rig, showing the temperature bath (1) (which has been lowered to show the coil and specimen), chromel-alumel thermocouple (3), heating coil (4) and specimen (5). The specimen is put into tension by the downward force exerted on the bottom end of the specimen by the downward movement of the cross-head and rig, while the top end of the specimen is kept stationary by the restraining rod (R), which is attached to the load cell.

The tests performed at 0°C were performed in an ice and water mixture, while those at 20°C were performed in air. Those at 60 and 120°C were performed in an oil bath, heated by a helical coil (4) which was coupled to the Eurotherm temperature controller. The coil was positioned over the gauge length of the specimen (5).

3.3.3 Data Analysis

The true stress-true strain curve was derived, with the aid of a computer spreadsheet package by using the equations:

$$e_t = \ln(1+e_n) \quad \sigma_t = \sigma_n(1+e_n) \text{.....(3.1)}$$

where σ_n and e_n are the engineering stress and engineering strain respectively and σ_t and e_t are

the true stress and true strain respectively. The work-hardening rate curve was obtained by using equation 3.2:

$$(\sigma_t^i - \sigma_t^{i-1})/(e_t^i - e_t^{i-1}).....(3.2)$$

where i refers to the i^{th} data point. Due to the intrinsic jagged nature of the stress-strain curve (especially one which exhibits accentuated serrated flow), the computed work-hardening rate curve has a large scatter if all data points collected on computer file are used (figure 3.3).

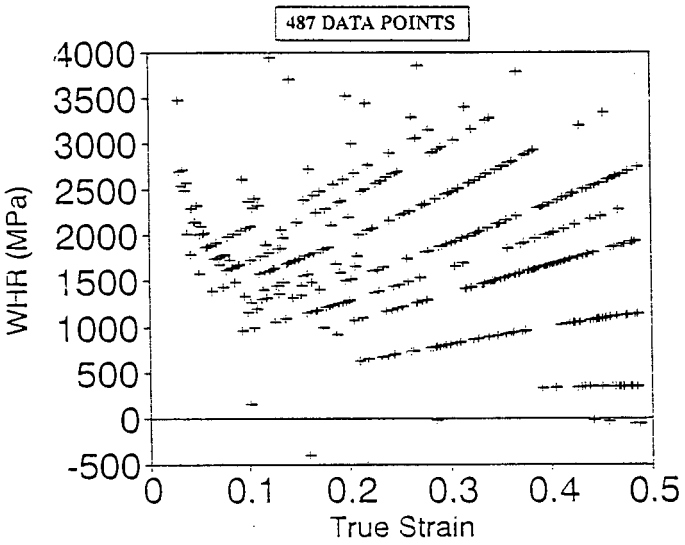

Figure 3.3 Large scatter in calculating work-hardening rate (WHR) using 487 data points.

The scatter can be reduced by the systematic elimination of every alternate data point (σ_t and its corresponding value of e_t), so that only half of the original data remains (243 data points). The work-hardening rate curve is then calculated and if the scatter is still too large, the process is repeated. This process of systematic data elimination was continued until the work-hardening rate curve was such that a definite trend could be observed (figure 3.4).

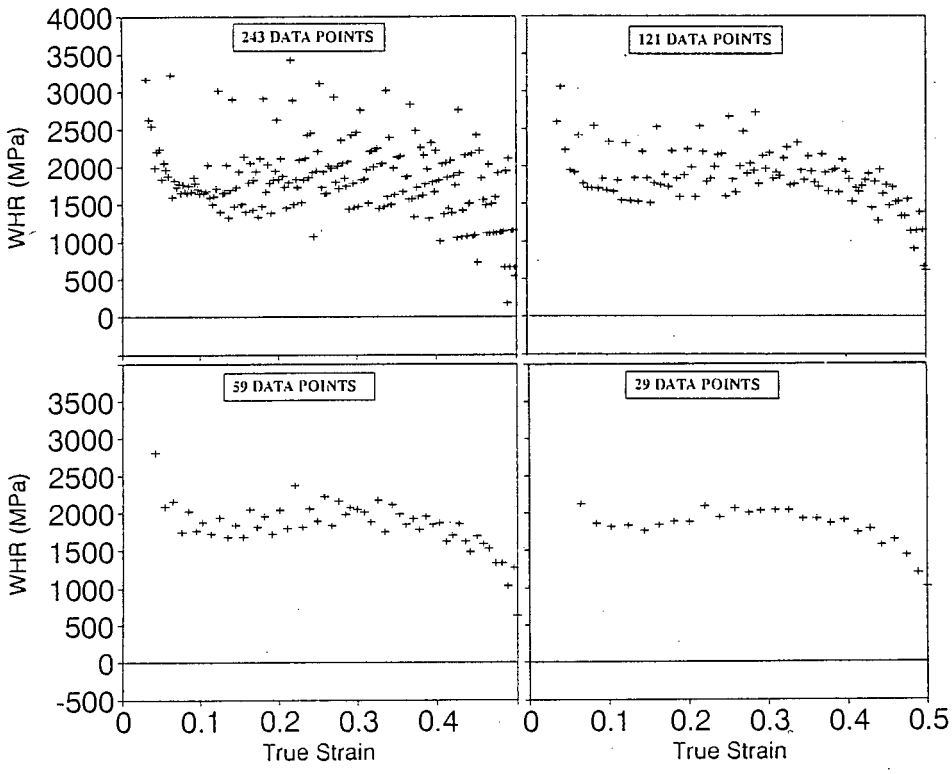

Figure 3.4 Systematic elimination of alternate data points to produce a smooth work-hardening rate curve.

This method was used in preference to including all data points and then having to use a smoothing procedure to obtain a work-hardening rate curve. The problem which arises when using a non-linear smoothing procedure (such as using polynomials of order 5 and less), is that the resultant curve contains maxima and minima which have a mathematical origin and have no real physical significance (figure 3.5).

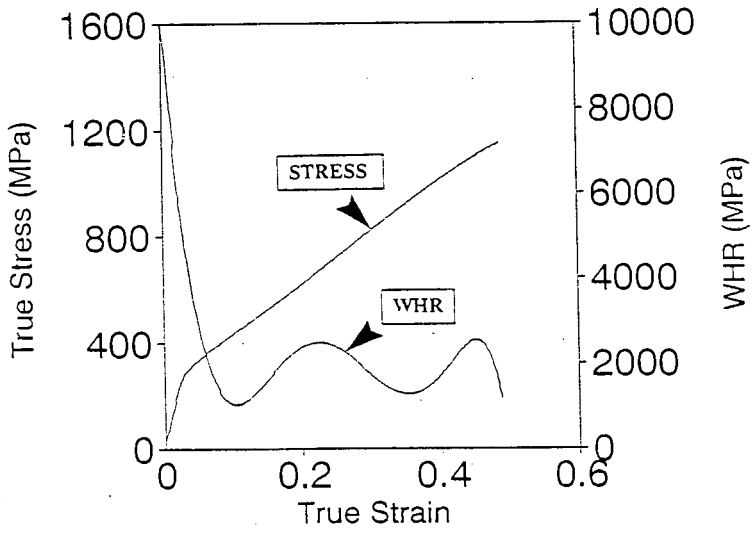

Figure 3.5 Non-linear smoothing using a 5th order polynomial to obtain the WHR curve from 487 data points showing the maxima and minima.

The uniform elongation was determined by measuring the plastic strain from the yield strain to

the strain at which the flow stress and the work-hardening rate are numerically equal. Thus at the point of specimen macro-necking:

$$\sigma = d\sigma/de \quad .....(3.3)$$

The strain-hardening exponent (n) of the equation:

$$\sigma = Ke^n \quad .....(3.4)$$

was determined by plotting log(σ) versus log(e) and performing linear regression on the desired strain interval to obtain the slope of the straight line (i.e. n).

3.4 IMPACT TESTS

For the purpose of establishing the room temperature impact fracture mode and toughness, sub-standard Charpy V-notch specimens were machined from the 10 mm plate shown in figure 3.6. Each impact test was repeated three or four times to ensure reasonable statistical accuracy.

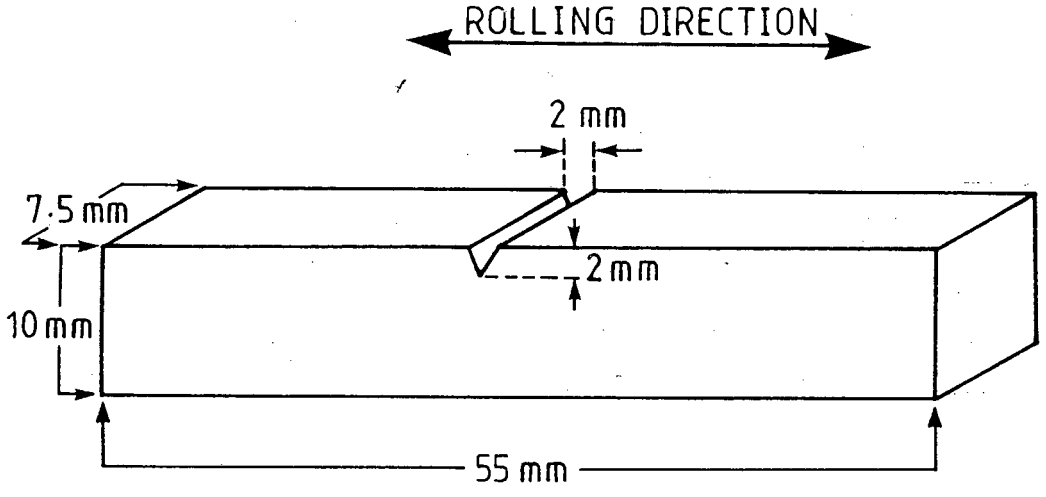

Figure 3.6 Sub-standard Charpy V-notch specimen for room temperature impact fracture mode and toughness evaluation (notched in through thickness direction).

The test was performed using a standard Charpy impact tester with a swinging pendulum of 300 joule striking the specimen resting on its side at a striking velocity of 5.5 ms^{-1}.

3.5 X-RAY DIFFRACTOMETRY (XRD)

The morphology of martensite militates against easy volume fraction measurement using light microscopy, in that plates occurring in sheaves or elongated clusters are too small to be resolved individually. As a result, optical microscopy indicates greater amounts of martensite than actually exists[57]. The X-ray diffraction technique is at present one of the most reliable methods of measuring martensite volume fractions, and has the advantage that it does not require a set of calibration samples[58].

3.5.1 Calculating Phase Volume Fractions by XRD

The diffraction pattern of a crystalline substance irradiated with X-rays is determined by the crystal structure of all phases within that substance and is predicted by Bragg's Law[59]:

$$n.\lambda = 2.d.\sin\theta \quad .....(3.5)$$

where : n = 1, 2, 3....

λ = X-ray wavelength

d = interplanar spacing

θ = angle between atomic plane and X-ray beam

The X-ray intensity diffracted from each phase is proportional to the volume fraction of that phase. If the X-ray intensity (peak height) were also proportional to the peak area, then the volume fraction could be calculated directly from the height of the peak. This is often not the case, and the volume fraction of each phase must therefore be calculated using the area under the peak (integrated intensity for a range of angles around θ), rather than the peak height itself (intensity at θ). (Diffraction line broadening occurs for a number of reasons[60]: (i) In a real polycrystalline sample the individual crystallites are slightly misoriented with respect to one another; (ii) Instrumental factors such as collimation; (iii) Natural wavelength distribution due to production of X-rays being a random process which follows the usual statistical laws. If the X-ray intensity is large, the X-rays follow a Gaussian distribution.) The integrated intensity of a particular (hkl) reflection in a phase can be expressed as[58]:

$$I_{hkl} = [I_0 e^4/m^2c^4] \,.\, [\lambda^3 A/32\pi r] \,.\, [1/v^2] \,.[\, FF \,.p.LP].e^{-2M}/2\mu].V \quad .....(3.6)$$

where : I_0 = intensity of incident beam

e, m = charge and mass of electron respectively

r = diffractometer radius

c = velocity of light

λ = incident wavelength radiation

A = cross-sectional area of incident beam

v = unit cell volume of particular phase

FF = product of structure factor and its complex conjugate

p = multiplicity factor of the (hkl) reflection

LP = Lorentz polarization factor

e^{-2M} = Debye-Waller or temperature factor

μ = linear absorption coefficient

V = volume fraction of particular phase

This equation can be simplified as follows:

$$I_{hkl} = [\, K \,.\, R_{hkl} \,.\, V \,] \,/\, [\, 2\mu \,] \quad .....(3.7)$$

where : $K = [I_0 e^4/m^2c^4] \,.\, [\lambda^3 A/32\pi r]$

$R_{hkl} = [1/v^2] \,.[\, FF \,.p.LP].e^{-2M}$

K is independent of the nature of the specimen, while R_{hkl} depends on the specimen crystal structure, the reflecting set of planes and θ. Hence R_{hkl} can be calculated from basic principles. The ratio of the volume fraction of austenite (V_γ) and martensite ($V_{\alpha'}$) can now be written as:

$$V_\gamma/V_{\alpha'} = I_\gamma^{hkl} R_{\alpha'}^{hkl} / I_{\alpha'}^{hkl} R_\gamma^{hkl} = \mathbf{S} \quad .....(3.8)$$

If $V_\gamma + V_{\alpha'} = 1$ (no third phase e.g. carbide or nitride is present) then:

$$V_{\alpha'} = 1/[1+\mathbf{S}] \text{ and } V_\gamma = \mathbf{S}/[1+\mathbf{S}] \quad .....(3.9)$$

If a third phase is present its volume fraction can be determined by other means (e.g. point counting) and included in equations (3.9).

3.5.2 Texture Effects

Equation (3.6) is only strictly true for a specimen which has effective infinite thickness and contains a completely random arrangement of crystals[58,61,62]. Dickson[58] defined a texture parameter (P) calculated from the values of I_{hkl} and R_{hkl} to assess the type and intensity of preferred orientation. Using this texture parameter it is found that large errors can arise by considering too small a number of (hkl) peaks of each phase, especially in heavily cold rolled metals which can exhibit high degrees of preferred orientation. Thus by including as many peaks as possible for each phase, the more accurate the final analysis. There are however

practical limitations such as peak overlap making some peaks difficult to resolve and also time constraint. One source advocates the use of at least four peaks for each phase[62] while another concludes that three peaks for each phase, in a heavily cold-rolled structure, are adequate for the result to be within the limits of experimental error[58]. Initially three peaks were used for both the austenite and martensite phase:

	CuKα[62]		MoKα[57]	
Peak	Bragg Angle(°θ)	$R_{(hkl)}$	Bragg Angle(°θ)	$R_{(hkl)}$
200α'	32.5	32	14.4	224
211α'	41.2	61	17.7	413
310α'	58.0	19	23.0	132
200γ'	25.4	82	11.4	481
220γ'	37.3	44	16.3	298
311γ'	45.5	51	19.2	314

Table 3.5 Bragg angles and R-factors of the three austenite and martensite peaks, which were initially used for both CuKα and MoKα radiation.

However, due to difficulty in resolving peak overlap between $310_{\alpha'}$ (θ_{Cu} = 58.0°) and 400_{γ} (θ_{Cu} = 59.3°) it was decided to use only the $200_{\alpha'}$ and $211_{\alpha'}$ peaks for the martensite phase. Further investigation showed that if only the 220_{γ} and 311_{γ} peaks were used for the austenite phase, the analysis yielded virtually the same results as for the analysis using three peaks for each phase. Generally martensite formed by tensile deformation does not have the same heavily preferred orientation as martensite formed by heavy cold rolling[58] and hence the use of two peaks for each phase suffices.

3.5.3 XRD Instrument Settings

The X-rays pass through two slits before reaching the detector. The first is the divergence slit and is situated between the tube and the specimen. This slit controls the amount of ray divergence which is determined by the focal size. It is matched with a scatter slit which is situated between the specimen and detector. This slit reduces scatter of the X-rays. The following combination gave the best peak to background ratio : receiving slit = 1°, scatter slit = 1°.

A β-filter was inserted between the tube and the specimen so as to allow only Kα radiation to strike the specimen. (A nickel filter was used for CuKα radiation and a zirconium filter for MoKα radiation). Since the β-filter, when used on its own, can never completely separate the Kα doublet from continuous radiation, a graphite monochromator was used in combination

with the filter to give optimum separation of the continuum from the Kα radiation. The voltage/current setting of the machine is determined by the maximum rating of the X-ray tube which in turn depends on the specific loading of the anode. Since high loading of an X-ray tube gives rise to filament heating and subsequent spectrum contamination, the voltage and current settings were optimized to protect the system. The following settings were used for both CuKα and MoKα radiation : current = 30 mA, voltage = 40 kV.

The X-ray intensity was measured as the number of counts detected by the scintillator in a pre-set time at pre-set angles. The data, which included diffraction angle, no. of counts/pre-set time and counting time, were collected on computer file. The motor control settings which gave optimum peak resolution, peak to background ratio and total running time are summarized in table 3.6:

CuKα Radiation	MoKα Radiation
Start angle = 62°2θ End angle = 93°2θ Step interval = 0.05°2θ Count time = 10 seconds	Start angle = 25°2θ End angle = 40°2θ Step interval = 0.05°2θ Count time = 10 seconds

Table 3.6 Optimum XRD motor control settings.

The spectrum was plotted using a computer spreadsheet package and the start angle (θ3) and end angle (θ4) for each peak were determined (figure 3.7). Appropriate angles for the background to the left (θ1 and θ2) and the right (θ5 and θ6) of each peak also had to be determined. The background under the peak was calculated in two ways: firstly by fitting a straight line through the left and right backgrounds and secondly by fitting a polynomial. Two integrated areas under the peak were thus obtained; one area corresponding to the total area minus the background fitted with the straight line, and the other area corresponding to the total area minus the background fitted with the polynomial. The two areas were then averaged to give the integrated intensity corrected for the background.

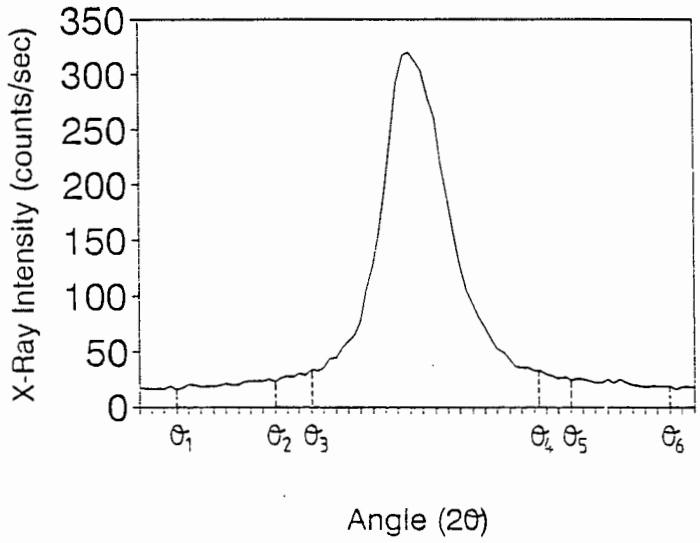

Figure 3.7 Determination of left and right peak angles (θ3 and θ4), as well as angles for determining the left and right backgrounds (θ1, θ2, θ5 and θ6).

3.6 SPECIMEN PREPARATION FOR XRD ANALYSIS

3.6.1 XRD Specimen Geometry

For the purpose of XRD, flat tensile specimens were machined from the 4 mm plate with the dimensions shown in figure 3.8.

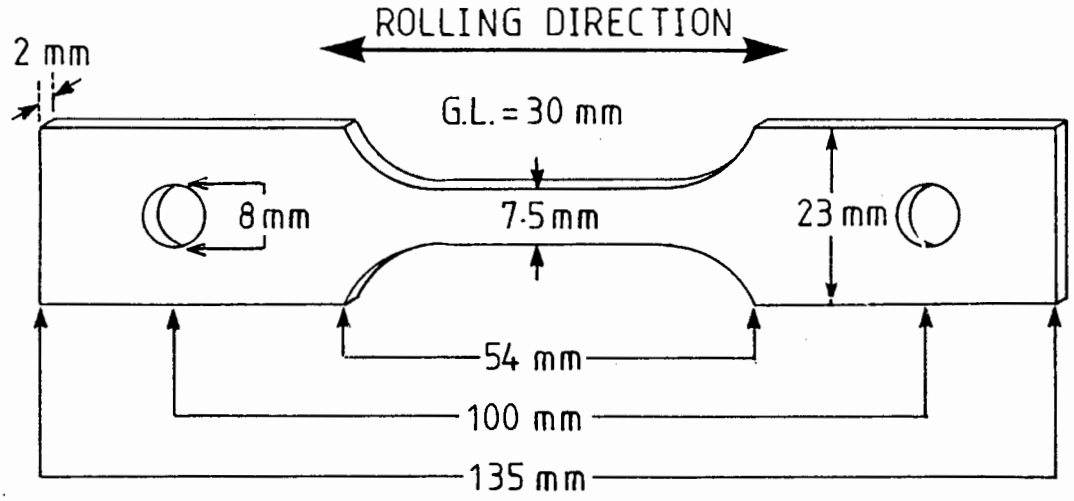

Figure 3.8 Flat tensile specimen for determining the volume fraction of deformation-induced martensite using XRD.

The gauge length was mechanically polished to remove machining marks before heat treating the specimen. After tensile deformation, two pieces each 10 mm long were cut from the centre of the gauge section and mounted side by side. This was necessary to obtain a XRD specimen which was at least 10 x 10 mm. It was found that the peak to background ratio decreased rapidly when the specimen dimensions were smaller than this. Kumar *et.al.*[40] showed that

due to nonhomogeneous distribution of plastic strain and variation in temperature along the gauge length, the volume fraction of martensite would be different near the end of the gauge length and the centre of the specimen. For this reason it was important to always use the centre portion of the gauge length.

3.6.2 Electrochemical-Polishing/Etching Conditions

During mechanical polishing of the alloy surfaces, metastable austenite can transform to martensite under suitable conditions. Since the resultant polished surface is not a true reflection of the underlying microstructure, this deformed layer has to be removed by means of an electrochemical-polishing process. Electrochemical-polishing is widely used in research and industry; however a standard procedure cannot be adopted[63]. Thus it is necessary to determine the optimum parameters such as electrolyte temperature, voltage, current density and polishing time by trial and error.

The specimen was mounted in a thermosetting plastic mould and prepared using conventional metallographic techniques. The final surface finish was obtained by mechanically polishing with 3 μm diamond paste. A stainless steel crocodile clip was then attached to it in such a way that only one of the teeth gripped the edge of the surface in order to minimize surface damage. This was the most efficient way of obtaining electrical contact with the specimen. A voltmeter was used to check that the circuit was complete before immersing the specimen. During the polishing process the temperature was monitored while the solution was gently stirred using a magnetic stirrer. The solution needed to be *gently* stirred for the following reasons :

(a) To prevent local heating from occurring at the specimen surface, which would reduce the viscosity of the polishing film;
(b) To dissipate heat from the electrolyte to the surrounding water bath more rapidly;
(c) To prevent air bubbles from forming at the surface which would result in uneven polishing.

The electrolyte used consisted of:

266 ml glacial acetic acid
50 g chromic acid (CrO_3)
14 ml distilled water

The voltage was kept constant at 20 V and the current density ranged between 0.10 - 0.25 A/cm^2 for electro-polishing purposes. The current density increased with electrolyte age, and the quality of the polish deteriorated rapidly if the electrolyte was used for a total of more than

about 1.5 hours.

In those cases where the specimen needed to be etched after it had been electro-polished, the voltage was reduced to 5 V and electro-etching was performed for between 5 and 10 minutes depending on the alloy and degree of etch required. For best results the specimen was rinsed in distilled water immediately afterwards and then cleaned in ethanol in an ultra-sonic bath.

In order to be sure that the deformed layer was completely removed, the martensite content vs. polishing time was measured for AISI 301 and is shown in figure 3.9. From this plot it can be seen that 5 minutes is adequate to remove the martensite induced by mechanical polishing. To avoid having to repeat this procedure for all experimental alloys each specimen was electro-polished for 9 minutes. It was found that the surface became very 'wavy' if this time was exceeded. The reduction in martensite volume fraction on increasing the electro-polishing time for up to 20 minutes in randomly selected alloys was found to be negligible within the accuracy of the XRD technique (i.e. within about 3%), and in some cases the martensite content even increased. Thus it appeared that in some alloys martensite was being formed during electro-polishing.

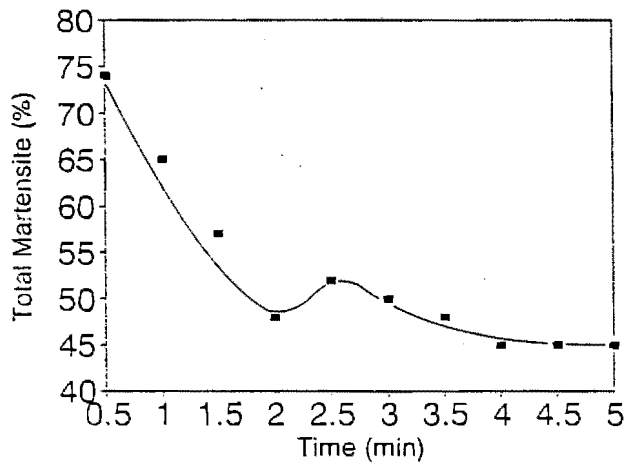

Figure 3.9 Removal of martensite induced by mechanical polishing from the surface of type 301 deformed by a true strain of 0.3 at 20°C.

3.6.3 Formation of Martensite During Electro-polishing

In order to quantify the amount of martensite induced during electro-polishing, martensite volume fractions were measured using both CuKα and MoKα radiation since these two radiations have different depths of penetration (table 3.7).

RADIATION	PENETRATION DEPTH (μm)
CuKα	2
MoKα	20

Table 3.7 Depth of penetration of CuKα and MoKα radiation in stainless steel[62].

The calculated martensite volume fraction using CuKα radiation minus the calculated volume fraction using MoKα radiation (ΔMVF) is determined, and gives an indication of the amount of martensite induced during electro-polishing (figure 3.10).

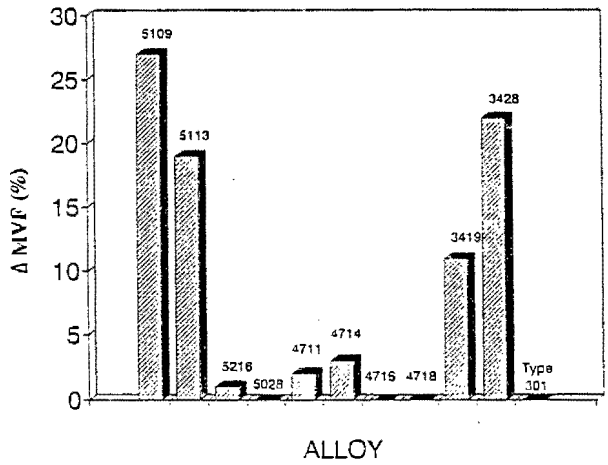

Figure 3.10 ΔMVF of solution-treated, undeformed alloys determined using CuKα and MoKα radiation.

It has been found that the introduction of hydrogen into the surface of type 304 austenitic stainless steel by cathodic hydrogen charging, can result in the formation of a FCC phase designated by γ^*, which has a lattice parameter approximately 5% greater than γ[64]. The formation of this phase during charging is accompanied by a volume expansion of approximately 15%, and the resulting high stresses in the region below this transformed and expanded surface layer result in plastic deformation accompanied by martensite transformation. On termination of charging, hydrogen is lost from the γ^* phase at the immediate sub-surface during subsequent room temperature ageing while a high concentration still exists one or two micrometers below the surface[65]. This produces high tensile stresses at the surface which induce elastic accommodation and/or plastic flow, resulting in surface relief and the formation of martensite at the surface[64]. It is expected that the amount of hydrogen absorbed during electro-polishing is considerably less than during cathodic charging, but is nevertheless sufficient to induce measurable quantities of martensite. While the minimum ageing time for equilibrium to be reached in type 304 was reported to be 24 hours at room temperature[64], it was found that equilibrium was reached in this study within a few minutes after electro-polishing followed by ageing at room temperature. (Specimens were aged at 50°C for 24 hours and no increase in martensite could be detected).

The results show that the amount of polish-induced martensite of the alloys deformed in tension to 0.3 true strain was negligible. In the undeformed alloys it appeared generally that the lower the austenite stability, the greater is the amount of martensite induced during electro-polishing. Set 34 however showed the opposite trend since alloy 3419 having lower austenite stability than alloy 3428 formed less polish-induced martensite. It is possible that reversal of the general trend is due to the considerable amounts of pre-existing martensite in alloy 3419 and 3428. (Alloy 3419 contains more pre-existing martensite than alloy 3428.) High levels of martensite present before polishing reduce the amount of hydrogen introduced into the surface, perhaps by providing paths for rapid diffusion away from the immediate surface, thus preventing build-up of hydrogen at the surface[66]. Also further production of martensite is likely to be hindered by the lack of suitable nucleation sites in the small volume of austenite remaining. The presence of pre-existing martensite may also constrain the austenite phase and prevent it from expanding to form γ^*.

3.7 METALLOGRAPHY

The microstructures of the various alloys were characterized using both light and electron (scanning and transmission) microscopy. Specimens were examined using light microscopy in the heat-treated condition after having been electro-polished and electro-etched as described in section 3.6.2. The presence of δ-ferrite was investigated using two tint etches[67] and an electro-chemical etch[63]:

Tint etch 1: Beraha colour etch II:

Stock solution : 48 g ammonium bifluoride, 800 ml distilled water and 400 ml concentrated hydrochloric acid.
Etch : 100 ml of stock solution mixed with 1 g potassium bisulphite.
Etching time : 60 - 90 seconds.

Tint etch 2: Lichtenegger-Bloech colour etch I:

Etch : 20 g ammonium bifluoride, 0.5 g potassium bisulphite and 100 ml hot distilled water.
Etching time : 1 - 5 minutes
(With this tint etch even the smallest δ-ferrite precipitates in the matrix can be detected since the austenite and martensite are coloured blue to brown while the δ-ferrite remains white.)

Electro-chemical etch:

Solution : 20% aqueous NaOH
Voltage : 20 V (d.c.)
Etching time : 60 - 120 seconds.

Light microscopy was carried out on a REICHERT MeF2 microscope using conventional brightfield imagery and Nomarski interference contrast. A Cambridge Stereoscan 200 electron microscope was used for the examination of the tensile and impact fracture surfaces. Secondary electron images were obtained at an accelerating voltage of 30 kV. A JEOL 200CX transmission electron microscope was used for the investigation of possible nitride formation in the highest nitrogen alloys. The following procedure was carried out for TEM specimen preparation:

(1) Small platelets were mechanically polished to a thickness of approximately 0.3 mm.
(2) Discs of 3 mm diameter were spark-eroded from the platelets.
(3) The spark-eroded discs were further mechanically polished to a thickness of 0.15 mm.
(4) The thinned spark-eroded discs were jet-polished to perforation at -10°C using a Struers Tenupol jet-polisher.

The solution used for jet-polishing consisted of:

80 ml Glycerol
300 ml Methanol
20 ml Perchloric acid

The polisher settings were : Flow Rate = 3.0 - 3.2, Current = 220 - 250 mA, Voltage = 50 V. An accelerating voltage of 200 kV was used and the majority of TEM micrographs were taken in the bright field mode.

3.8 DILATOMETRY

The austenite to martensite transformation is accompanied by a volume expansion of 3 - 4%[11] and can be determined from a dilatometric trace (figure 3.11). The M_S and M_f temperatures can be measured using this technique. Dilatometer specimens of 50 mm length (4 x 4 mm cross-section) were heated at a rate of 4°C/min to ensure a homogeneous temperature distribution throughout the specimen during heating. Specimens were heated to about 950°C and upon reaching this temperature were then immediately furnace cooled. The

set-up facilitated the capture of temperature and dilation on computer file. It was not possible to cool the specimen below room temperature and hence M_s temperatures which are below 20°C could not be determined using this technique. Ideally the specimens should have been rapidly cooled from 950°C to assimilate the quenching procedure of the tensile and impact specimens, but rapid cooling was unfortunately not possible with the existing set-up.

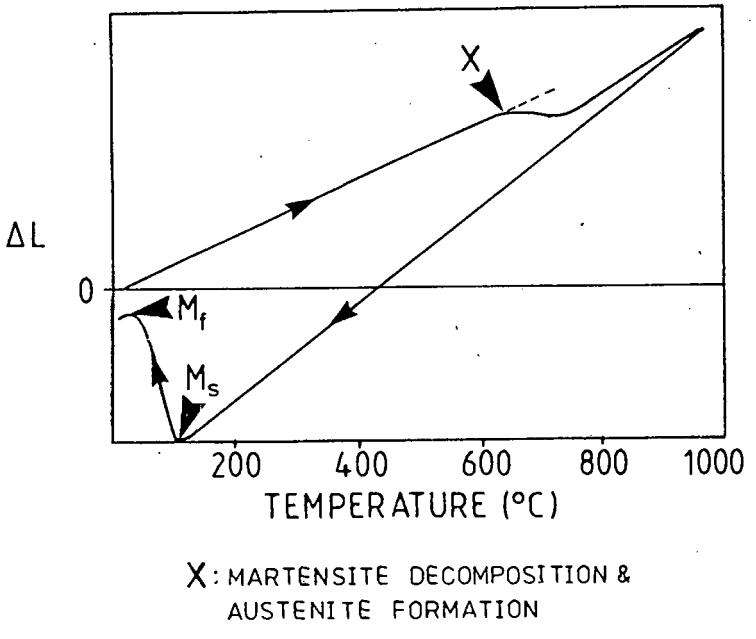

Figure 3.11 Typical dilatometric trace of an alloy with M_s around 100°C and M_f close to room temperature.

CHAPTER 4

RESULTS

4.1 MICROSTRUCTURAL CHARACTERIZATION

4.1.1 Optical Microscopy and XRD

The microstructures of the ten experimental alloys solution-treated at 1050°C are shown in figures 4.1 to 4.3. The martensite (bulk) volume fractions, indicated in the figure captions, were determined by XRD (using MoKα radiation). Figures 4.1(a) and (b) show that the surface martensite content is considerably greater than that of the bulk.

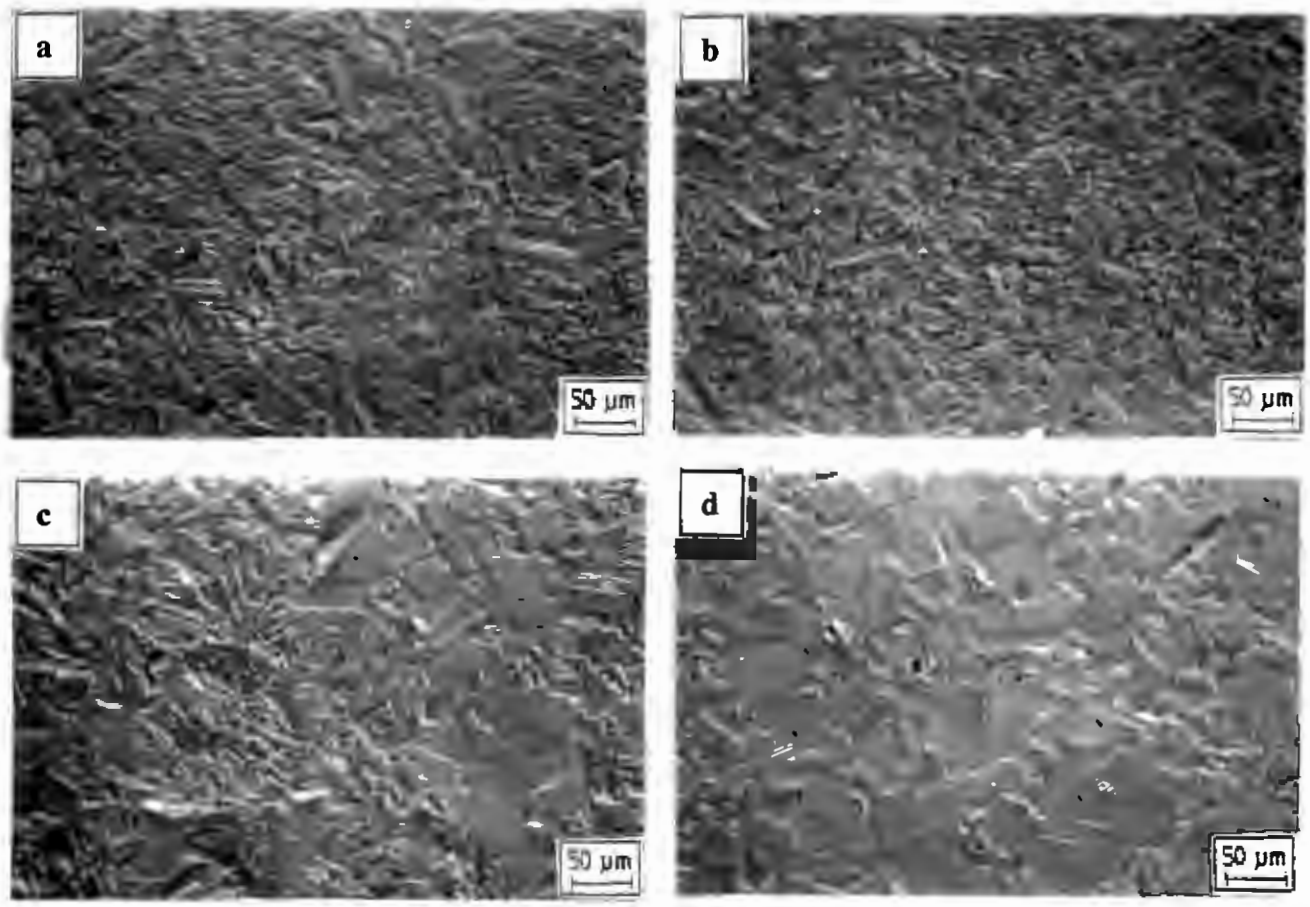

Figure 4.1 Microstructures of set 51, solution-treated at 1050°C for 30 minutes followed by oil quench. Electro-polished and electro-etched. Surface relief enhanced by Nomarski interference contrast.
[A = Austenite; M = Martensite]
(a) **Alloy 5109 (A = 84%; M = 16%)** (b) **Alloy 5113 (A = 87%; M = 13%)**
(c) **Alloy 5216 (A = 89%; M = 11%)** (d) **Alloy 5028 (A = 95%; M = 5%)**

The surface martensite content exceeds that of the bulk in alloys 5109 and 5113, due to the formation of martensite during electro-polishing as discussed in section 3.6.3. The alloys of set 47 in general are more resistant to martensite formation during electro-polishing than the

alloys of set 51, and the martensite volume fractions visible in the optical micrographs, are in close agreement with the bulk volume fractions determined by XRD (figure 4.2)

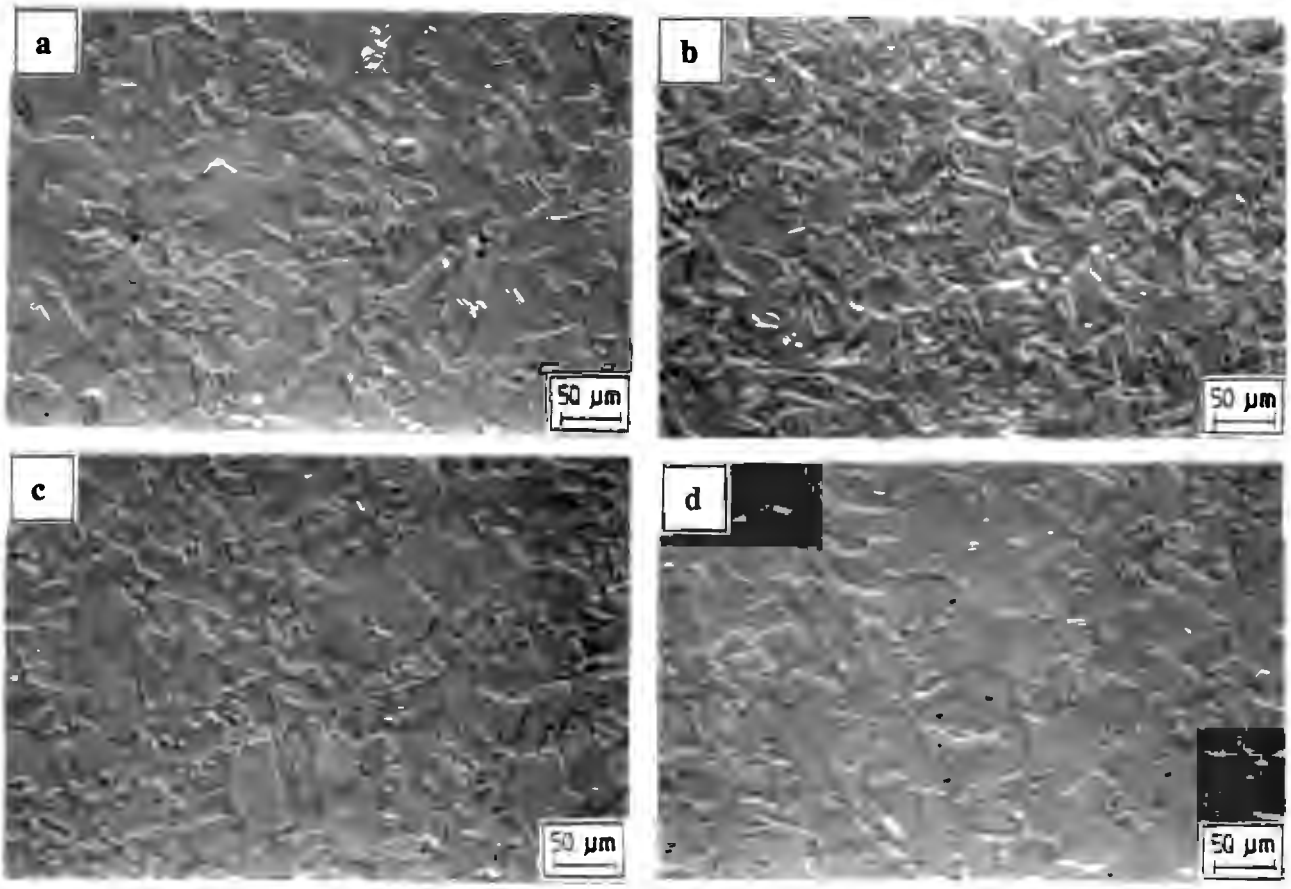

Figure 4.2 Microstructures of set 47, solution-treated at 1050°C for 30 minutes followed by oil quench. Electro-polished and electro-etched. Surface relief enhanced by Nomarski interference contrast.
[A = Austenite; M = Martensite]
(a) Alloy 4711 (A = 94%; M = 6%) (b) Alloy 4714 (A = 95%; M = 5%)
(c) Alloy 4716 (A = 96%; M = 4%) (d) Alloy 4718 (A = 97%; M = 3%)

The formation of martensite during electro-polishing is pronounced in the alloys of set 34 as can be seen in figure 4.3. Martensite, which is thought to have formed in the electro-polishing process, can be seen to encroach on a neighbouring austenite region (figure 4.3(b)). (It is generally not possible to distinguish between martensite formed during quenching and martensite formed during electro-polishing). The microstructures of the experimental alloys in the solution-treated and quenched condition reveal no traces of δ-ferrite and show that the microstructures consist only of a martensite-austenite mixture. The colour etchants and electro-chemical etch, enabling the detection of very small traces of δ-ferrite, also failed to reveal δ-ferrite, and it can be inferred that the experimental alloys are thus fully austenitic at the solution heat treatment temperature. The calculated chromium equivalents (Cr′), nickel equivalents (Ni′) as well as the calculated and measured M_S temperatures (M_S(calc) and M_S(meas) respectively) are given in table 4.1. The increase in retained austenite content with increasing nitrogen content is shown in figure 4.4.

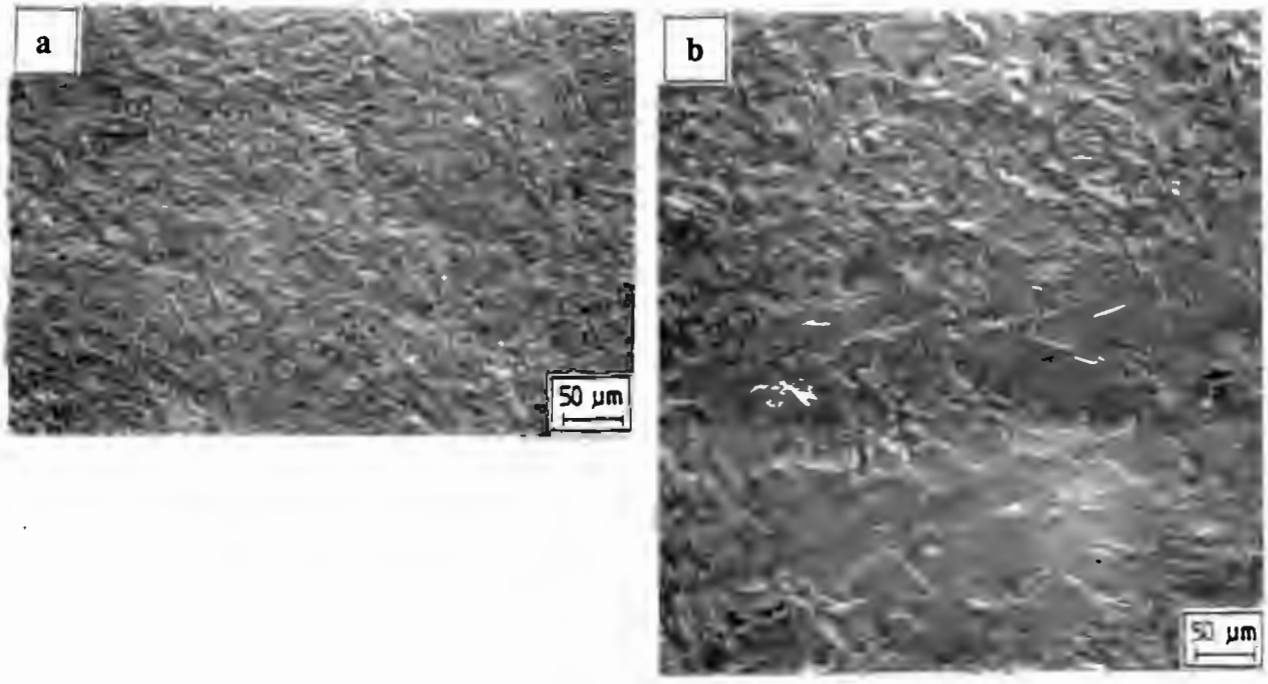

Figure 4.3 Microstructures of set 34, solution-treated at 1050°C for 30 minutes followed by oil quench. Electro-polished and electro-etched. Surface relief enhanced by Nomarski interference contrast.
[A = Austenite; M = Martensite]
(a) **Alloy 3419** (A = 45%; M = 55%)
(b) **Alloy 3428** (A = 63%; M = 37%) Martensite, which is thought to have formed during electro-polishing, encroaching on a neighbouring austenite region.

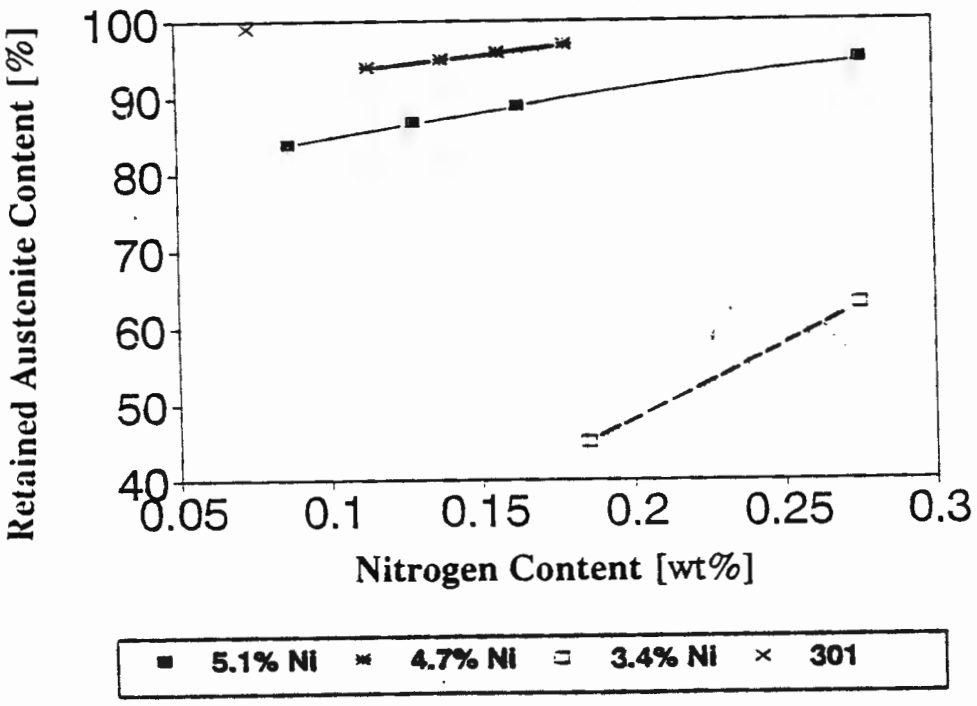

Figure 4.4 Variation of retained austenite content with nitrogen content.

HEAT NO.	ALLOY	Cr' wt%	Ni' wt%	M_S(calc) °C	M_S(meas) °C	AUSTENITE %
901891	5109	18.95	10.67	-81	+31	84
901911	5113	19.31	11.77	-167	<RT	87
902121	5216	19.32	12.32	-220	<RT	89
902131	5028	19.18	14.84	-388	<RT	95
901971	4711	20.00	11.29	-160	<RT	94
901981	4714	20.04	11.75	-197	<RT	95
901991	4716	20.10	12.47	-246	<RT	96
902001	4718	20.27	12.52	-261	<RT	97
902101	3419	19.25	11.16	-153	<RT	45
902111	3428	19.23	13.12	-287	<RT	63
AISI 301		18.91	11.02	-125	<RT	99

Table 4.1 Variation of retained austenite content with nickel and chromium equivalents and M_S temperature.

The dilatometer set-up did not facilitate rapid cooling and the measured M_S temperatures in table 4.1 apparently contradict the measured martensite content (i.e. martensite having formed in spite of the M_S being below room temperature). It is possible that in relatively unstable alloys such as alloys 3419 and 3428, martensite is formed not only by electro-polishing, but also by the action of thermal stresses during quenching.

4.1.2 Transmission Electron Microscopy (TEM)

Since nickel lowers nitrogen solubility, the alloy containing the highest nickel and nitrogen content (alloy 5028) is the most likely to contain nitrides. Figure 4.5(a) and (b) show partial dislocations in alloy 5028, separated by stacking faults, which is indicative of a low stacking fault energy. Nitride formation was not evident from the bright field, nor the dark field image (figure 4.5(a) and (b) respectively). Also the diffraction pattern in figure 4.5(c) did not reveal any diffraction spots corresponding to nitrides. Evidence of nitride precipitation in alloy 4718 (which is the alloy of set 47 with the highest nitrogen content) was also found to be absent. Figure 4.6(a) and (b) show the characteristic stacking faults in alloy 4718, separating partial dislocations, while figure(b) also shows the presence of some martensite. Nitrides are even less likely to occur in alloy 3428 (which is the alloy of set 34 with the highest nitrogen content) than in alloy 5028, since the former contains less nickel. In figure 4.7(a), two co-planar arrays of partial dislocations separated by stacking faults can be clearly seen, while figure 4.7(b) shows an array of dislocation dipoles. There are no nitrides evident in these figures and the diffraction pattern in figure 4.7(c) does not reveal any nitride spots.

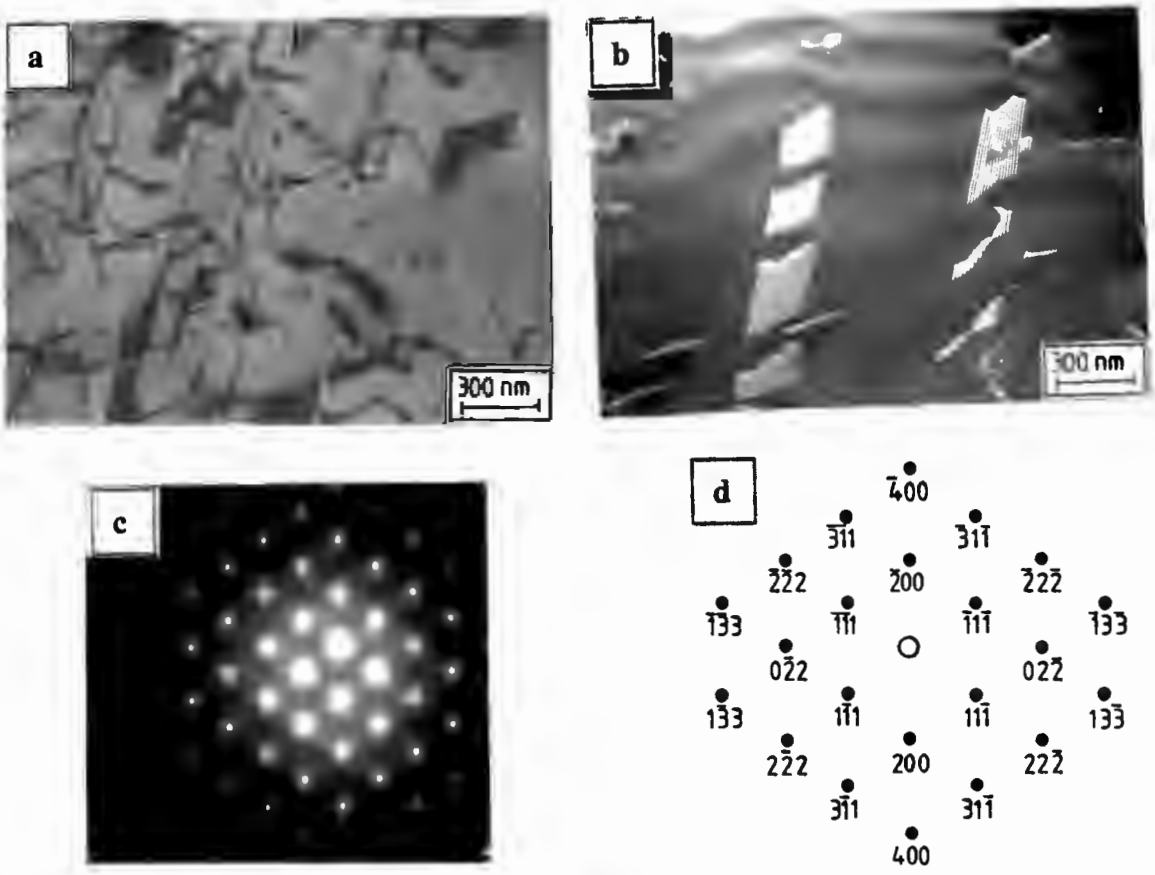

Figure 4.5 **Alloy 5028** (a) Bright field image showing partial dislocations separated by stacking faults.
(b) Dark field image showing co-planar arrays of partial dislocations separated by stacking faults.
(c) Diffraction pattern along [011] zone axis. Note the absence of diffraction spots corresponding to nitride precipitates.
(d) Diffraction index map of (c).

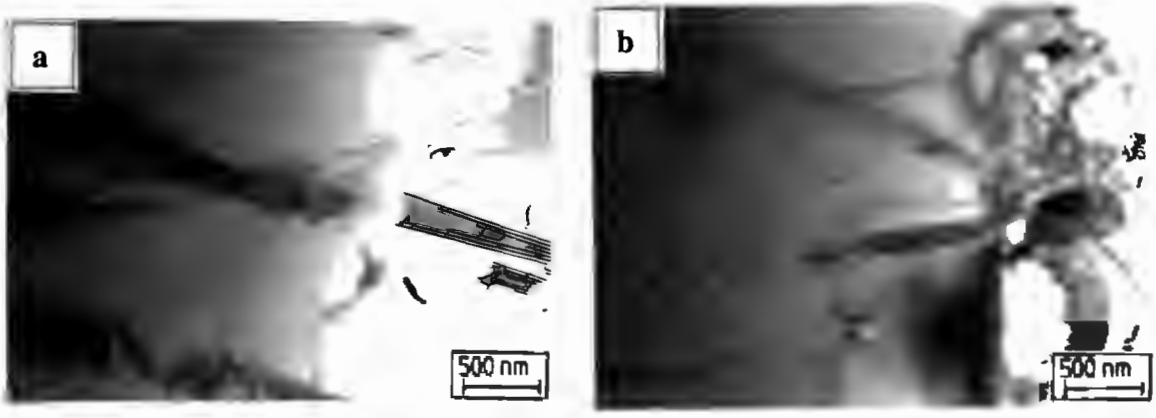

Figure 4.6 **Alloy 4718** (a) Bright field image showing partial dislocations separated by stacking faults. No nitrides are evident.
(b) Bright field image showing martensitic region adjacent to austenitic region.

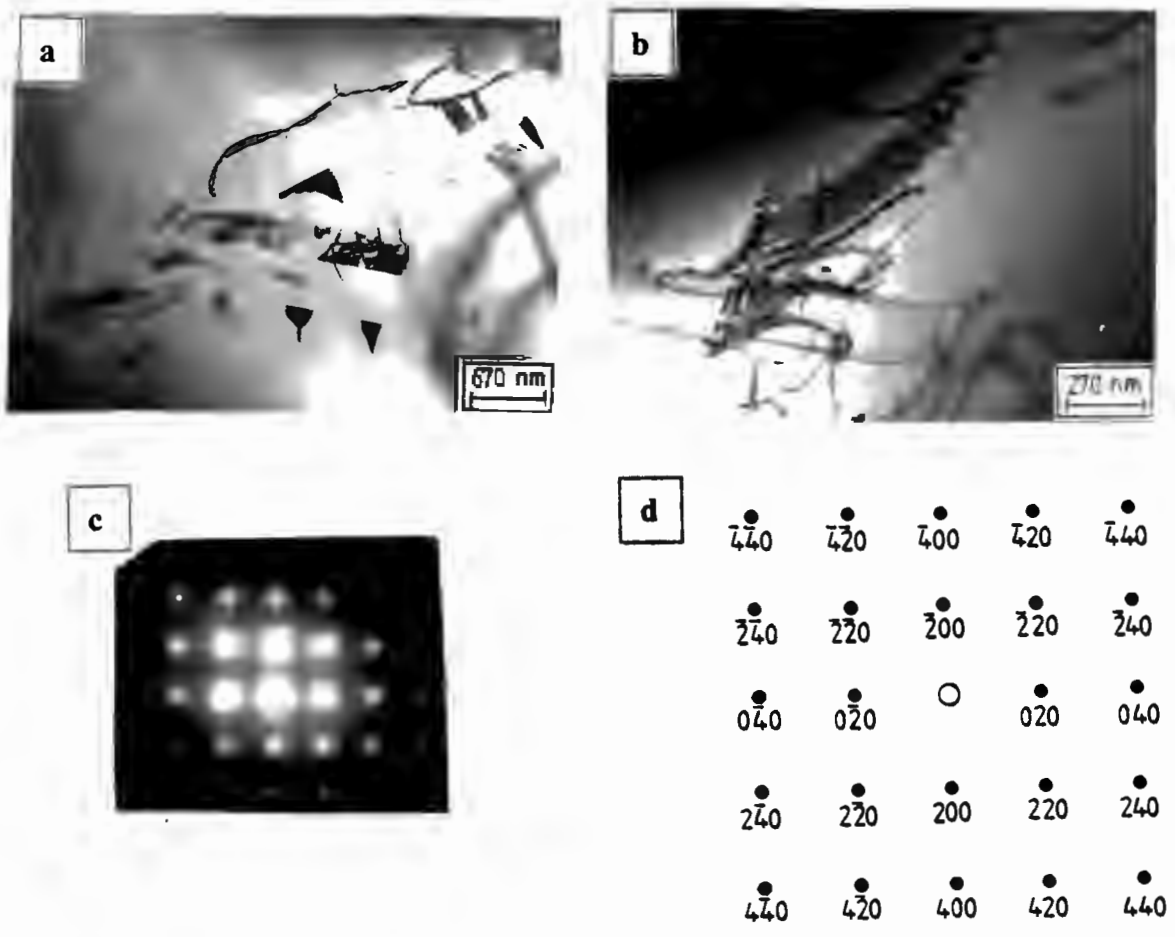

Figure 4.7 **Alloy 3428** (a) Two co-planar arrays of partial dislocations separated by stacking faults.
(b) Bright field image of an array of dislocation dipoles.
(c) Diffraction pattern along [001] zone axis. No nitride diffraction spots are present.
(d) Diffraction index map of (c).

From the above figures, it can be concluded, that the nitrogen solubility has not been exceeded in any of the experimental alloys at 1050°C. Thus it can be assumed that for all practical purposes, nitrogen is confined to solid solution.

4.2 TENSILE DEFORMATION BEHAVIOUR

The shape of the true stress - true strain curve of a metastable austenitic steel is an indication of the amount of martensite formed during deformation. A parabolic shape (with concave-down curvature) indicates that little or no martensite formed, whereas a sigmoidal shape (or S-shape) indicates the formation of an appreciable amount of deformation-induced martensite. The true stress - true strain curves in figure 4.8 are sigmoidal at 20°C for sets 51 and 47, as well as type 301. The curves become increasingly parabolic in shape as the temperature increases.

This trend is attributed to the increased suppression of martensite formation due to increased austenite stability as the temperature is raised[25]. The shapes of the curves observed for set 34 tend to be parabolic rather than sigmoidal at all three temperatures. Pronounced serrated flow occurred at 60°C in the experimental alloys, with serration amplitude decreasing as nitrogen increases. At 20 and 120°C such flow was not observed in any of the alloys. Type 301 in contrast did not exhibit the same pronounced serrated flow at 60°C, but the presence of very fine serrations occurred instead. It thus appears that the pronounced serrated flow observed in some of the experimental alloys is influenced by nitrogen content and temperature.

4.2.1 True Stress - True Strain Curves

The true stress - true strain curves of the lowest and highest nitrogen alloys in each set, including type 301 are shown in figures 4.8 (a) - (d).

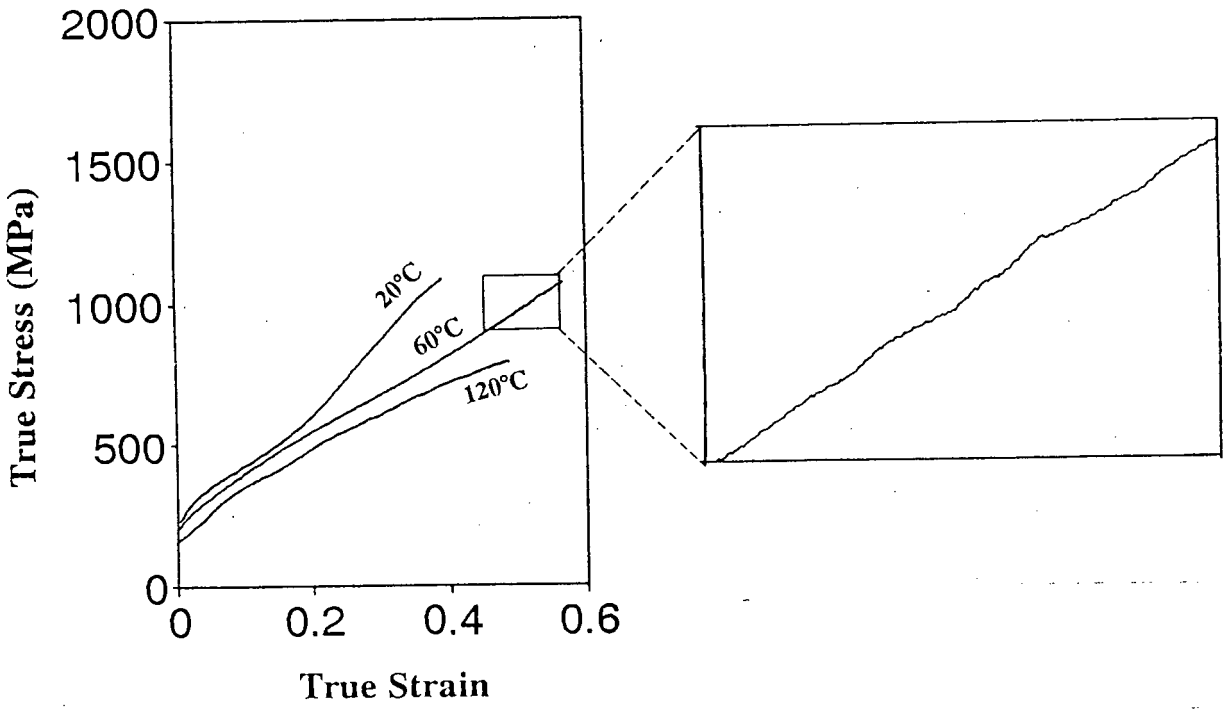

Figure 4.8(a) True stress-true strain curves of type 301 at 20, 60 and 120°C. Pronounced serrations as they occur in some of the experimental alloys are not present in this alloy. Instead very fine serrations are visible.

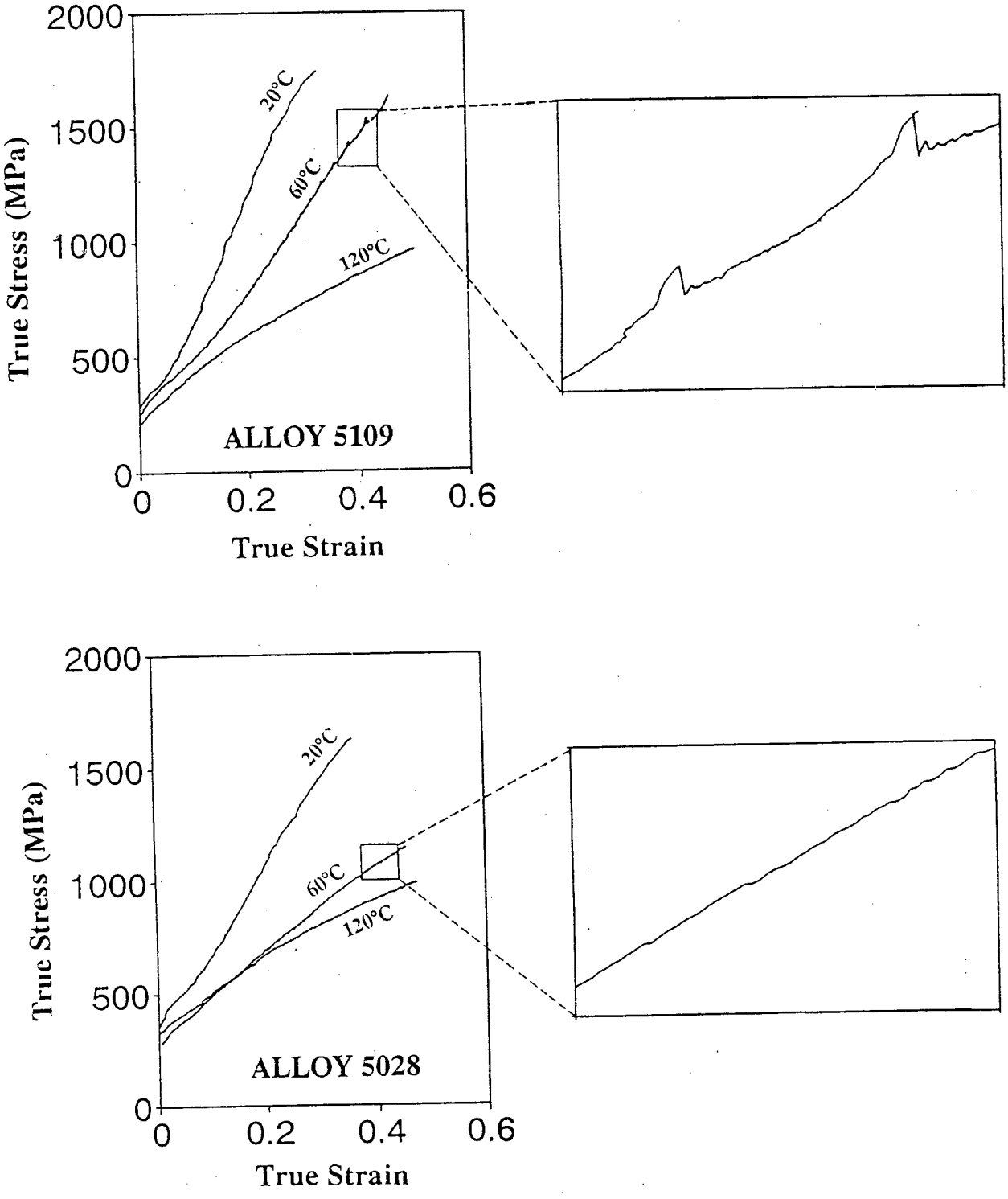

Figure 4.8(b) True stress-true strain curves of set 51 alloys at 20, 60 and 120°C, showing pronounced serrations at 60°C for alloy 5109, which are not observed in alloy 5028.

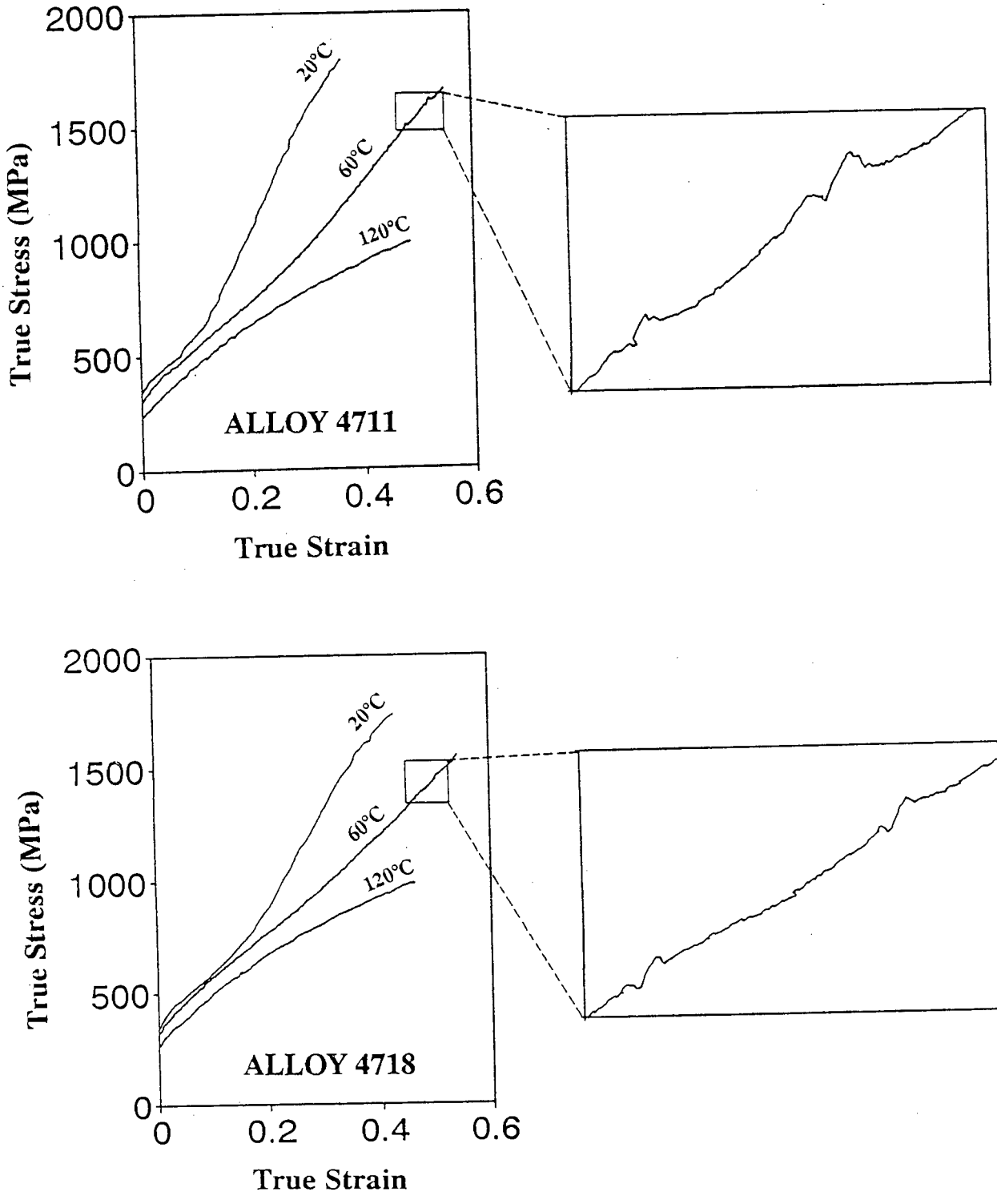

Figure 4.8(c) True stress-true strain curves of set 47 alloys at 20, 60 and 120°C. Pronounced serrations at 60°C occur in both alloys, but are smaller in alloy 4718.

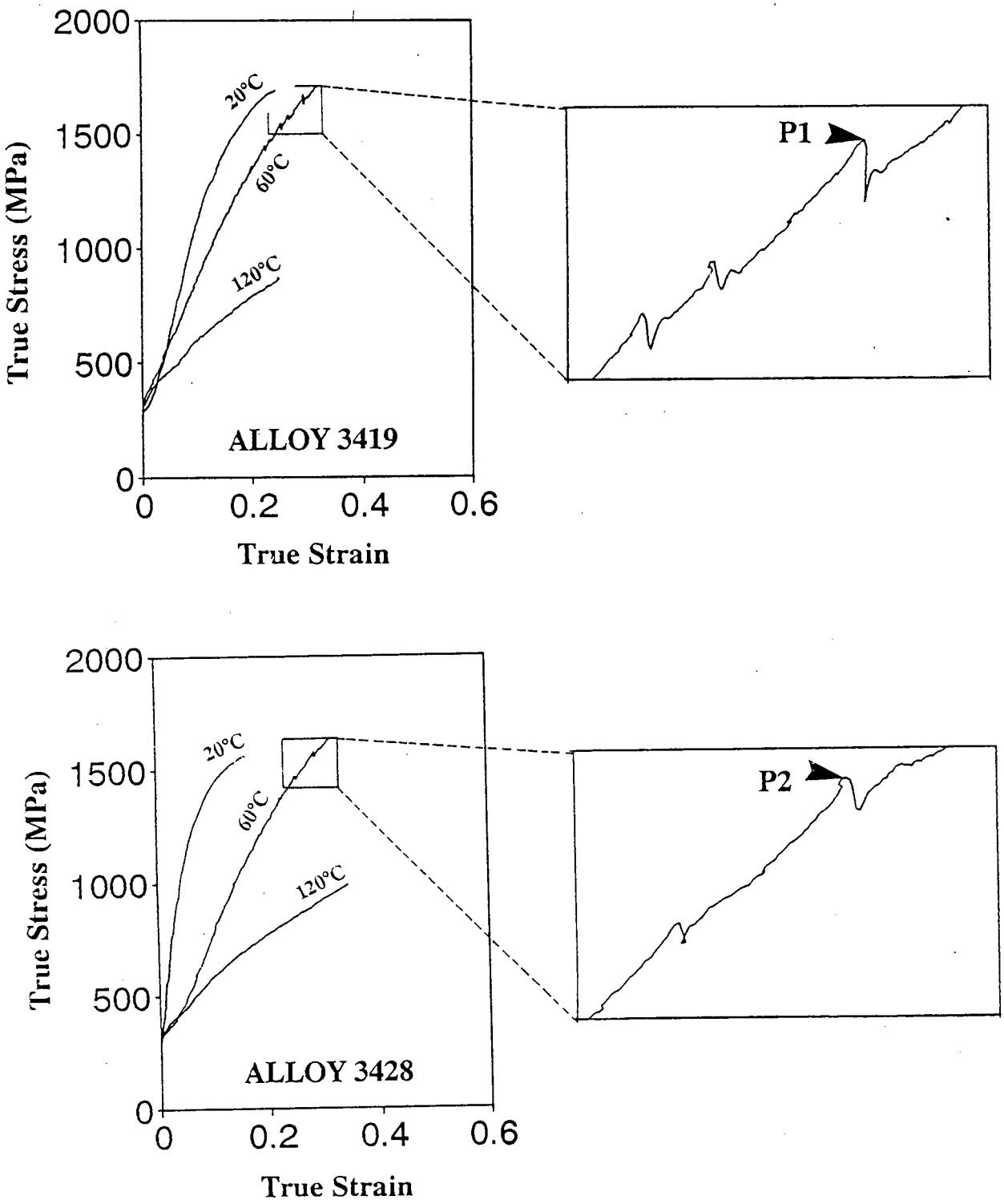

Figure 4.8(d) True stress-true strain curves of set 34 alloys at 20, 60 and 120°C. Pronounced serrations occur in both alloys at 60°C, and increasing the nitrogen content decreases the serration amplitude (as in alloy 3428), but not as effectively as in set 51.

4.2.2 Work-Hardening Rate (WHR) Behaviour

The work-hardening rate of metastable alloys is closely related to the formation of martensite during deformation[68], and it has been established that the onset of positive work-hardening

occurs as a consequence of martensite formation[26]. The work-hardening rate does not only indicate the formation of martensite, but also the rate and strain interval at which it occurs. Figures 4.9 - 4.12 show the changes which occur in the work-hardening rate and true stress at various temperatures for the type 301 alloy and the experimental alloys.

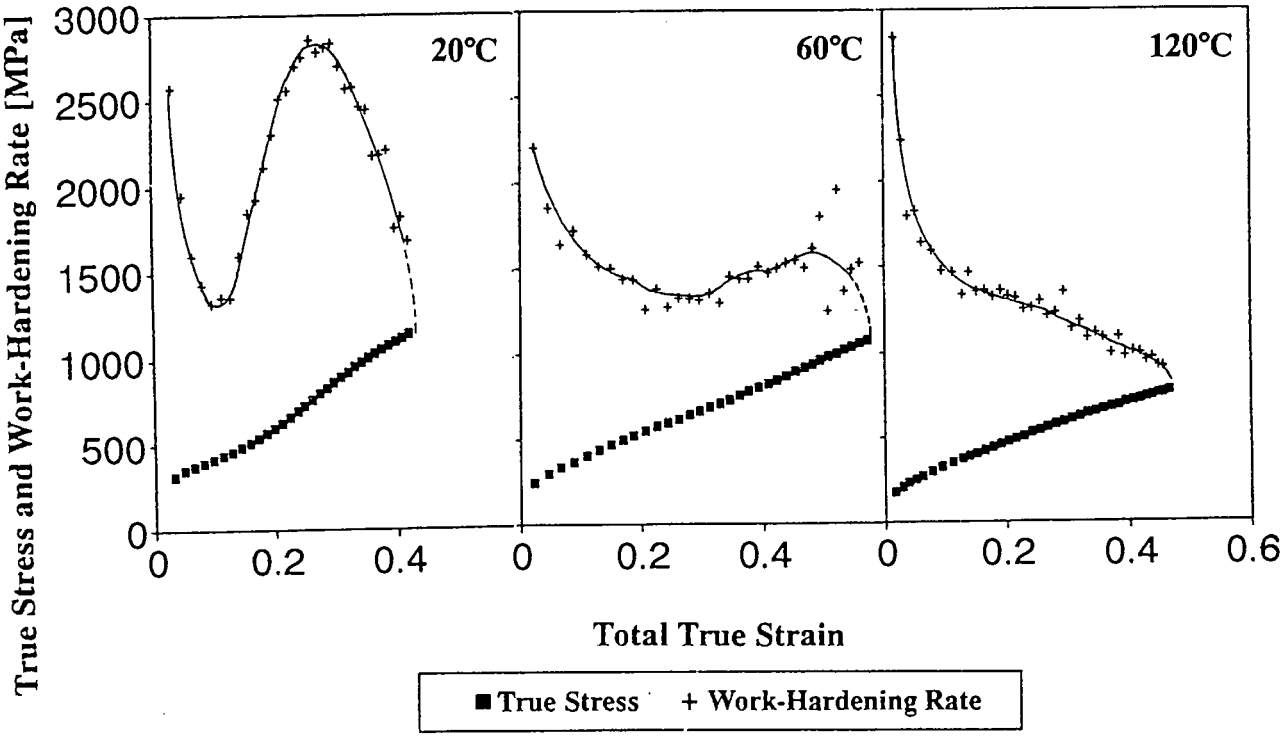

Figure 4.9 Work-hardening rate and true stress as a function of true strain : Type 301 deformed at 20, 60 and 120°C.

Figure 4.10 shows that the work-hardening rates of set 51 increase rapidly towards the maximum when deformed at 20°C, whereas at 60°C the rate of increase is lower and the WHR maxima are reached at higher strain values. In addition, the magnitudes of the maxima at 20°C are greater than those at 60°C. These observations indicate that martensite formation occurs at a more controlled and slower rate at 60°C, resulting in higher uniform elongations. At 120°C the work-hardening rates decrease continuously as a function of strain, and it can be concluded from this that little or no martensite is formed at this temperature. Similar trends are observed for set 47 (figure 4.11), but the difference in maximum uniform strain recorded at 60 and 120°C for this set is more pronounced than for set 51 (the maximum uniform strains at 60°C being consistently higher than at 120°C).

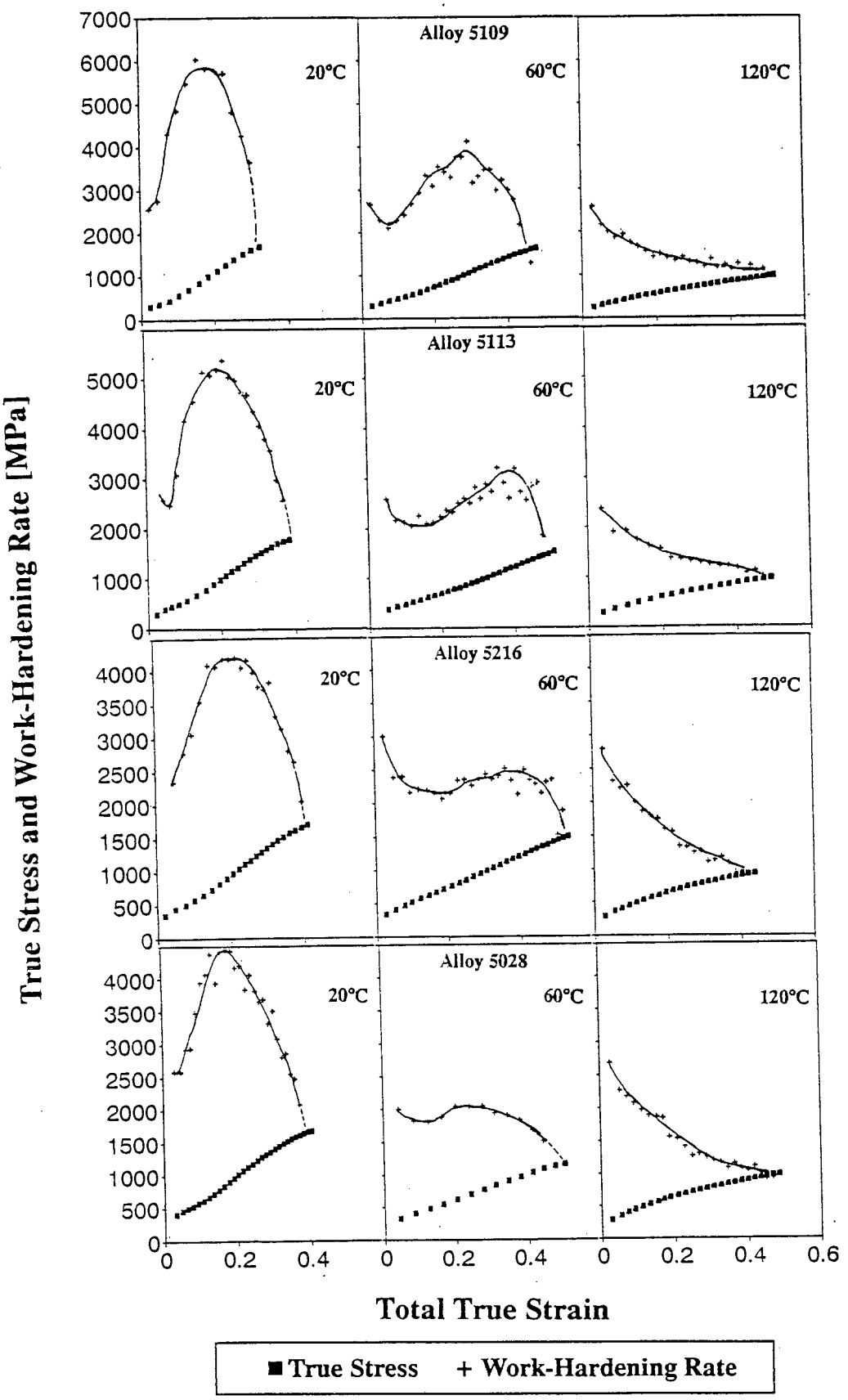

Figure 4.10 Work-hardening rate and true stress as a function of true strain : Set 51 deformed at 20, 60 and 120°C.

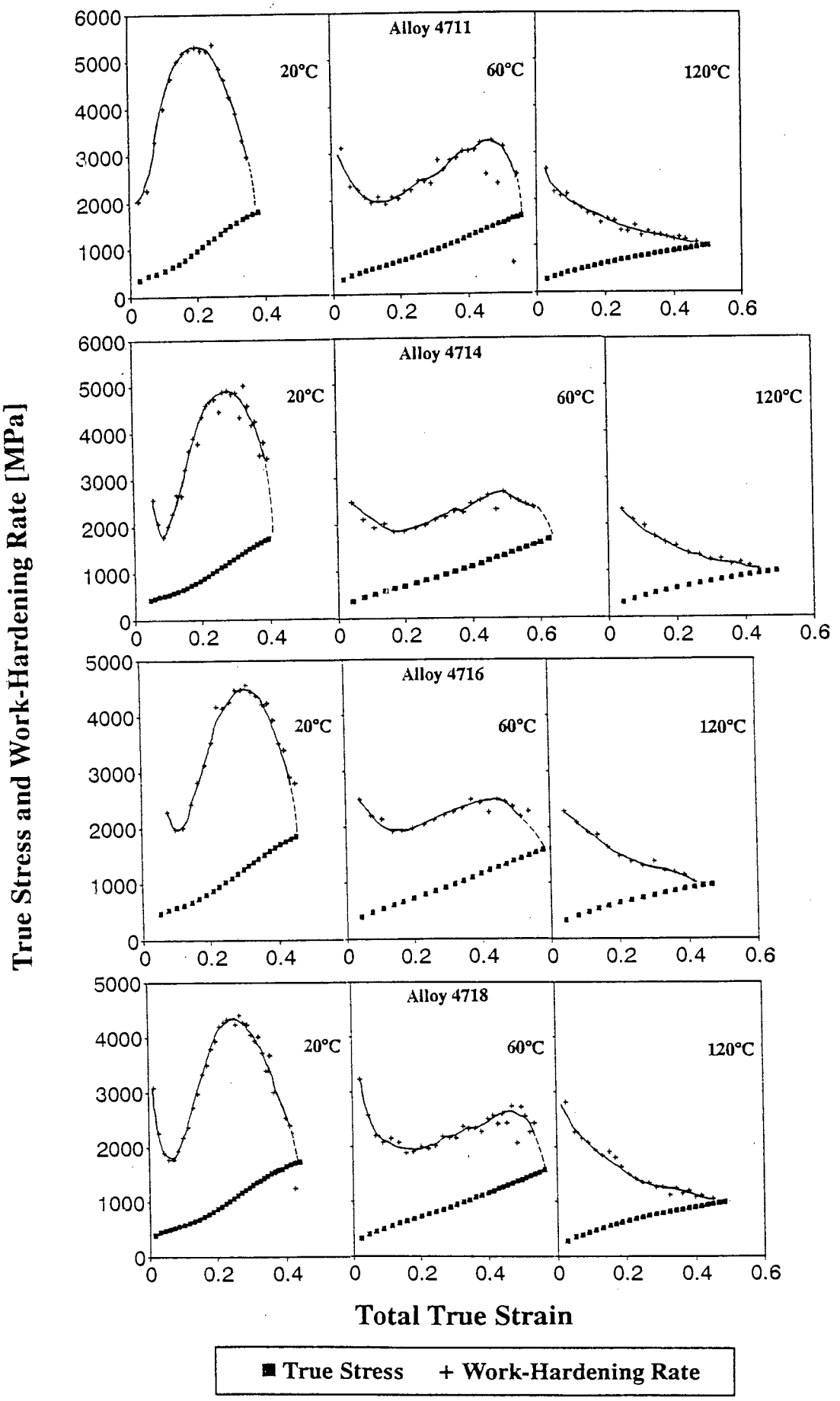

Figure 4.11 Work-hardening rate and true stress as a function of true strain : Set 47 deformed at 20, 60 and 120°C.

The work-hardening rates of set 34 increase very rapidly at very low strains at 20 and 60°C. At

120°C, the work-hardening rate decreases continuously as for sets 51 and 47 (figure 4.12). The rapid increase in work-hardening rate at very low strains is due to both the presence of a substantial volume fraction of pre-existing martensite (which means that relatively little retained austenite is available for transformation) and to the low stability of the retained austenite phase, resulting in rapid transformation, so that the WHR maxima are reached at much lower strains than in sets 51 and 47.

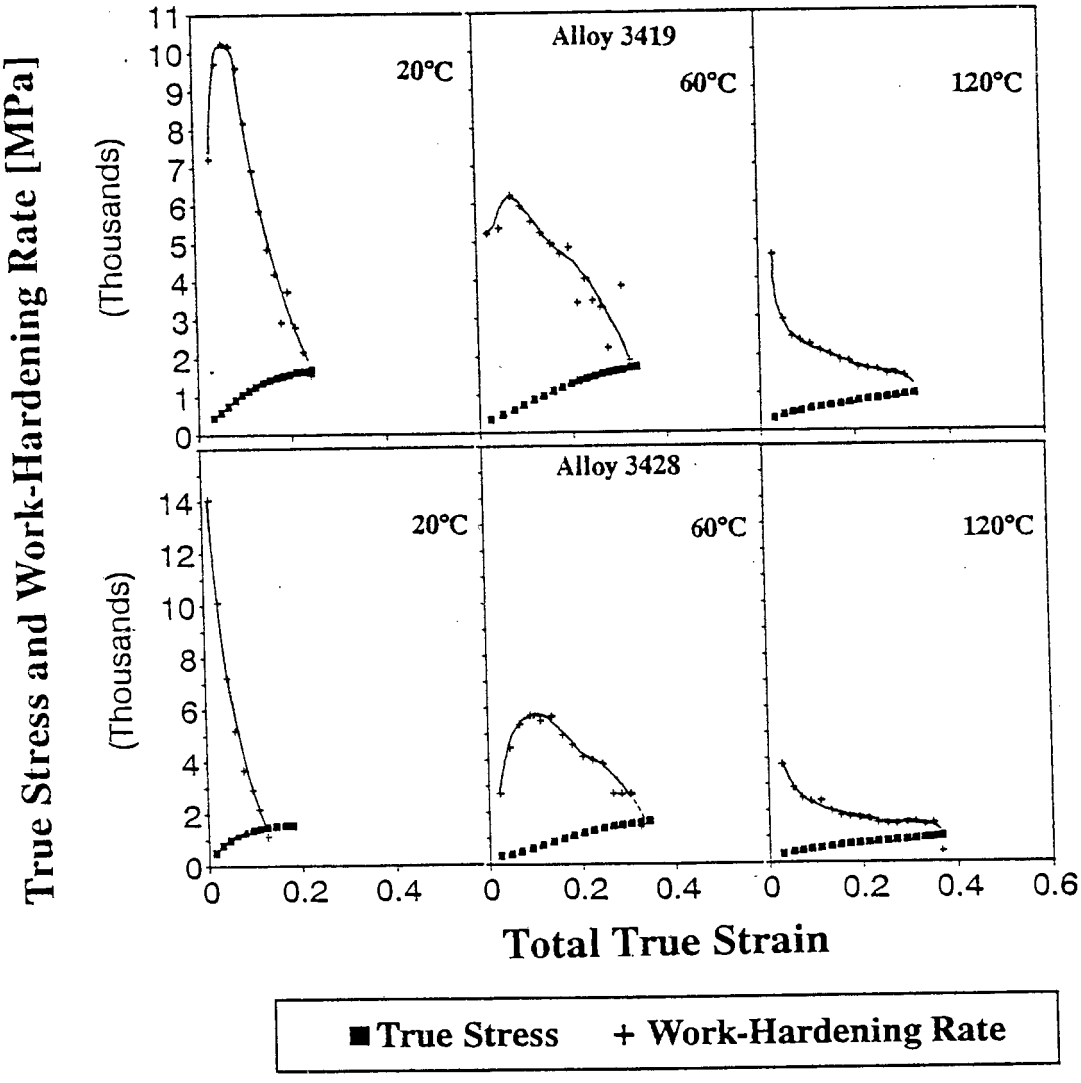

Figure 4.12 Work-hardening rate and true stress as a function of true strain : Set 34 deformed at 20, 60 and 120°C.

4.2.3 Tensile Fractography

Figures 4.13 and 4.14 show that the fracture surfaces of set 51 and 47 produced during tensile testing at 20°C, are predominantly ductile, and have the characteristic dimpled appearance.

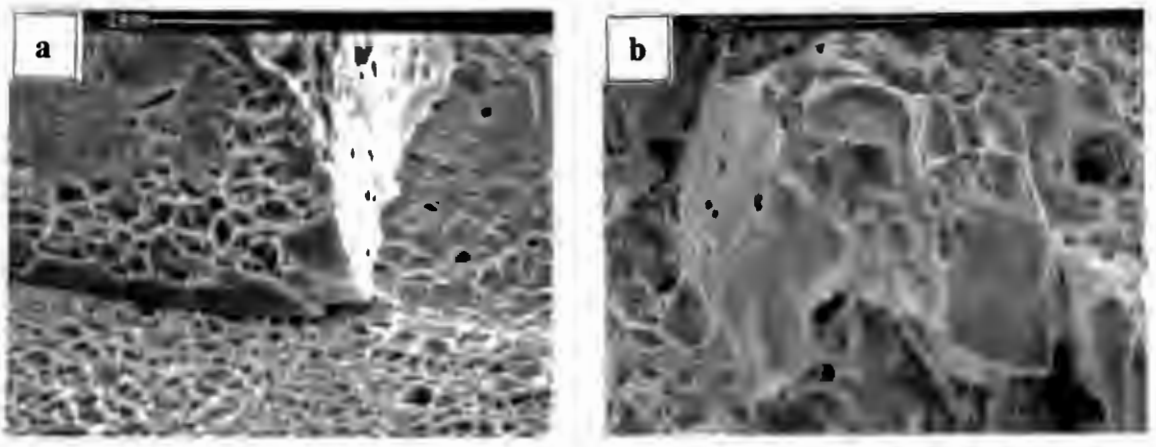

Figure 4.13 Ductile fracture surfaces of tensile test at 20°C of:

(a) **Alloy 5109** (Pre-existing martensite = 16%; Martensite induced up to 0.3 true strain = 80%).
(b) **Alloy 5028** (Pre-existing martensite = 5%; Martensite induced up to 0.3 true strain = 53%).

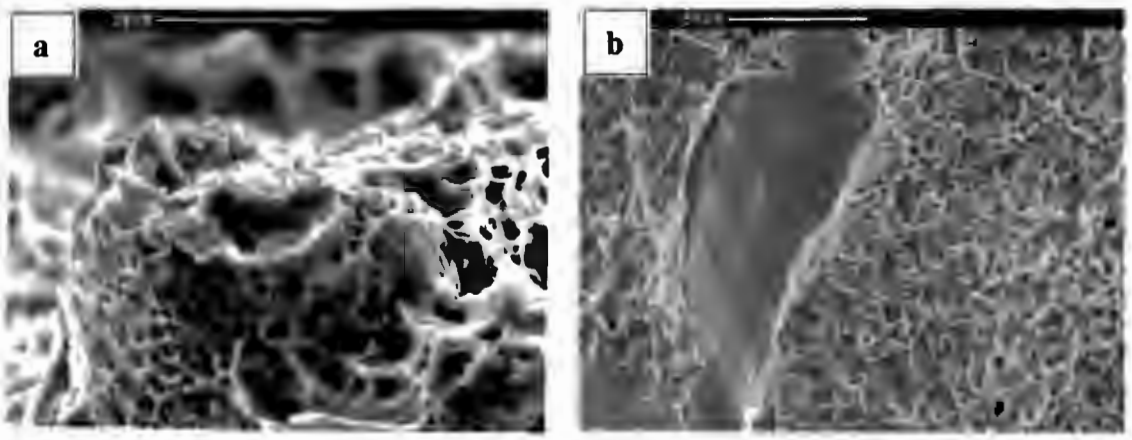

Figure 4.14 Ductile fracture surfaces of tensile test at 20°C of:

(a) **Alloy 4711** (Pre-existing martensite = 6%; Martensite induced up to 0.3 true strain = 69%).
(b) **Alloy 4718** (Pre-existing martensite = 3%; Martensite induced up to 0.3 true strain = 58%).

The two alloys of set 34, alloys 3419 and 3428, which contain 55 and 37% pre-existing martensite respectively, exhibit rift-like cracking in conjunction with ductile rupture (figure 4.15). In view of the high pre-existing martensite content of these alloys, the rift cracks are probably due to fracture in martensite.

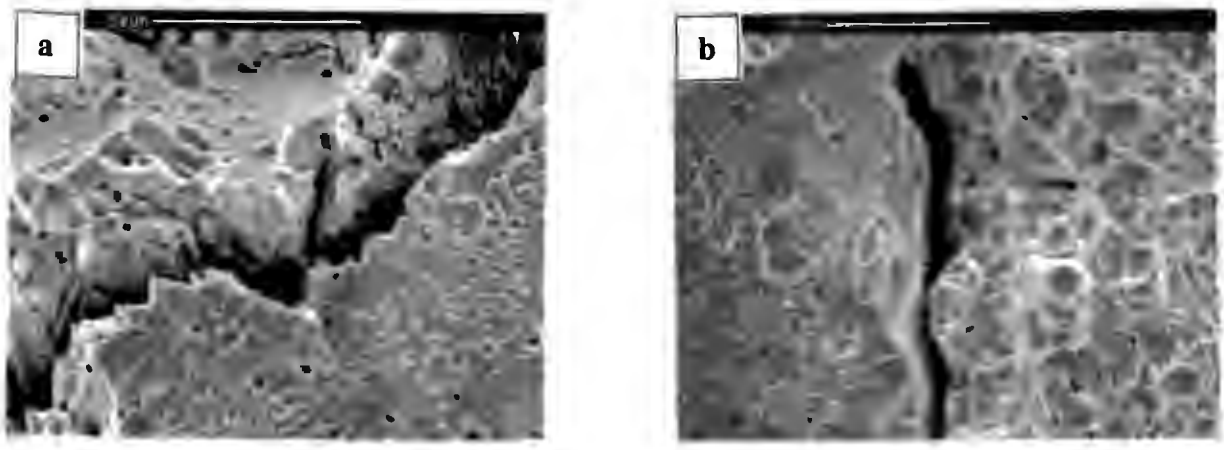

Figure 4.15 Fracture surface of tensile test at 20°C:

(a) **Alloy 3419.** Predominantly ductile fracture surface. Rift crack is probably associated with fracture in martensite. (Pre-existing martensite = 55%; Martensite induced up to 0.18 true strain = 37%)

(b) **Alloy 3428.** Predominantly ductile fracture surface. (Pre-existing martensite = 37%; Martensite induced up to 0.18 true strain = 51%)

4.2.4 Deformation-Induced Martensite Content

The amount of martensite induced from 0 to 0.3 strain in the type 301 alloy increases with decreasing temperature as shown in figure 4.16, and is in accordance with the trend observed by Rosen et. al.[27]. In contrast the amount of deformation-induced martensite of set 51 peaks around 20°C. The peak is absent in set 47, with alloys 4714 and 4716 behaving in a similar fashion to type 301. Alloy 4711 appears to reach the martensite saturation level around 20°C (although it is possible that below 0°C the amount of martensite induced up to a strain of 0.3 decreases).

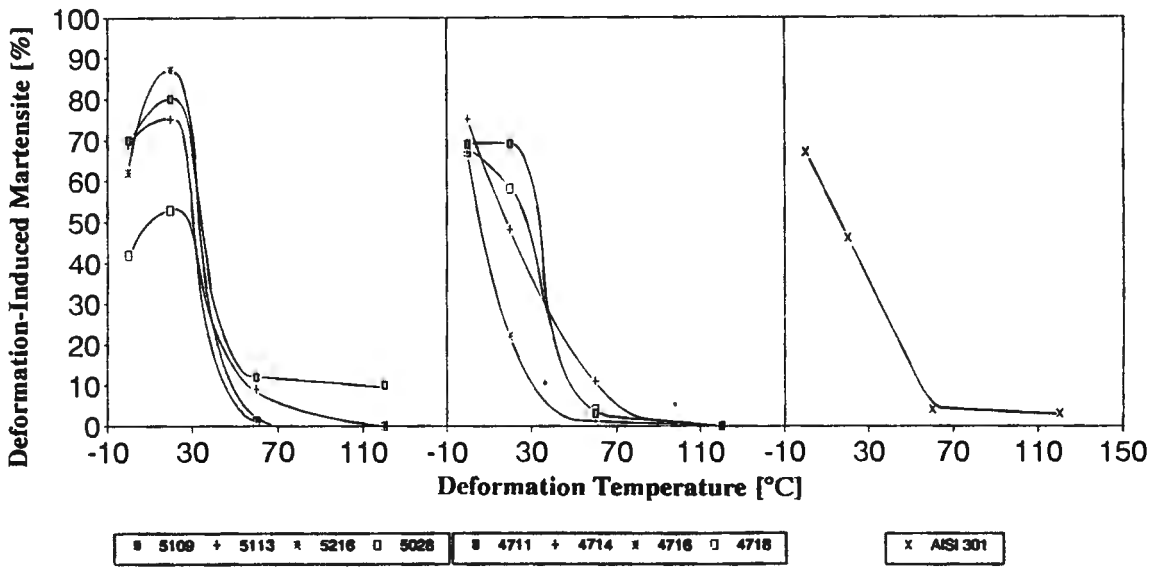

Figure 4.16 Deformation-induced martensite content of experimental alloys and type 301 at 0.3 true strain.

4.2.5 Microstructure of Alloys 4711, 4718 and Type 301 at 0.3 True Strain

The microstructures of alloys 4711 and 4718 at 0.3 strain were compared with the microstructure of type 301 at the same strain level. The micrographs below show the microstructures parallel to the tensile direction.

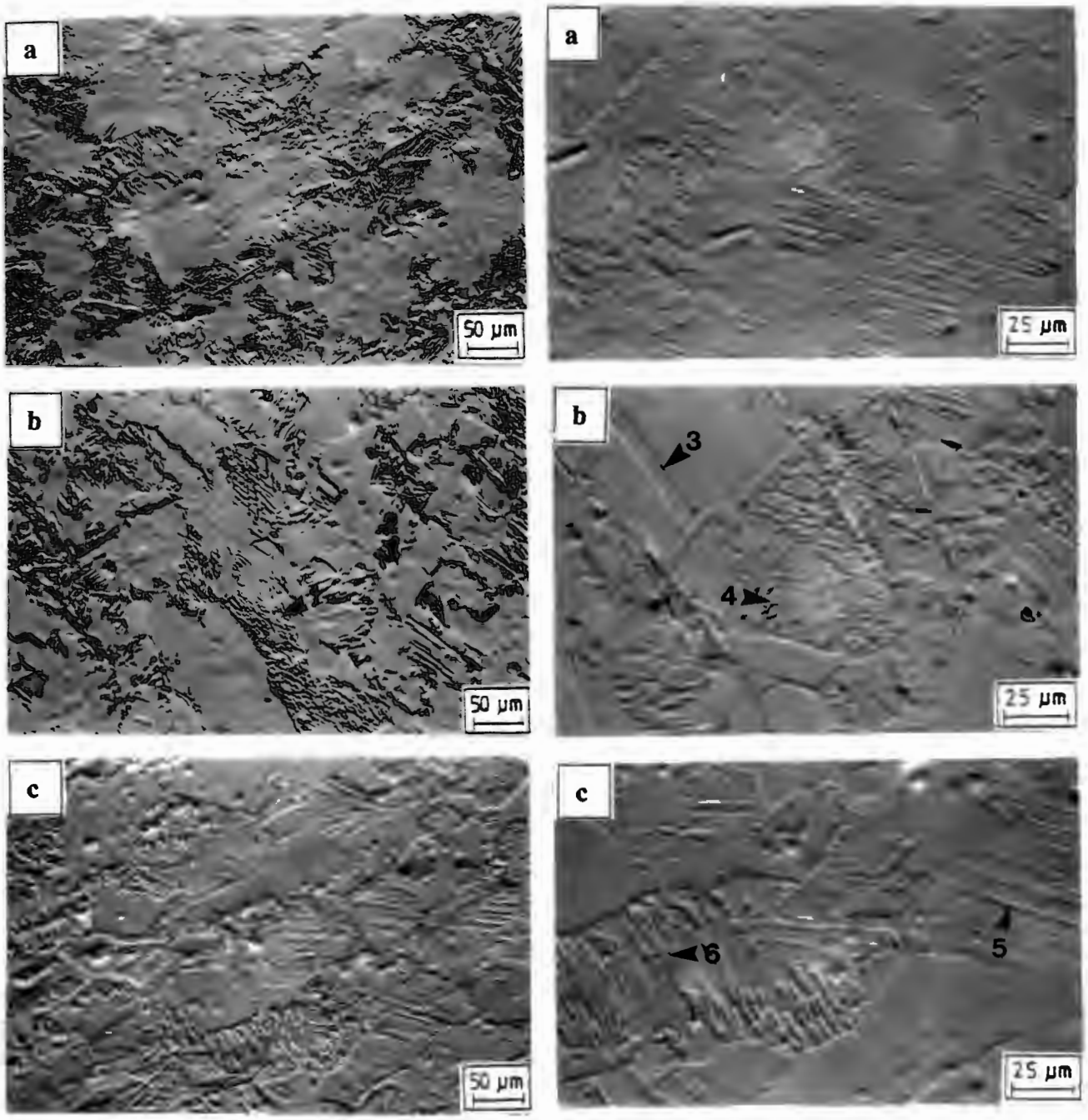

Figure 4.17 **Alloy 4711** deformed to 0.3 true strain at:

(a) 0°C [Total martensite = 72%]; (b) 60°C [Total martensite = 10%]; (c) 120°C [Total martensite = 6%]

Microstructural features : 1 : Lath martensite; 2 : Untransformed austenite grain; 3 : Austenite twin; 4 : Martensite laths forming on austenite slip lines; 5 : Austenite slip bands; 6 : Clusters of martensite within austenite grain.

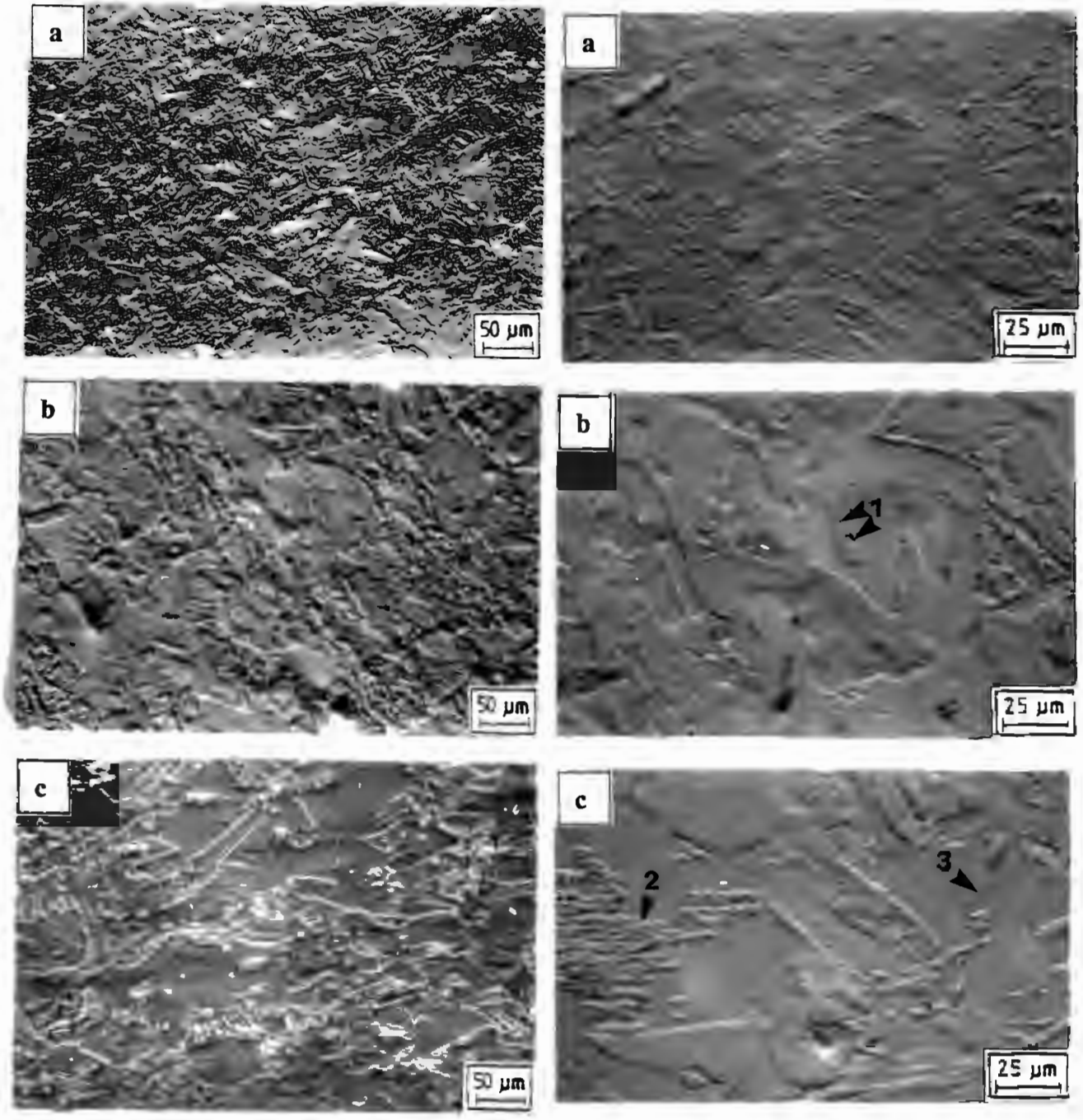

Figure 4.18 **Alloy 4718 deformed to 0.3 true strain at:**

(a) 0°C [Total martensite = 69%]; (b) 60°C [Total martensite = 7%]; (c) 120°C [Total martensite = 3%]

Microstructural features : 1 : Martensite laths occurring on slip lines within an austenite twin; 2 : Martensite cluster; 3 : Austenite slip lines.

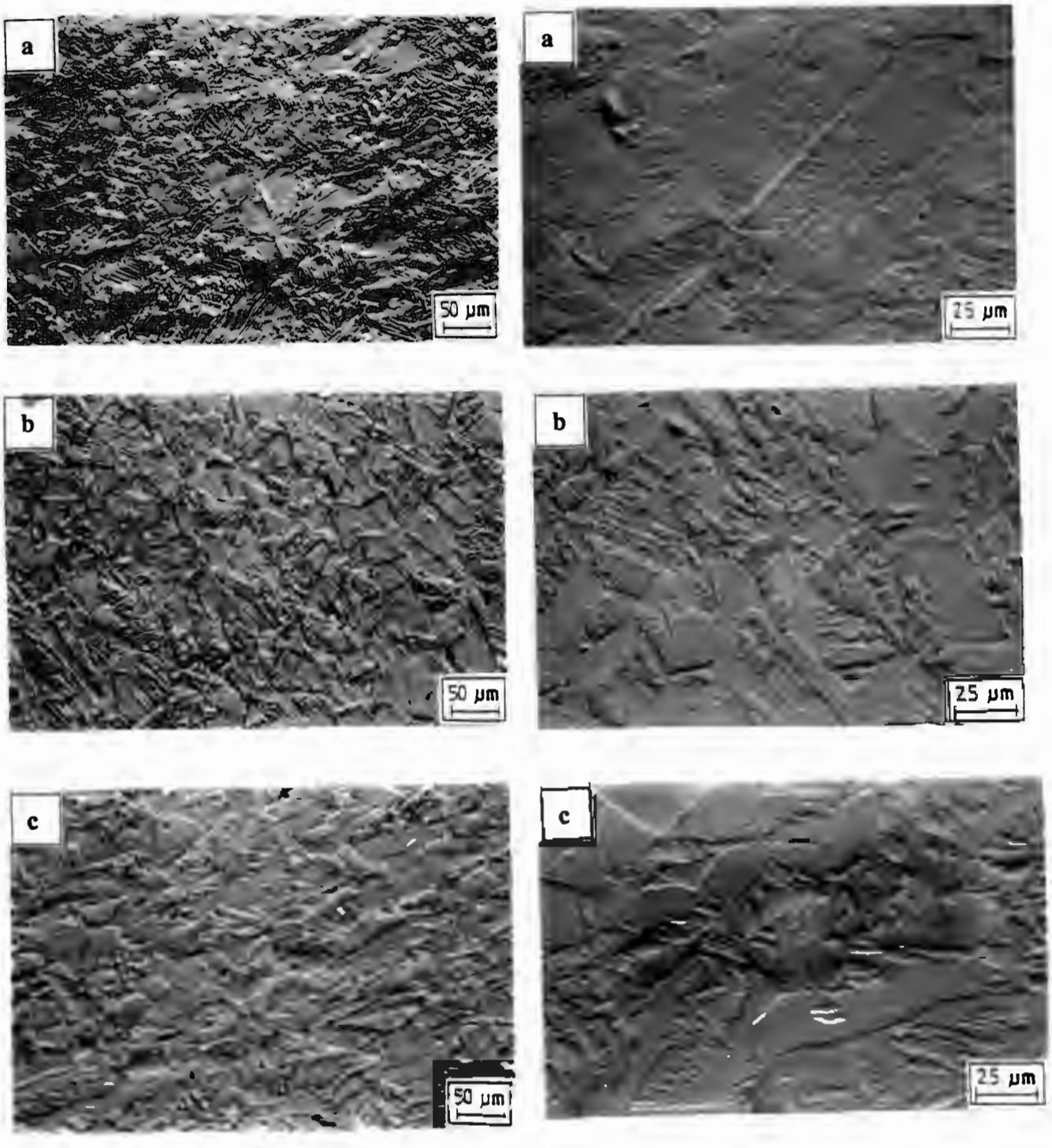

Figure 4.19 **Type 301 deformed to 0.3 true strain at:**

(a) 0°C [Total martensite = 67%]
(b) 60°C [Total martensite = 4%]
(c) 120°C [Total martensite = 4%]

4.2.6 Bulk Hardness

(a) Bulk Hardness Of Solution Treated Alloys

The experimental alloys have inherently higher bulk hardnesses than the type 301 alloy due to the interstitial strengthening ability of nitrogen. Generally with increasing nitrogen content, the hardness increases due to the solid solution hardening effect of the nitrogen. However, once the structure contains approximately 90% retained austenite, the increase in hardness with increasing nitrogen is small (e.g. for set 51 in figure 4.20). This is because the hardening effect of nitrogen in martensite is much more pronounced than in austenite, as shown by the increase in hardness by set 34 (which contains 40 - 55% pre-existing martensite).

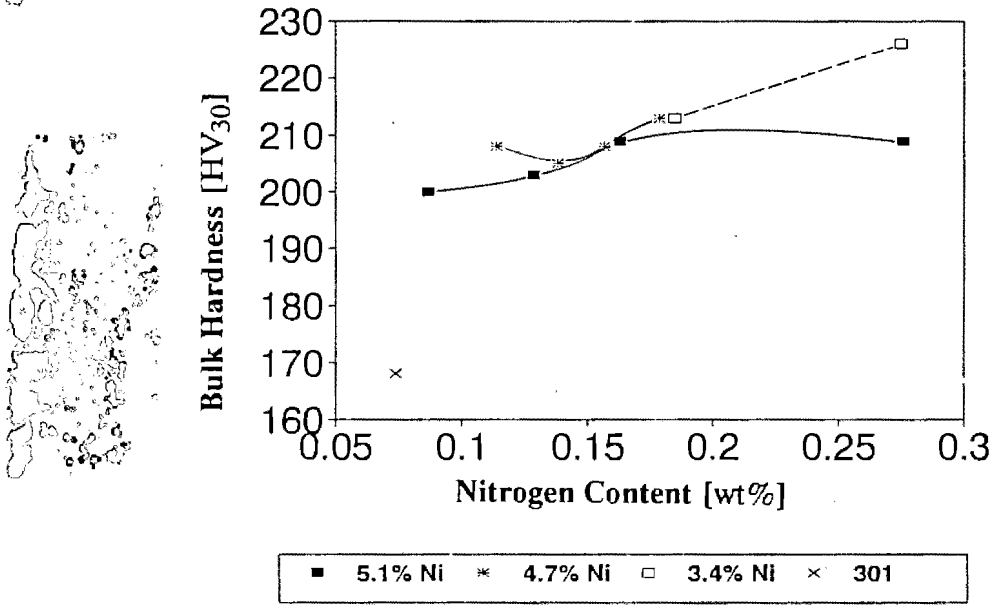

Figure 4.20 Bulk hardness of sets 51, 47 and 34 displaying the effects of decreasing martensite content and increasing solid solution hardening, with increasing nitrogen content.

(b) Bulk Hardness at 0.3 True Strain

The bulk hardnesses at a strain of 0.3 closely follow the same trend with temperature as the amount of deformation-induced martensite (compare figure 4.21 and 4.16). Thus the bulk hardness is a reliable single parameter by which to rank alloys with respect to their tendency to form martensite during deformation.

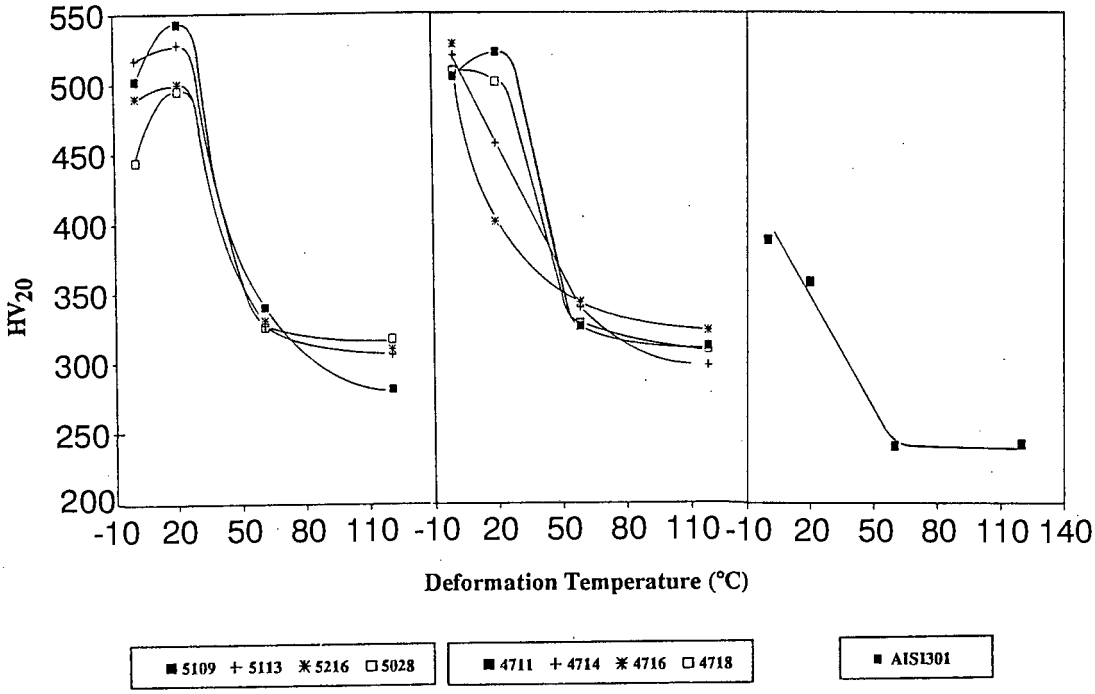

Figure 4.21 Bulk hardness of experimental alloys and type 301, at 0.3 true strain.

4.2.7 Plastic Deformation Energy (PDE)

The plastic deformation energy absorbed during deformation depends both on the increase in flow stress and the concomitant increase in uniform strain. In an austenitic structure which does not transform during straining, PDE is low since the increase in flow stress is moderate compared to that of a martensitic structure. Similarly PDE of a martensitic structure is low due to the much reduced uniform straining ability compared to that of a stable austenitic structure. In a TRIP alloy, the ability of the austenitic structure to work-harden due to its transformation to martensite, produces a high value for PDE compared to that of a martensitic or stable austenitic structure.

The area under the force-displacement curve is mathematically equal to the amount of energy required to deform the tensile specimen and has the units (N.mm). The area under the true stress-true strain curve has the dimensions ($N.mm^{-2}$) and this is equivalent to the deformation energy per unit volume ($N.mm/mm^3 = N.mm^{-2}$). PDE was evaluated by calculating the area under the true stress-true strain curve from the yield strain to (a) 0.3 true strain and (b) to e_u.

(a) PDE absorbed between yield strain and 0.3 strain (PDE_{30})

Figure 4.22 shows that the PDE_{30} of the type 301 alloy increases continuously with decreasing temperature, whereas it peaks around 20°C for sets 51 and 47. There is a similarity between the trend for PDE_{30}, and the trends for deformation-induced martensite at 0.3 strain (figure 4.16), and bulk hardness at 0.3 strain (figure 4.21). However, it will be shown in section 4.3.3 that there is an even closer resemblance between PDE_{30} and the tensile stress at 0.3 strain, σ_{30}

(figure 4.29).

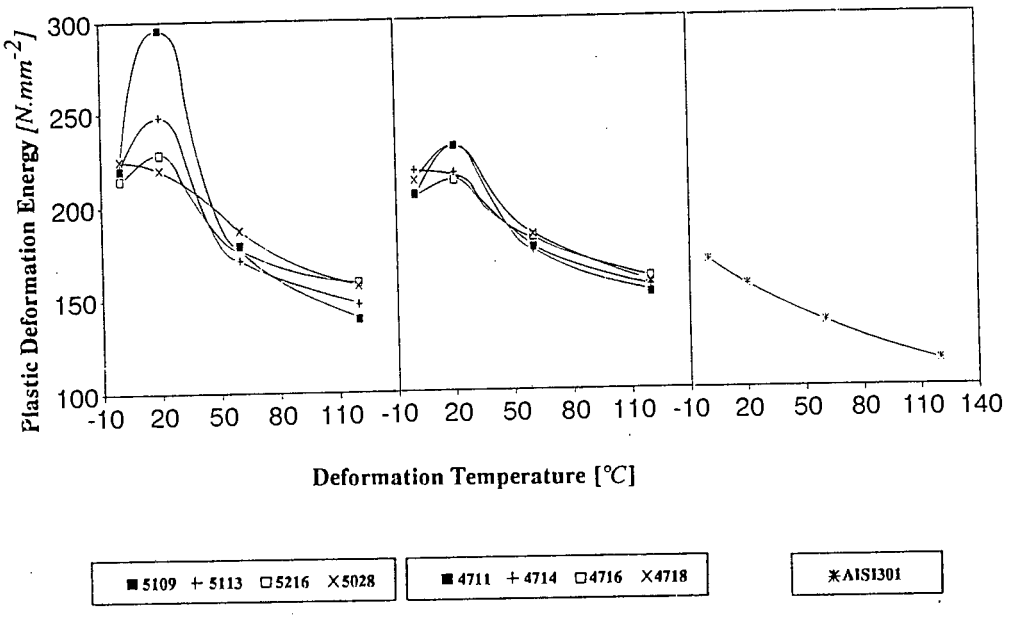

Figure 4.22 Plastic deformation energy of experimental alloys and the type 301 alloy absorbed between the yield strain and 0.3 true strain, as a function of deformation temperature.

(b) PDE absorbed between yield strain and e_u (PDE_u)

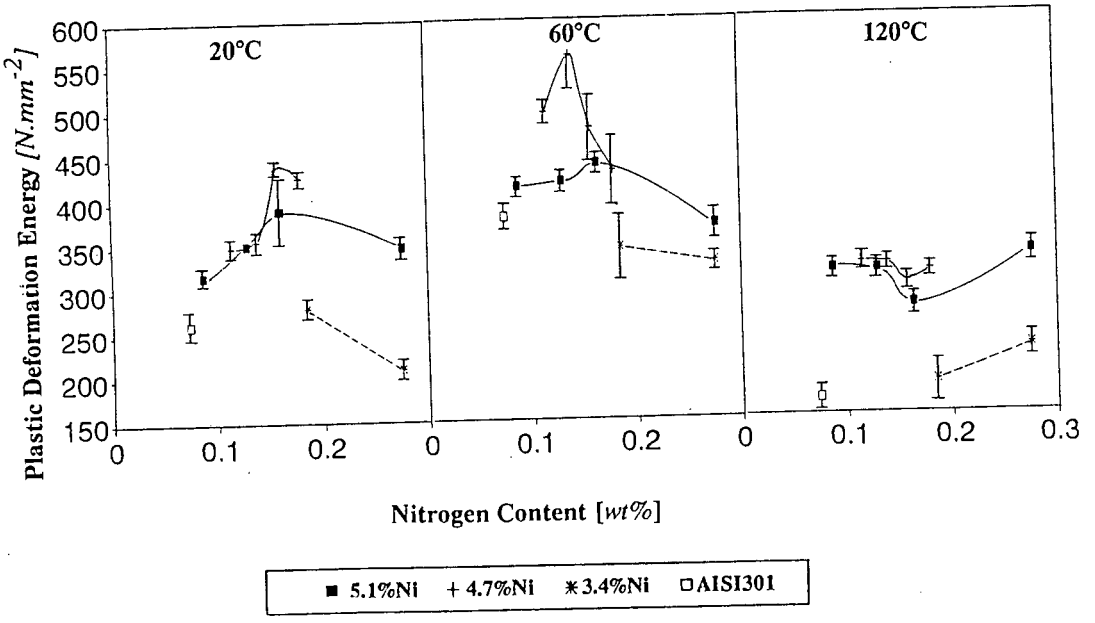

Figure 4.23 Plastic deformation energy of experimental alloys and the type 301 alloy absorbed between yield strain and e_u, as a function of nitrogen content.

The PDE_u values of the type 301 alloy are lower than the PDE_u values of sets 51 and 47 at 20, 60 and 120°C. Only set 34 has comparable PDE_u values to those of type 301. The values of set 47 are consistently greater than those of set 51 and this becomes especially noticeable at 60°C, where the maximum PDE_u value of set 47 (at 0.14% nitrogen) is significantly greater than the maximum PDE_u value of set 51 (at 0.16% nitrogen).

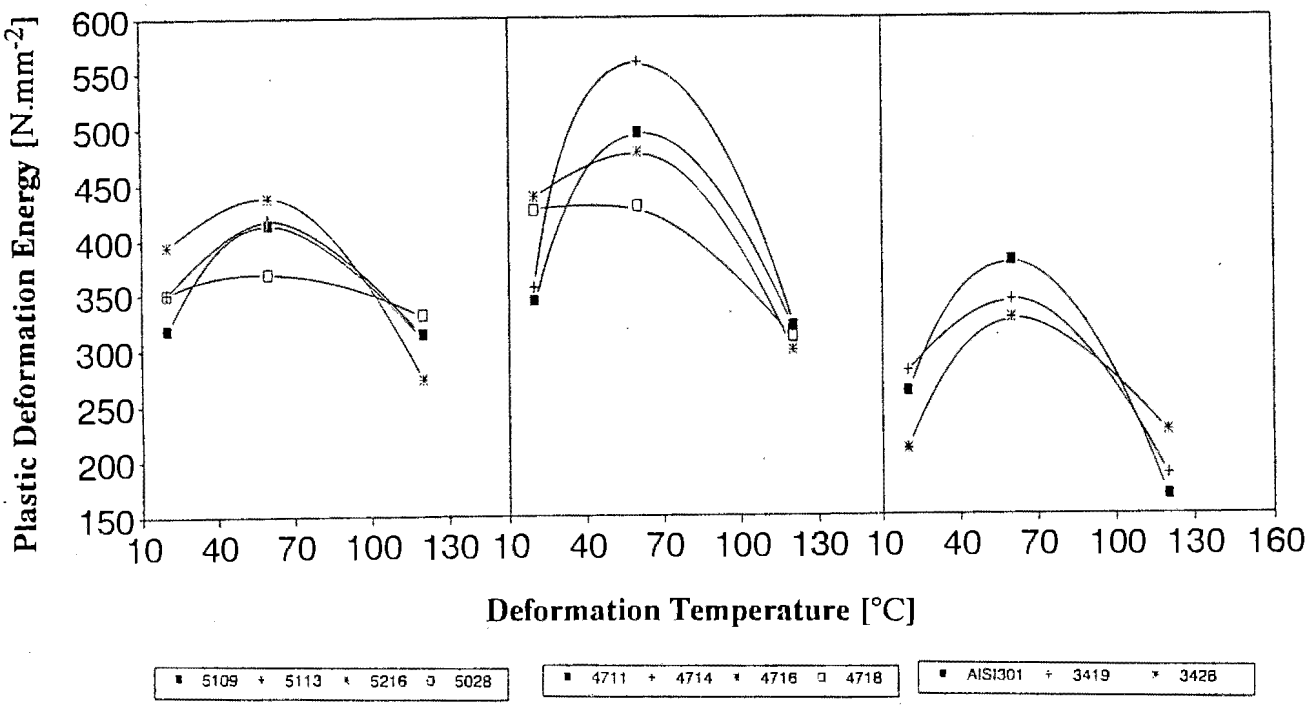

Figure 4.24 Plastic deformation energy of experimental alloys and the type 301 alloy absorbed between yield strain and e_u, as a function of deformation temperature.

Figure 4.24 shows that the maximum PDE_u is absorbed at 60°C for all alloys (including the type 301 alloy). From the limited data points that are available for each alloy it appears that the peak moves towards 20°C as nitrogen content increases. Furthermore, the peak height varies according to the nitrogen content, with the heighest peaks occurring at intermediate nitrogen content of 0.14 - 0.16% (nickel = 4.7 - 5.1%), and alloys containing the highest amount of nitrogen have the lowest PDE_u values at 60°C. It is noteworthy that for sets 51 and 47, the temperature at which the maximum PDE_{30} occurs, is 20°C, whereas the temperature at which the maximum PDE_u occurs, is 60°C. Thus the temperature of deformation needs to be adjusted according to the required final strain value in order to achieve optimum energy absorption.

4.3 MECHANICAL PROPERTIES

The mechanical properties investigated are the maximum uniform strain (e_u), yield strength and tensile strength at e_u (σ_u).

4.3.1 Maximum Uniform Strain (e_u)

Figure 4.25 shows that at 20 and 60°C, e_u has a maximum at a particular nitrogen content whereas at 120°C a minimum occurs. The occurrence of the maxima is associated with the formation of deformation-induced martensite at the optimum rate i.e. the nitrogen content at a particular maximum enables the TRIP phenomenon to occur at the optimum rate. At 120°C,

insufficient martensite is formed, and e_u is determined by the ability of austenite to work-harden and to resist incipient necking.

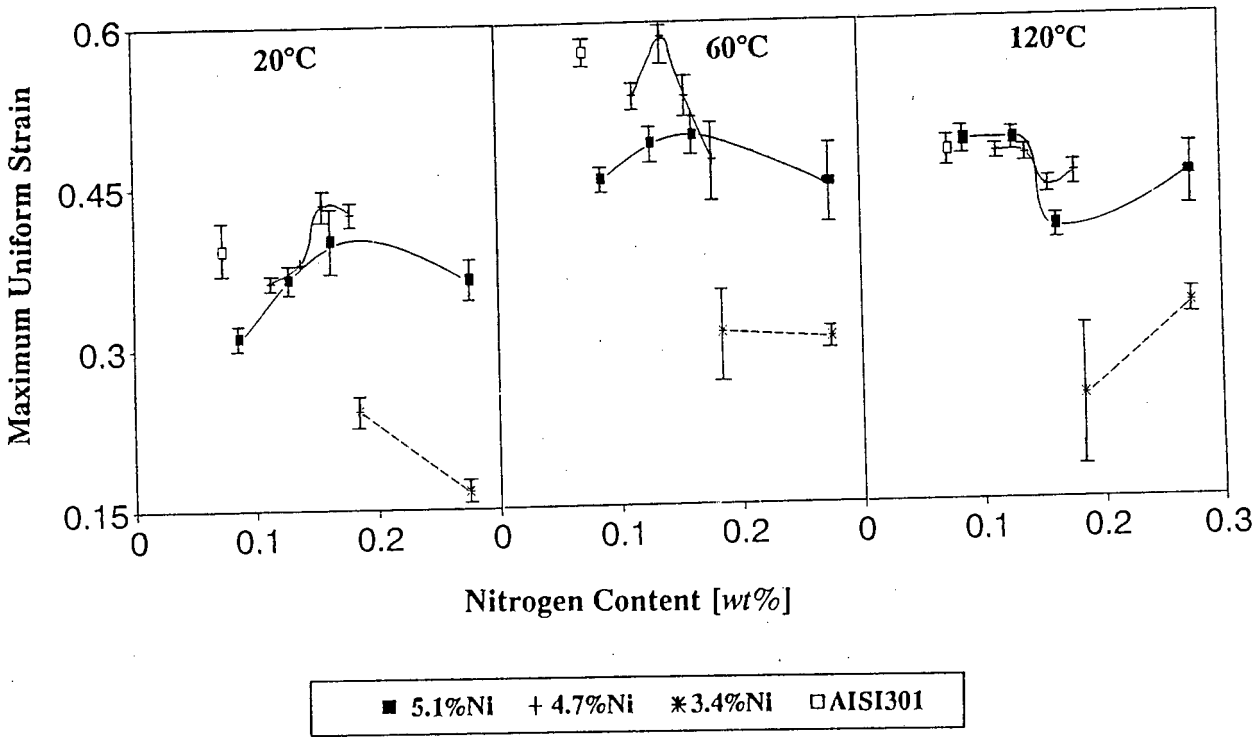

Figure 4.25 Maximum uniform strain (e_u) of experimental alloys and the type 301 alloy as a function of nitrogen content.

Although set 47 contains on average only 0.4% less nickel than set 51, the pronounced effect that this has on the peak sharpness can be clearly seen at 20 and 60°C, with set 47 having a significantly greater incline and decline at 60°C than set 51. Set 34 has low e_u values which are attributed to the both presence of 40 - 55% pre-existing martensite, and to the rapid formation of martensite during deformation. It can be inferred from the virtually identical trends of e_u (figure 4.25) and PDE_u (figure 4.23), that the maximum uniform strain of the experimental alloys is directly proportional to the plastic deformation energy. Figure 4.26 shows that the variation of e_u with temperature of alloy 4714 is similar to that of the type 301 alloy. Since the maximum elongation temperature (MET) lies between the M_s and M_d[31], the lowering of the M_s and M_d on raising the nitrogen level should also decrease the MET. It is difficult to see this trend from figure 4.26 due to the lack of data points available for each curve.

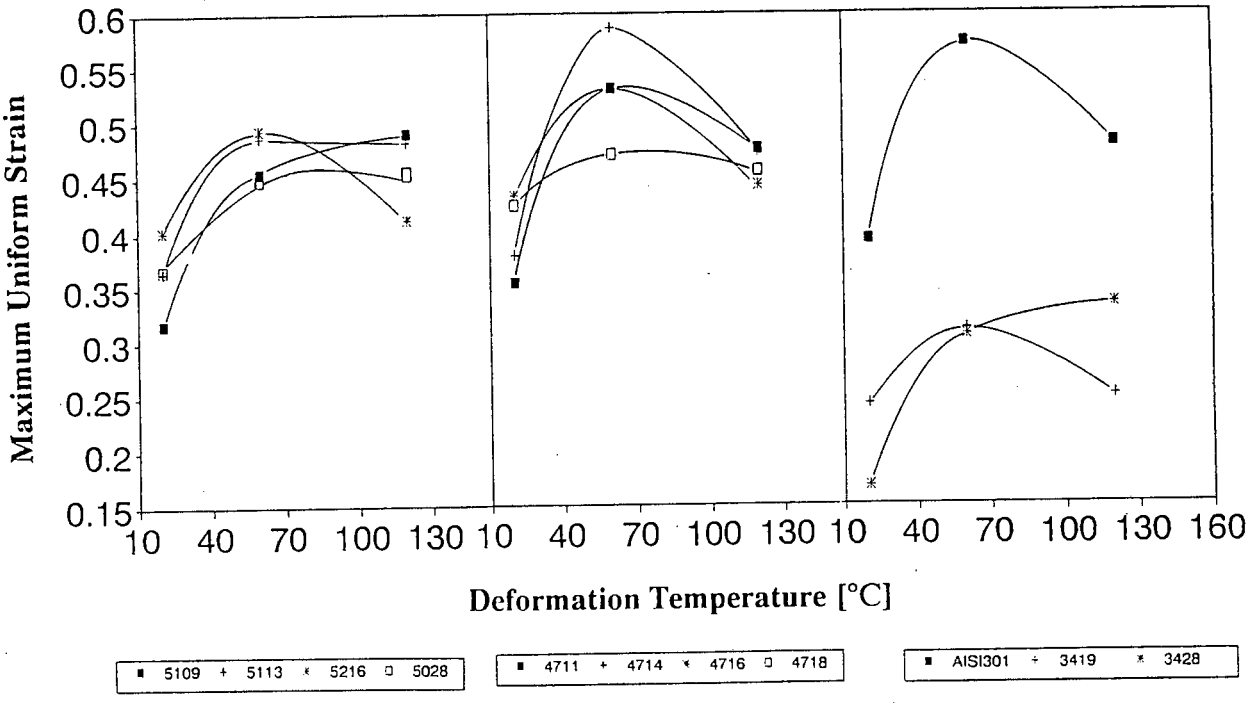

Figure 4.26 Maximum uniform strain (e_u) of experimental alloys and the type 301 alloy, as a function of deformation temperature.

4.3.2 Yield Strength

Yielding in TRIP steels can occur as a result of stress-assisted martensite formation or due to slip in austenite[16]. In the former case, the volume expansion of the austenite to martensite transformation results in a transformation strain and consequent yielding. Since the experimental alloys favour the formation of strain-induced martensite, yielding occurs primarily as a result of slip in austenite.

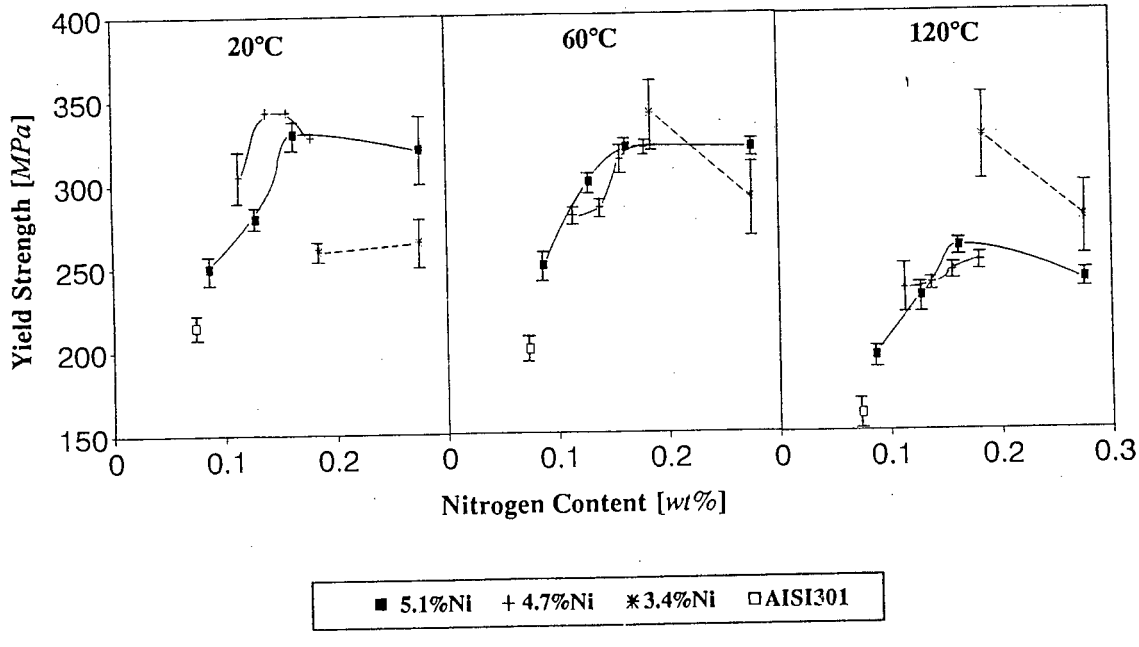

Figure 4.27 Yield strength of experimental alloys and the type 301 alloy, as a function of nitrogen content.

The yield strength of the experimental alloys is generally higher than that of the type 301 alloy, due to their relatively high nitrogen contents. Figure 4.27 shows that the yield strengths of the experimental alloys exceed that of the type 301 alloy at all three temperatures. The figure also shows that the yield strength of sets 51 and 47 at 20 and 120°C decreases above a certain nitrogen content. The yield strength of sets 51 and 47 at 20°C, is higher than the yield strength of set 34, but as the temperature increases, the yield strength of set 34 becomes increasingly greater than that of sets 51 and 47. Figure 4.28 shows that the yield strength of the experimental alloys and of the type 301 alloy decreases with increasing temperature, except for alloy 3419. The seemingly different behaviour of the latter alloy is possibly due to the formation of stress-assisted martensite at the lower temperatures. The dilational strain associated with the formation of martensite within the elastic region gives rise to an off-set which is sufficient to indicate premature yielding. As the temperature increases the tendency to form stress-assisted martensite decreases.

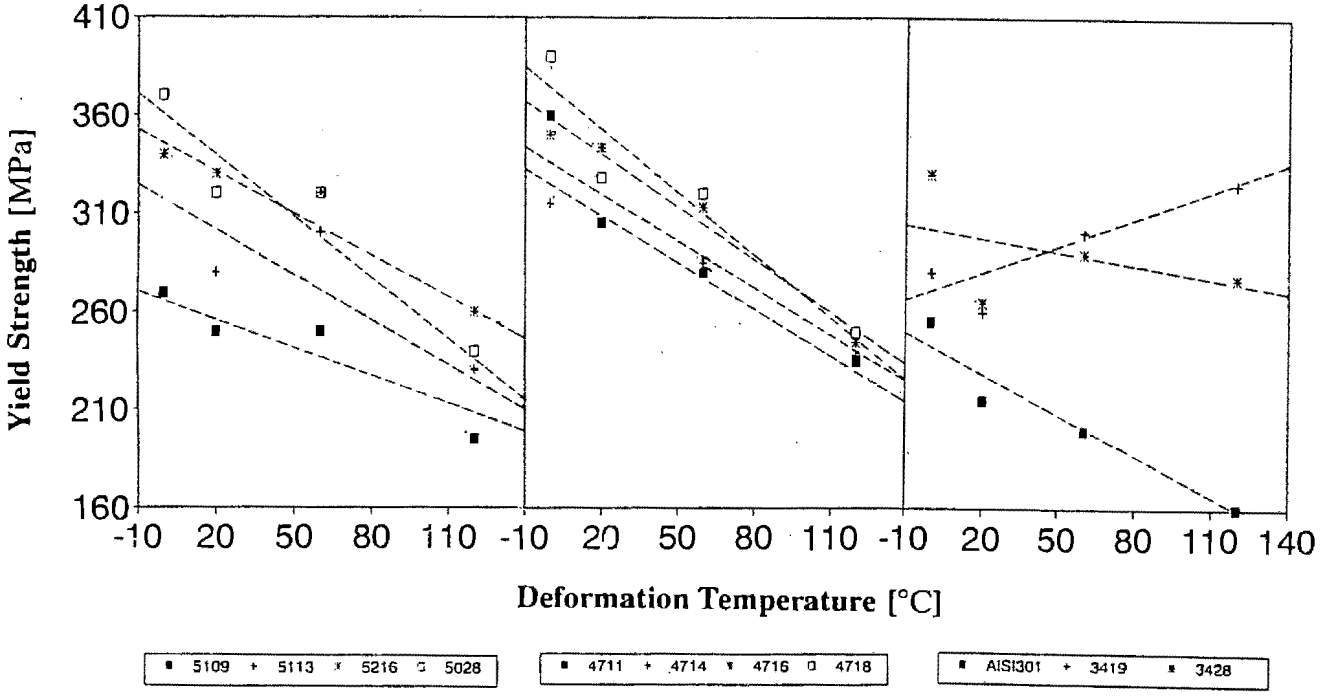

Figure 4.28 Yield strength of experimental alloys and the type 301 alloy, as a function of temperature.

4.3.3 Tensile Stress

(a) Tensile Stress at 0.3 True Strain(σ_{30})

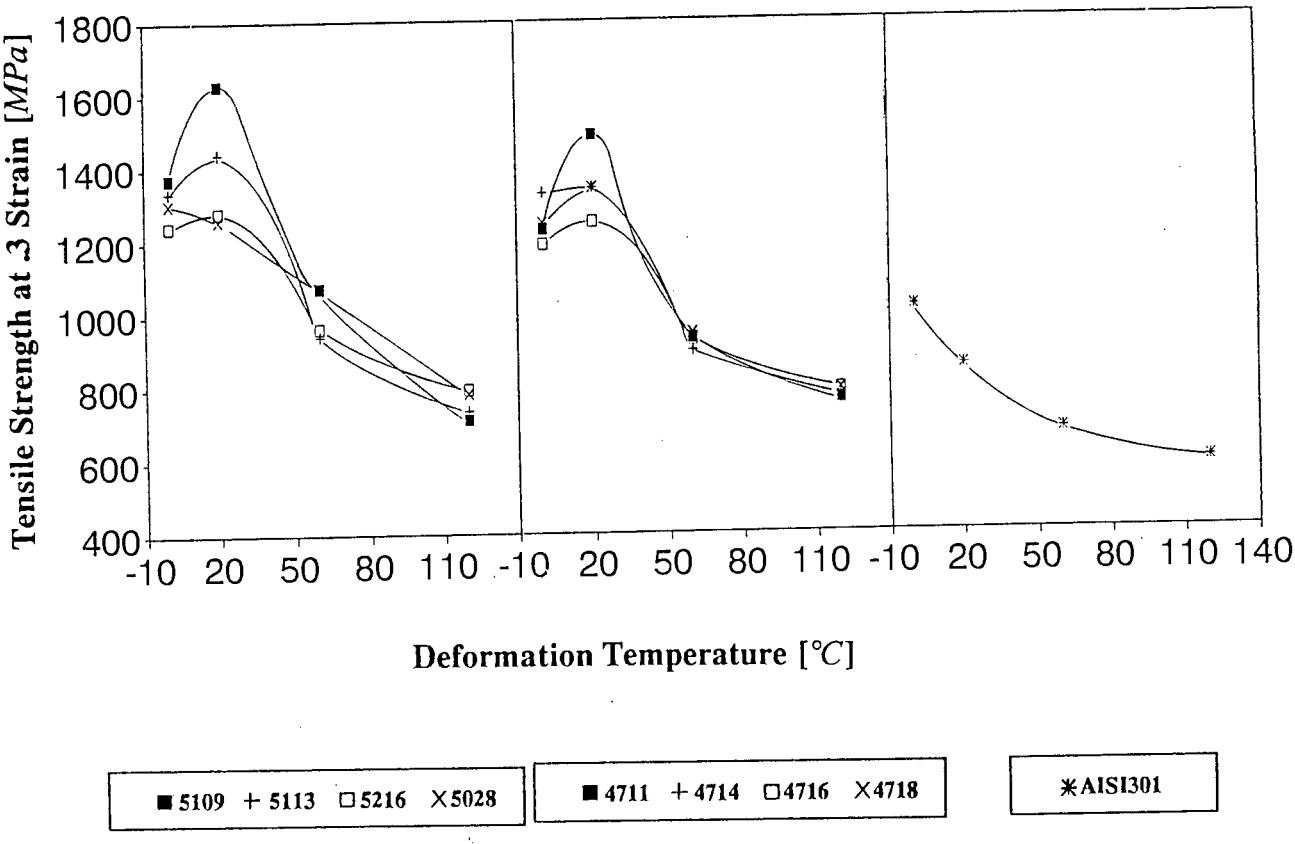

Figure 4.29 True stress at 0.3 true strain of experimental alloys and the type 301 alloy as a function of temperature.

The tensile stress of the experimental alloys at a strain of 0.3 has a maximum at 20°C (except for alloy 5028). In contrast, the measured value of σ_{30} for the type 301 alloy increases continuously with decreasing temperature, in accordance with the martensite content and bulk hardness trends (figures 4.16 and 4.21 respectively). The trend of σ_{30} (figure 4.29) is virtually identical to the trend of PDE_{30} (figure 4.22) for all alloys, including type 301. It can be inferred that at 0.3 strain, the plastic deformation energy is directly proportional to the tensile stress. Figure 4.30 shows that σ_{30} for the experimental alloys is consistently greater than σ_{30} for the type 301 alloy, and that the values for sets 51 and 47 are similar at all four temperatures.

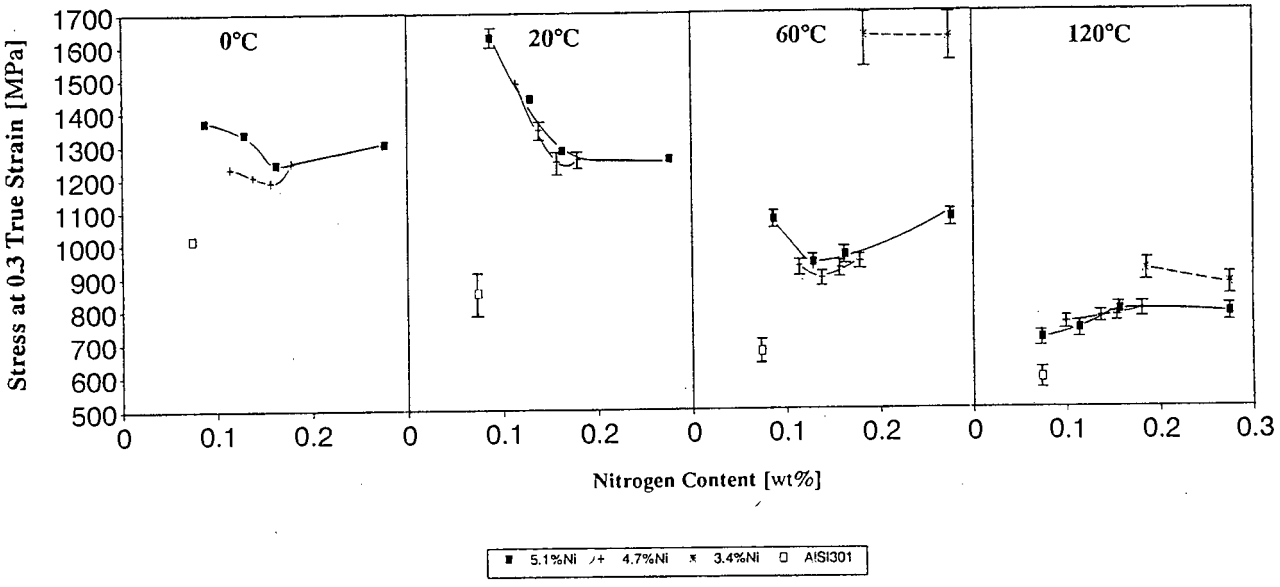

Figure 4.30 True stress at 0.3 true strain of experimental alloys and the type 301 alloy, as a function of nitrogen content.

(b) Tensile Stress at Maximum Uniform Strain (σ_u)

Figure 4.31 shows that at 20°C, set 47 has a maximum σ_u value which is higher than that of set 51, and the shape of the curve for the former set is also sharper than that of the latter. As temperature increases the maxima of both sets apparently move to the left i.e. towards lower nitrogen contents.

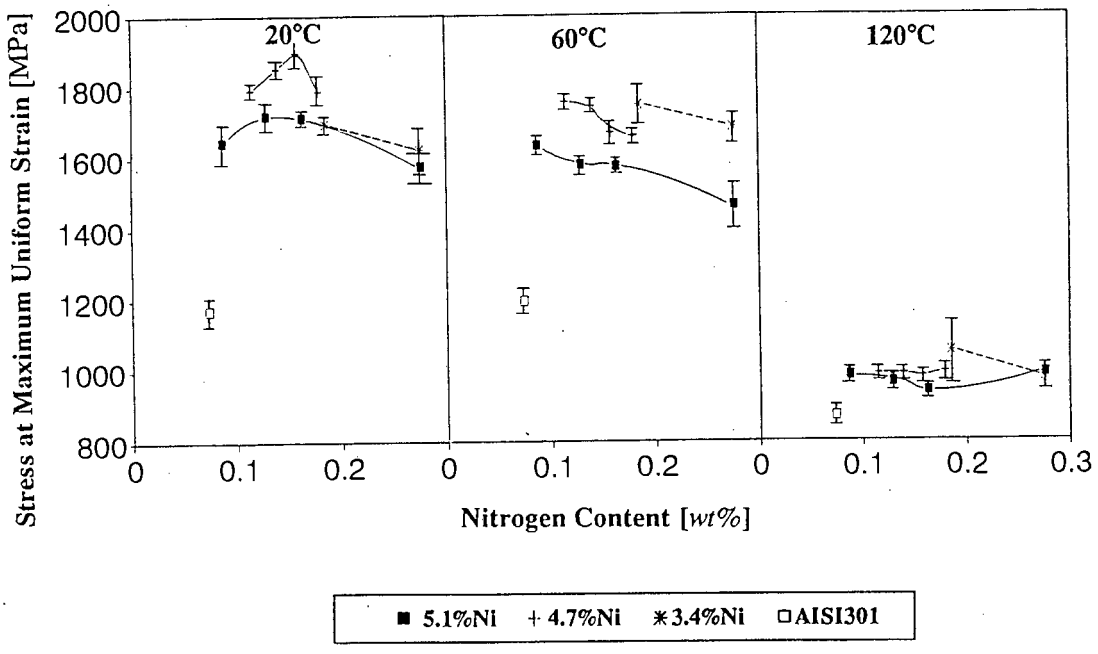

Figure 4.31 Tensile stress (σ_u) at maximum uniform strain of experimental alloys and the type 301 alloy, as a function of nitrogen content.

The rate at which σ_u increases with decreasing temperature is greater in the experimental alloys than in the type 301 alloy (figure 4.32). This rate decreases as nitrogen increases, but even in the highest nitrogen alloys (5028, 4718 and 3428) it is still relatively high compared to that of the type 301 alloy. An interesting observation is that σ_u of the type 301 alloy and of set 34 both peak at 60°C whereas those of sets 51 and 47 peak somewhere below 20°C.

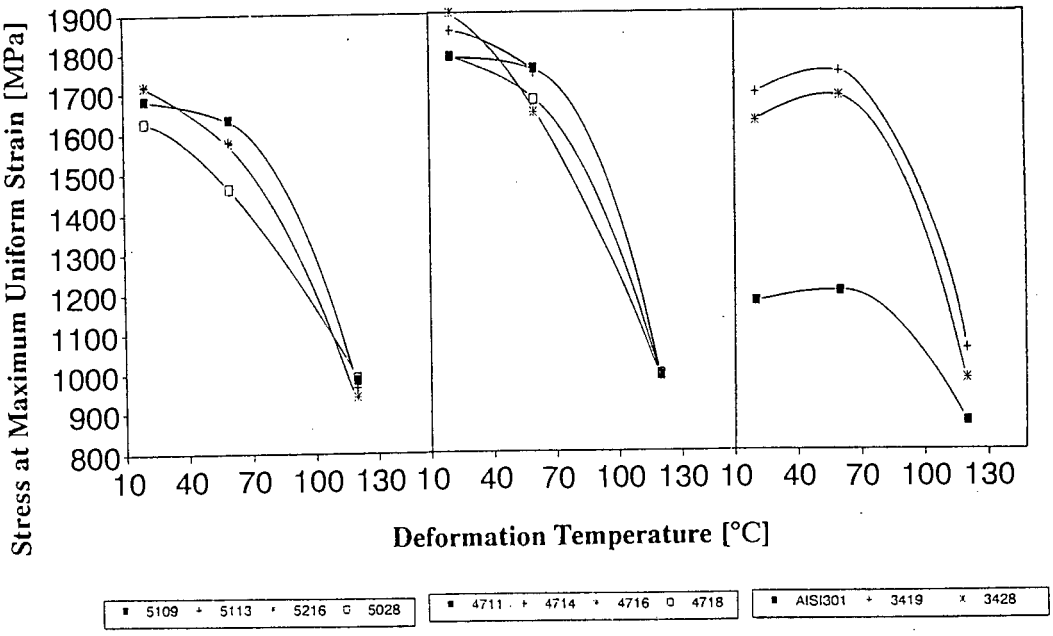

Figure 4.32 Tensile stress (σ_u) at maximum uniform strain of experimental alloys and the type 301 alloy, as a function of temperature.

4.3.4 Room Temperature Impact Properties

Adiabatic heating increases considerably at high strain rates[40] (i.e. strain rates of the order of 10^3 s^{-1} and above), and thus very little or no martensite is expected to form during impact. The observed trends of impact energy are thus primarily attributed to the effect of nitrogen in solid solution. The impact toughness of set 51 increases with increasing nitrogen content (the retained austenite content also increases with increasing nitrogen content) up to 0.16% nitrogen and decreases slightly as nitrogen increases to 0.28%. (Set 51 contains 90% retained austenite at 0.16% nitrogen). The impact toughness of set 47 decreases continuously with increasing nitrogen content (all alloys of this set contain more than 90% retained austenite), while the impact toughness of set 34 increases continuously (both alloys of this set contain less than 90% retained austenite).

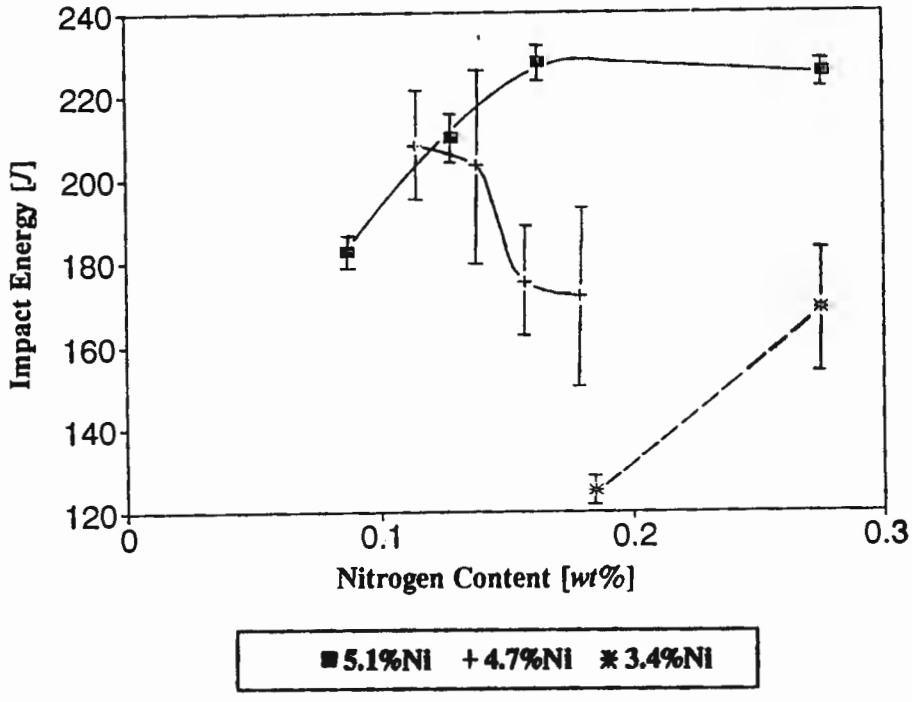

Figure 4.33 Impact energy absorbed by experimental alloys at room temperature.

The ductile impact fracture surfaces of alloys 5109, 4718 and 3419 are shown in figure 4.34. The principal fracture mode is crack propagation due to void coalescence.

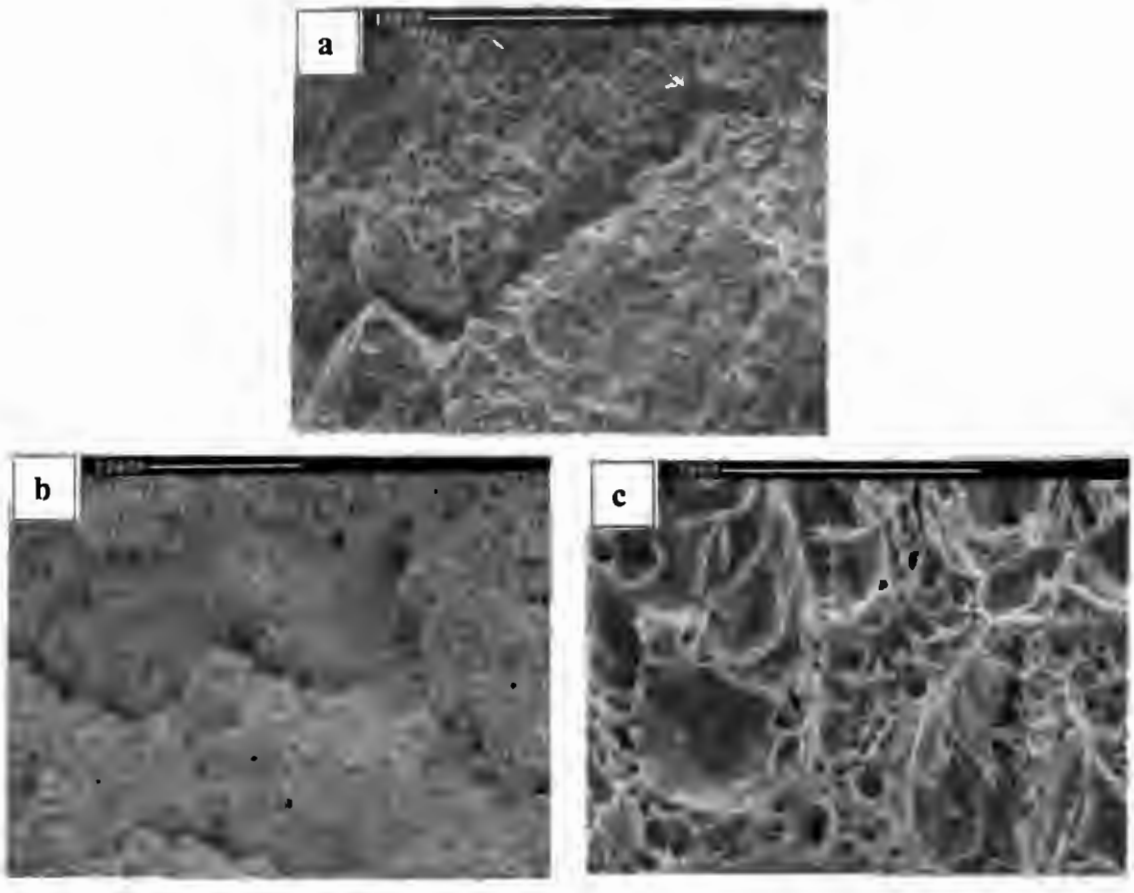

Figure 4.34 Impact fracture surfaces of tests at 20°C.

(a) **Alloy 5109** [Impact energy = 183 J] (b) **Alloy 4718** [Impact energy = 177 J] (c) **Alloy 3419** [Impact energy = 125 J]

CHAPTER 5

DISCUSSION

5.1 MICROSTRUCTURAL CHARACTERIZATION

5.1.1 Austenite Forming and Stabilizing Ability

The pseudo-ternary phase diagram in figure 5.1 shows that at 1000°C (which is 50°C below the solution treatment temperature) the experimental alloy compositions fall into the austenite region (γ) only. The confirmed absence of δ-ferrite at the solid solution treatment temperature in all experimental alloys, shows that the compensatory increase in nitrogen for the decrease in nickel, has successfully maintained the austenite forming ability of the type 301 alloy.

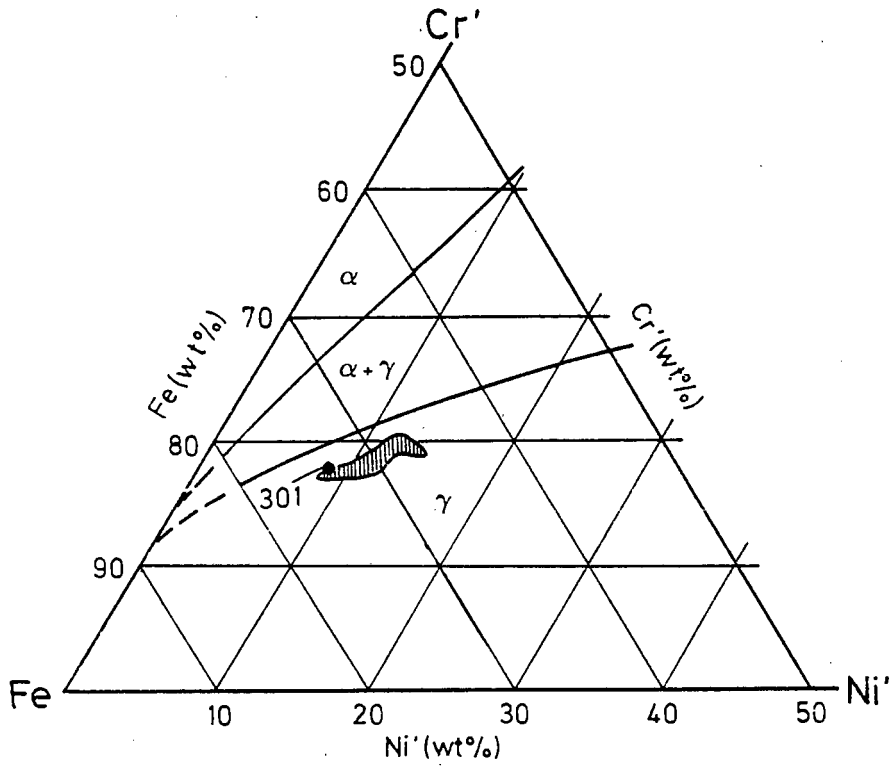

Figure 5.1 Fe-Cr'-Ni' ternary phase diagram (1000°C isothermal section). Experimental alloy compositions fall into hatched area[69].

The absence of δ-ferrite in austenitic microstructures generally improves the hot ductility and hot workability[10]. This is true for low nitrogen levels (approx. 0.03 wt%), but it has been shown that at high nitrogen levels (approx. 0.20 wt%) the absence of δ-ferrite results in a reduction in hot ductility as shown in figure 5.2. It has been proposed that the decrease in ductility is due to Cr-N clusters retarding recovery and recrystallization by segregating to austenite grain boundaries[42].

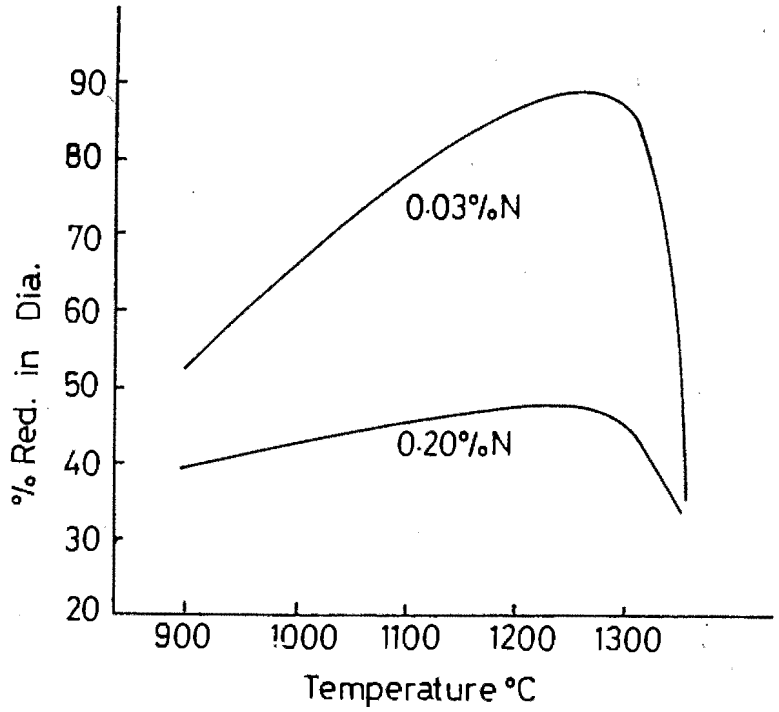

Figure 5.2 The effect of nitrogen content on the hot workability of austenitic stainless steels containing no δ-ferrite[42].

It would therefore be advantageous to have some δ-ferrite present, since in fact a small amount of δ-ferrite can be beneficial as it dissolves impurities which lead to intergranular cracking. Also the additional interfacial area created by δ-ferrite can lower the concentration of impurities segregated to the boundaries[42].

The austenite stabilizing ability of set 47 compares very favourably with that of the type 301 alloy, since the amount of retained austenite of the respective alloys in this set ranges between 94 and 97%. The stabilizing ability of set 51 also compares well with that of the type 301 alloy and the amount of retained austenite varies between 84 and 95%. Set 34 in contrast shows that the partial substitution of 4 wt% nickel with up to 0.28 wt% nitrogen does not provide a stabilizing ability comparable to that of the type 301 alloy. Since the levels for carbon, manganese and chromium vary slightly over the alloy range, including the type 301 alloy, (ideally the base composition of all the experimental alloys and the type 301 alloy should be *identical* but this is not viable in practice), minor deviations also occur in the expected trend of retained austenite with nitrogen content. For example, alloy 4716 contains 7% more austenite after solution treatment than alloy 5216 and this can be attributed to the fact that set 47 contains slightly higher carbon and manganese contents than set 51.

5.1.2 Nitrogen solubility

Transmission electron microscopy revealed no nitride precipitates in the highest nitrogen alloys (5028, 4718 and 3428). This is not surprising in view of the fact that type 304 austenitic stainless steel containing 8 - 12 wt% nickel, comfortably retains 0.2 wt% nitrogen when solution heat-treated at 1050°C[51]. Since nickel lowers nitrogen solubility, lowering the nickel level will provide increased nitrogen solubility. Co-planar arrays of dislocations separated by

stacking faults have been directly linked with the presence of nitrogen and can be clearly seen in figures 4.5(b) and 4.7(a)[50]. The formation of deformation-induced nitrides has been reported[42] but it is unlikely that this phenomenon would occur in the experimental alloys.

5.2 TENSILE DEFORMATION BEHAVIOUR

5.2.1 True Stress - True Strain Curves

The true stress - true strain curves of set 51 at 20, 60 and 120°C are very similar to those of set 47 (compare figure 4.8(a) and (b)). In contrast those of set 34 show distinct differences, which are attributed in part to the effect of the relatively large amounts of pre-existing martensite in this particular set (figure 4.8(c)). A striking feature of the tensile behaviour of the experimental alloys is the pronounced serrations, which occur only at 60°C in the experimental alloys. The type 301 alloy exhibits very fine serrations at 60°C, which are more uniformly distributed and by far not as pronounced as the ones which occur in the experimental alloys. In the experimental alloys, the serration amplitude increases with decreasing nitrogen content and increasing strain. In particular, serrations occur with increasing amplitude as the maximum uniform strain is approached.

It is unlikely that the pronounced serrated flow occurring in the experimental alloys is the result of adiabatic heating since it should then also be present at 20°C. Furthermore, it is unlikely that dynamic strain ageing is the primary cause, since the serration amplitude should then increase with increasing nitrogen content. It is proposed that the serrations are the result of martensitic transformation and that they occur only at very specific austenite stabilities. At 20°C austenite stability is not favourable for serration formation presumably because the stability is 'too low'. At 60°C stability is higher and this suggests that serrations do not occur below a minimum threshold stability. Furthermore, since serrations are also absent at 120°C, a maximum threshold stability exists, above which no serrations are formed. Pronounced serrations only occur beyond 0.3 true strain and since a negligible amount of deformation-induced martensite has formed at 60°C up to this strain (figure 4.16), it is plausible that serrations only start to form when the average flow stress reaches the required stress for transformation. The formation of some martensite before the average flow stress reaches the transformation stress, is attributed to the occurrence of local stress concentrations, which are greater than the average flow stress.

It is proposed that serrations occur as a result of an incubation period, coupled with a type of burst phenomenon. The three stages in the formation of a serration are shown in figure 5.3. Between A and B slip occurs in the austenite, while martensite formation is suppressed, but

this does not necessarily imply complete transformation suppression. At B, the critical stress is reached for slip in austenite to be succeeded by martensite formation.

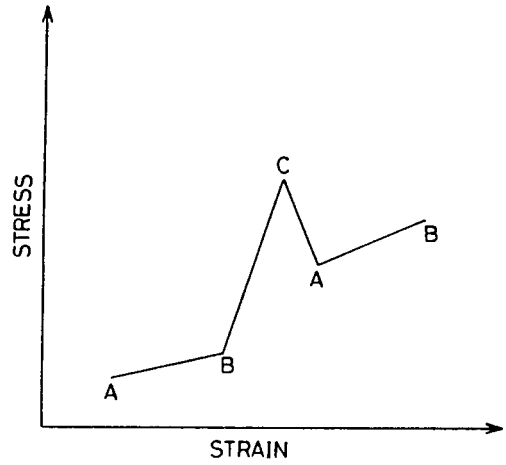

Figure 5.3 The three stages of formation of serration peak at 60°C.

A→B : Slip in austenite. Very little or no martensite formed.
B : Slip in austenite is succeeded by martensite formation.
C : Martensite burst.

The transformation proceeds at a relatively slow rate and the flow stress increases as martensite is formed. At C, the critical stress for rapid martensite formation is reached (martensite is probably forming in bursts). Tomota *et.al.* have shown that when martensite forms rapidly, the stress relief accompanying the transformation strain can lead to a lowering of the overall applied stress[68]. (Martensitic shear transformation results in a 4% volumetric expansion or equivalently 1.3% linear dilatation, and hence a certain positive value of transformation strain occurs along the direction of applied stress). The cycle is then repeated. Serrations do not occur at low strains since the flow stress values are below the critical stress required for rapid martensite burst transformation at C.

It appears that as austenite stability increases the stress drop (C→A) becomes more gentle (compare peak P1 with P2 in figure 4.8(d)). The presence of nitrogen has been associated with the occurrence of burst phenomena[70], but the exact role played by nitrogen in the process of serration formation cannot be determined from the experiments performed, and further work would be required to this end.

5.2.2 Work-Hardening Rate (WHR) Behaviour

Type 301:

At 20°C, the decrease in WHR at strains below 0.2 is typical of the continuously decreasing WHR of stable austenite (figure 4.9). It has been shown, that at strains just prior to the minimum in WHR, deformation-induced transformation begins[26]. Martensite embryos become supercritical and begin to grow[13] due to the increase of local stress concentrations at

the intersection of slip bands[73] and/or the pile up of dislocations at grain boundaries[12]. Beyond 0.2 strain, the transformation rate and correspondingly the martensite volume fraction increases, resulting in an increase in strength, due to composite strengthening by continual refinement of the austenite and martensite mixture. At 0.3 strain, the maximum WHR is reached, and about 40% martensite has been induced (figure 4.16). The most energetic or the most favourably oriented martensitic embryos have been consumed, and more energy is required to activate embryos of successively less favourable orientation, and the transformation rate decreases[13]. The amount of martensite formed per nucleus gradually decreases, due to the partitioning of austenite into smaller and smaller volumes by the martensite laths that are formed. The transformation gradually peters out, the composite microstructure begins to deform, and dynamic recovery results in a decrease of WHR with increasing strain[24].
At 60°C, the extent of transformation at a given strain is significantly lower, and the magnitude of the maximum value attained by WHR decreases.
At 120°C, WHR decreases continuously since transformation is largely suppressed. It is not suppressed completely, as can be seen by the laths that have formed (figure 4.19(c)), but the growth of martensite embryos is very slow, with the result that deformation occurs primarily as slip in austenite.

5.1% Ni alloys:

At 20°C, the onset of positive work-hardening of all 4 alloys occurs toward lower strains (i.e. below 0.1) than in the type 301 alloy, and is relatively insensitive to changes in nitrogen content. The earlier onset of positive work-hardening in set 51 is accompanied by the formation of 15 - 45% more martensite up to 0.3 strain than in the type 301 alloy.

At 60°C, the onset of positive work-hardening also occurs at lower strains than in the type 301 alloy (i.e. at approx. 0.2 strain), and relatively little martensite ($<10\%$) is induced up to 0.3 strain. The value of the peak WHR with its corresponding strain value are plotted in figure 5.4. The greater the strain at which the peak WHR value occurs, the greater will be the elongation.

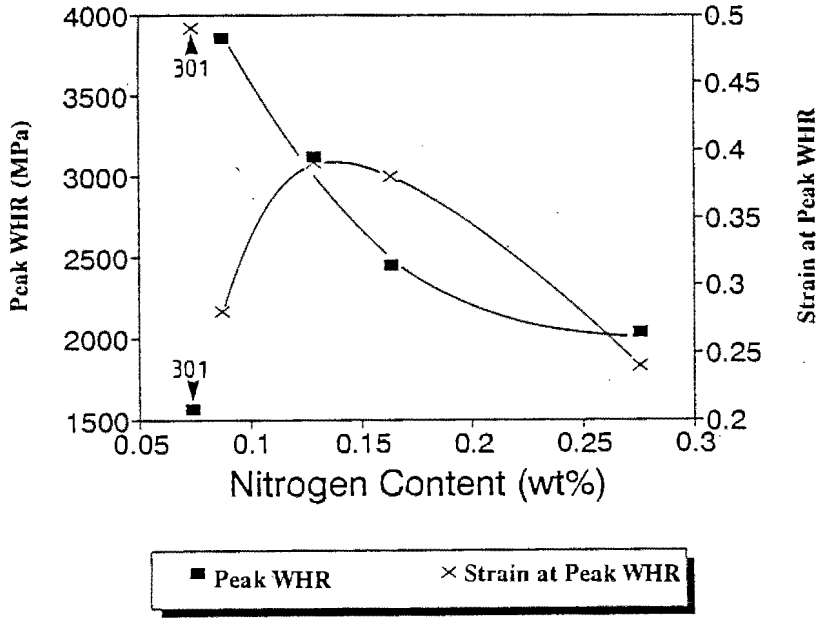

Figure 5.4 The peak work-hardening rates and the corresponding strain values of set 51 compared to that of the type 301 alloy at 60°C.

The curve of peak WHR of set 51 decreases continuously with increasing nitrogen content, and the curve of the corresponding strain values at the peak WHR has a maximum at a nitrogen content of approximately 0.13%. This represents the nitrogen content at which TRIP can occur at the optimum rate. The value of the peak WHR for each of the alloys in set 51, exceeds that of the type 301 alloy, and none of the alloys has a value for the strain at peak WHR which is greater than that of the type 301 alloy. Alloys 5216 and 5028 have similar work-hardening behaviours to the type 301 alloy, except that in the former, the onset of positive work-hardening occurs at lower strains, the magnitude of the peak WHR values are higher and are reached at lower strains, resulting in lower elongations.

At 120°C, transformation is suppressed, and the work-hardening behaviour of set 51 is very similar to that of the type 301 alloy, with elongations being similar.

4.7% Ni alloys :

At 20°C, the strain at which the onset of positive work-hardening occurs, increases with increasing nitrogen content, with the onset in alloy 4716 occurring at approximately the same strain as in the type 301 alloy. This experimental alloy contains 20% less deformation-induced martensite than the type 301 alloy at 0.3 strain, while the other alloys of set 47 contain 10-30% more martensite than the type 301 alloy. The work-hardening behaviour of the 4 experimental alloys at 20°C is very similar to that of set 51 at the same temperature, with little difference between the peak WHR for alloys of equivalent nitrogen content.

At 60°C, onset of positive work-hardening commences at a strain of approximately 0.2 for all 4 alloys. The peak WHR and corresponding strain values are shown in figure 5.5.

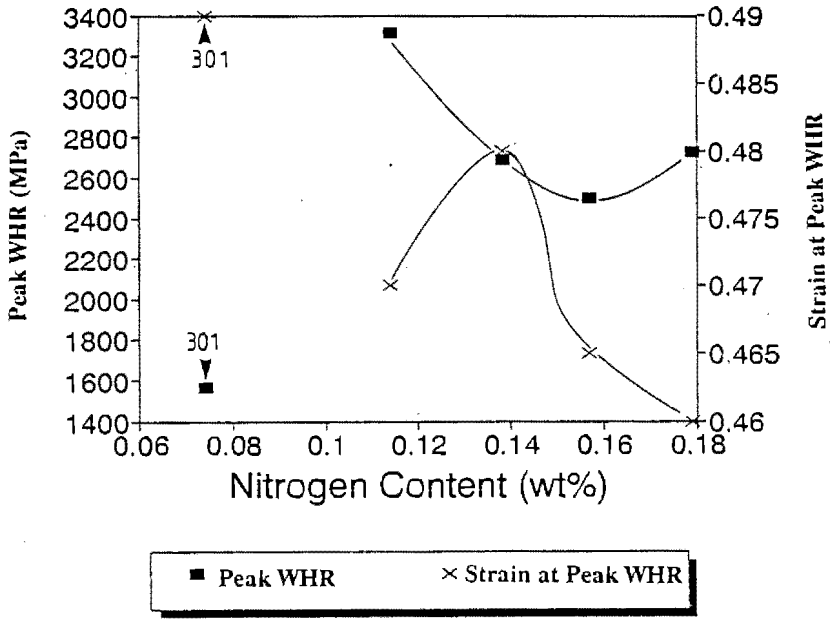

Figure 5.5 The peak work-hardening rates and the corresponding strain values of set 47 compared to that of the type 301 alloy at 60°C.

The curve of peak WHR of set 47 has a minimum at about 0.16% nitrogen, and that of the corresponding strain values has a maximum occurring at a nitrogen content of approximately 0.14%. This is very close to the optimum nitrogen content of set 51. Set 47 has a higher maximum peak strain value than set 51, the two values being 0.48 and 0.40 respectively. The high elongations to fracture, particularly in alloy 4714, indicate that conditions at 60°C are favourable for elongations to be increased by the transformation-induced plasticity mechanism.

At 120°C, transformation is suppressed, and the work-hardening behaviour of set 47 is very similar to that of the type 301 alloy, with elongations being similar.

3.4% Ni alloys :

At 20°C, the WHR of set 34 increases very rapidly at low strains, reaching a value of more than 10^4 MPa at strains below 0.1, indicating that martensite formation is rapid at low strains. Beyond the peak, the WHR decreases rapidly resulting in low elongation to fracture. Hence the formation of 40-50% martensite during deformation is too rapid to prevent incipient necking; the TRIP phenomenon therefore does not occur.

At 60°C, the onset of positive work-hardening still occurs at very low strains in both alloys. The peak WHR values are considerably lower than at 20°C, and the reduced rate of martensite formation does result in greater elongations, but these are low compared to that of the type 301 alloy.

At 120°C, the WHR decreases continuously, indicating the suppression of martensite formation during deformation, but the recorded elongations are nevertheless comparable to those at 60°C.

The work-hardening behaviours show that transformation-induced plasticity enhances the ductilities of set 51 and 47 at 60°C, but not of set 34. This is attributed to the presence of 40-55% pre-existing martensite in set 34 and the rapid formation of martensite at low strains. The work-hardening rate curves of the experimental alloys differ from those of the type 301 alloy, in that, generally onset of positive work-hardening occurs at lower strains, the peak WHR is higher, and corresponding strain values at which the peak WHR occurs, are lower than in the type 301 alloy. Nevertheless, in spite of these differences, the ductilities of some of the alloys in sets 51 and 47, compare favourably with the ductilities of the type 301 alloy recorded at 20, 60 and 120°C.

5.2.3 Microstructural Examination of Strained Alloys

The microstructures (parallel to the tensile direction) of the lowest and highest nitrogen alloys in set 47 (4711 and 4718 respectively) deformed by a tensile strain of 0.3, are compared to those of the type 301 alloy in figures 4.17 to 4.19. The microstructural features of the three alloys are examined after straining at 0, 60 and 120°C. It is not always easy to distinguish martensite from slip lines, but the deformation temperature gives a guideline, since martensite formation dominates at the lower temperatures, and slip dominates at the higher temperatures.

The microstructure of alloy 4711 deformed at 0°C, consists predominantly of fine lath strain-induced martensite (figure 4.17(a)). At 60°C (figure 4.17(b)), a number of austenite grains can be seen which have resisted slip and transformation [area (2)]. The slip lines have widened and a twin can also be seen [area (3)], although this twin may have formed during quenching. Martensite has formed more selectively at 60°C, than at 0°C, and therefore results in an increase in uniform straining ability at 60°C. At 120°C, some austenite grains exhibit microstructural features which resemble slip bands [area (5)]. The presence of martensite clusters [area (6)] could be the result of martensite formation during electro-polishing since similar such clusters occur in the undeformed structure (figure 4.2(a)).

The microstructure of alloy 4718 at 0°C (figure 4.18(a)) is very similar to that of alloy 4711. (The alloys contain 69% and 72% martensite respectively). At 60°C, martensite occurs as isolated laths, and clusters are less prevalent than in alloy 4711 (figure 4.18(b)). Two martensite laths (presumably strain-induced) occur on the slip lines in an austenite twin [area (1)]. At 120°C features resembling slip are again visible [area(3)], and some martensite clusters occur [area (2)] (figure 4.18(c)).

The microstructure of the type 301 alloy at 0°C, is similar to that of alloy 4711 and 4718, and contains 67% martensite (figure 4.19(a)). At 60°C, the microstructure appears very similar to that of alloy 4718. Martensite occurs only in the form of laths not in clusters (figure 4.19(b)).

At 120°C, clusters of martensite are also absent. Features thought to be slip bands, which span whole grains of austenite as in alloy 4711 at 120°C (figure 4.17(c)), are not evident in the type 301 alloy.

5.2.4 Deformation-Induced Martensite Content

The formation of deformation-induced martensite in the present experimental alloys is largely attributed to strain in the matrix. The ease with which critical levels of strain can occur in the austenite is expected to influence the formation of martensite. At any specific temperature, local stress variations may result in the average stress being lower than the local stress. Since the propensity for slip to occur is enhanced with increase in temperature, it is possible for an increase in local stress to arise from increased local slip even when the average stress level is still low. This could lead to martensite formation at some point. However, as the temperature is reduced, the ease with which slip might occur at low average stress levels is reduced and the occurrence of local slip becomes less significant, thereby restricting the formation of martensite. This might explain why the amount of martensite measured after 0.3 strain in some experimental alloys is greater at 20°C than at 0°C, although the total martensite induced up to fracture may be equivalent in both situations.

In addition the amount of pre-existing martensite must influence the formation of deformation-induced martensite. It is expected that martensite formed during quenching (after solution treatment) will be influenced by the existence of favourable nucleation sites. The formation of deformation-induced martensite is similarly affected by nucleation sites, and if a proportion of initial favourable sites is already consumed, it is more difficult for martensite to form in regions of low stress/strain. Therefore the increase in the formation of deformation-induced martensite in the type 301 alloy up to 0°C, can be explained on the basis that very little or no martensite (<2%) exists in the microstructure prior to deformation. Three of the set 47 alloys behave in the same manner for similar reasons.

The formation of deformation-induced martensite results in a substantial increase in bulk hardness measured for the experimental alloys. Figure 4.20 shows that their hardness values after solution treatment ranges between 200-230 HV_{30}. After straining by 0.3, the hardness values have increased to between 300-550 HV_{20} (the hardness increase at 0 and 20°C being considerably higher than at 60 and 120°C). In contrast, the bulk hardness of the type 301 alloy after straining by 0.3, increased from 170 HV_{30} (after solution treatment) to between 250-400 HV_{20} depending on temperature. The experimental alloys, which contain considerably higher amounts of nitrogen than the type 301 alloy, undergo greater strengthening during deformation due to the inherently high strengthening effect of nitrogen in martensite. The close correlation between the increase in deformation-induced martensite and the concomitant increase in bulk

hardness can be observed by comparing figures 4.16 and 4.21.

5.3 MECHANICAL PROPERTIES

5.3.1 Maximum Uniform Strain (e_u)

(a) Variation with temperature

From the limited data available, it can be said that the maximum elongation temperature (MET) of the type 301 alloy is in the vicinity of 60°C (figure 4.26). (The MET of the type 301 alloy has been reported to vary from 50 to 55°C[27,32,33].) The MET's of the alloys in set 47 are also in the vicinity of 60°C, while those of the alloys of set 51 occur more in the 60 to 120°C temperature range. It has been well substantiated during previous investigations that the MET decreases as the stability of the austenite microstructure increases[12,31]. This can be similarly illustrated with some degree of confidence from the limited data available from the set 51 alloys. The curves drawn in figure 5.6 are approximated, but indicate how the MET might be influenced by increasing nitrogen content.

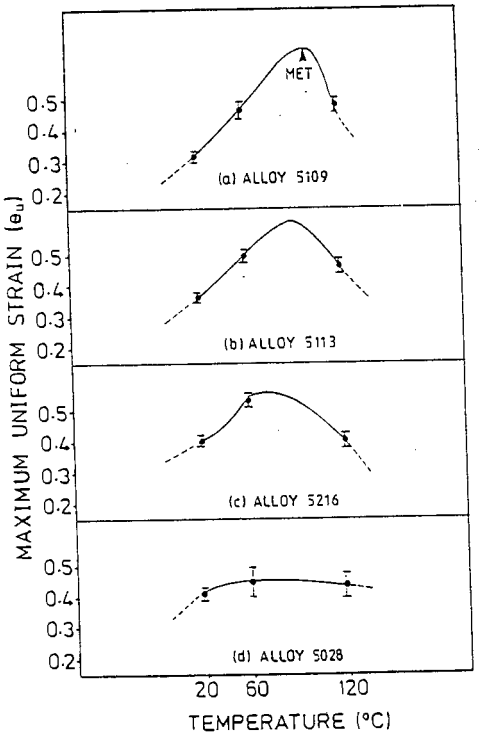

Figure 5.6 Schematic approximation of influence of nitrogen on the MET. The position of the MET is presented qualitatively and <u>not</u> quantitatively.

The schematic approximation shows not only that the MET decreases with increasing nitrogen, but also that the peak becomes shallower as nitrogen increases in accordance with previous findings[27,31].

(b) Variation with nitrogen content

The occurrence of a maximum uniform strain as a function of temperature implies that there should also be a maximum uniform strain as a function of nitrogen content, since the effect of a variation in temperature on austenite stability is equivalent to a variation in nitrogen content. Figure 4.25 shows that sets 51 and 47 do have a maximum uniform strain at a particular nitrogen content, but only at 20 and 60°C and not at 120°C. It was shown in section 5.2.2, that the manner in which work-hardening occurs during straining, is crucial in determining uniform straining ability. The maximum uniform strains of sets 51 and 47 at 60°C are generally greater than at 20 or 120°C, since incipient necking is delayed by the gradual and selective formation of martensite. In contrast, the formation of martensite at 20°C is less selective and more rapid, and is even more detrimental to the uniform straining ability, than had no martensite (or very little) formed, as at 120°C, since the values of e_u in general are greater at 120°C than at 20°C. Some alloys in sets 51 and 47 do have higher uniform strains at 20°C than at 120°C, but the majority have higher uniform strains at 120°C. The maximum uniform strain measured for the experimental alloys at 20, 60 and 120°C, is directly proportional to the plastic deformation energy (PDE_u), as can be seen by the similar trends of figures 4.25 and 4.23. The measured values of PDE_u should therefore provide a basis on which to rank the experimental alloys according to their ductilities.

There are two salient features which can be observed in figure 4.25:

(1) The peak of set 47 at 20 and 60°C is sharper and higher than that of set 51. There is a similarity between this observation and the results of Rosen *et.al.*, who found that the peak of their type 301 alloy was sharper and higher than of type 304[27]. Type 301 contains less nickel than type 304, and set 47 also contains less nickel than set 51. The nickel content may have a significant effect on the height and sharpness of the peak, but it may be that any alloying elements, which affect the austenite stability, influence the peak height and sharpness. The sharpness of the peak is an indication of the sensitivity of the alloy to changes in nitrogen (and temperature), and in view of the peaks of set 47 being sharper than the peaks of set 51 (at 20 and 60°C), it is possible that set 51 may be more suited for practical purposes than set 47, in spite of the attractively high uniform strains achieved by set 47. It is difficult to control strain rates precisely during fabrication, and strain rates are likely to vary within a particular component in the manufacturing process. Varying strain rates make it more difficult to control adiabatic heating, which in turn has a pronounced effect on martensite formation.

(2) At 120°C, sets 51 and 47 have a minimum uniform strain instead of a maximum. Since the

steels are stable at this temperature, their deformation behaviour can be compared to that of 17% chromium ferritic steels. A minimum in tensile ductility is observed in the latter at about 40% martensite (figure 5.7) suggesting that a similar minimum tensile ductility occurs at a particular martensite content in the experimental alloys at 120°C.

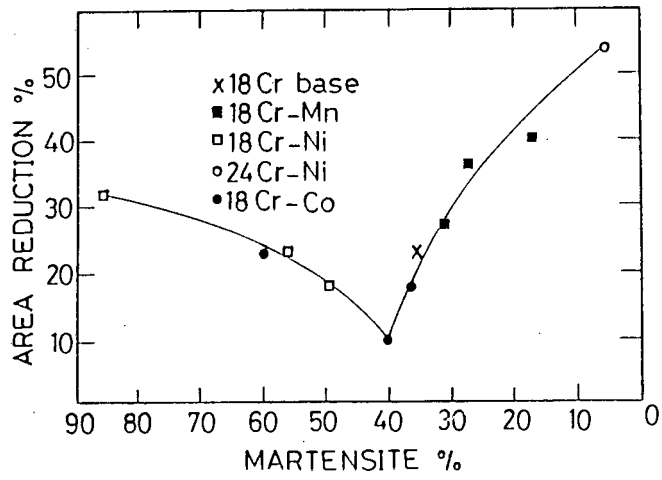

Figure 5.7 Effect of martensite content on the tensile ductility of 17% chromium steels[71].

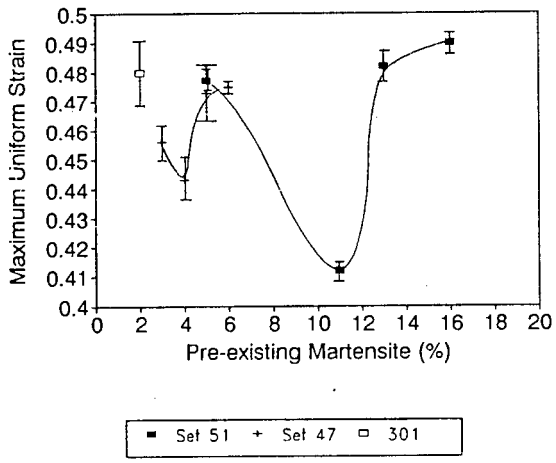

Figure 5.8 Minimum in ductility of sets 51 and 47 at about 11 and 4% pre-existing martensite respectively.

Figure 5.8 shows that a minimum in ductility occurs for set 51 at 11% pre-existing martensite, and for set 47 at 4%. The decrease in ductility as the amount of pre-existing martensite increases from 0%, indicates that the presence of martensite must be having some adverse influence on the deformation behaviour of austenite during the latter stages of straining. Obviously two-phase mixtures do influence uniform deformation as shown by the ferrite-martensite steel in figure 5.7, but further work would be required to clarify this in the present steels.

5.3.2 Yield Strength

The yield strength of the experimental alloys exceeds that of the type 301 alloy at all temperatures (figure 4.27), and this can be attributed to the intrinsic high strengthening ability of nitrogen in solid solution as shown in figure 5.9.

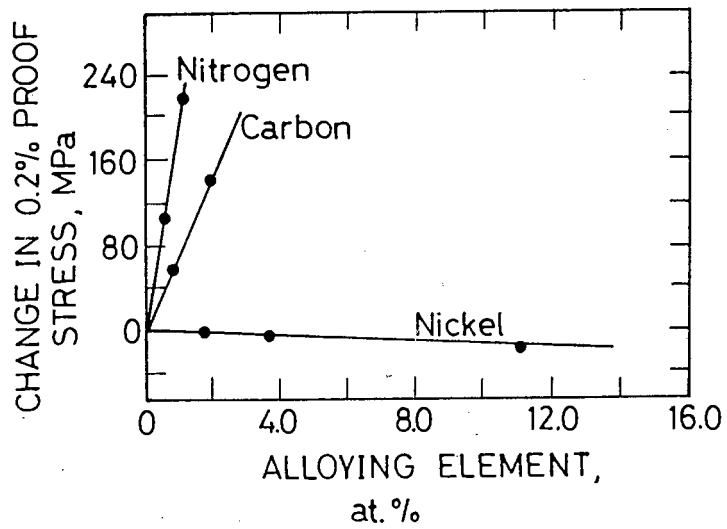

Figure 5.9 Yield strengthening ability of nitrogen compared to that of carbon and nickel[42].

The yield strength of the alloys in sets 51 and 47, as well as that of the type 301 alloy, decreases with increasing temperature as shown in figure 4.28, which is consistent with previous observations of the decrease of yield strength in FCC metals[72]. In contrast, the yield strength of alloy 3419 increases with temperature. This trend is unexpected and could be due to the formation of some stress-assisted martensite at the lower temperature. The formation of stress-assisted martensite would cause yielding due to the dilatation associated with the transformation. Less stress-assisted martensite is expected to form as temperature increases, and yielding will then only occur when slip occurs in the austenite, and will consequently be delayed to higher stress levels. Stress-assisted martensite is less likely to form in alloy 3428, which follows the same normal trend as the other alloys, because of its considerably higher nitrogen content.

5.3.3 Tensile Stress

(a) Variation with temperature

The observed tensile stress is dependent on the existing microstructure at the start of the tensile test, and the manner in which the microstructure work-hardens during deformation.

The difference between σ_{30} and σ_u depends on the extent of work-hardening between 0.3 strain and e_u. Figure 5.10 shows that (σ_u - σ_{30}) for the type 301 alloy is considerably smaller than (σ_u - σ_{30}) for sets 51 and 47. This is partly due to the martensite phase being strengthened to a greater degree in the experimental alloys than in the type 301 alloy, because of the higher nitrogen contents in the former alloys. Furthermore, nitrogen strengthens martensite considerably more than austenite, and since the experimental alloys generally contain more martensite at a given strain interval than the type 301 alloy, strengthening is much more pronounced between 0.3 strain and e_u in the former alloys.

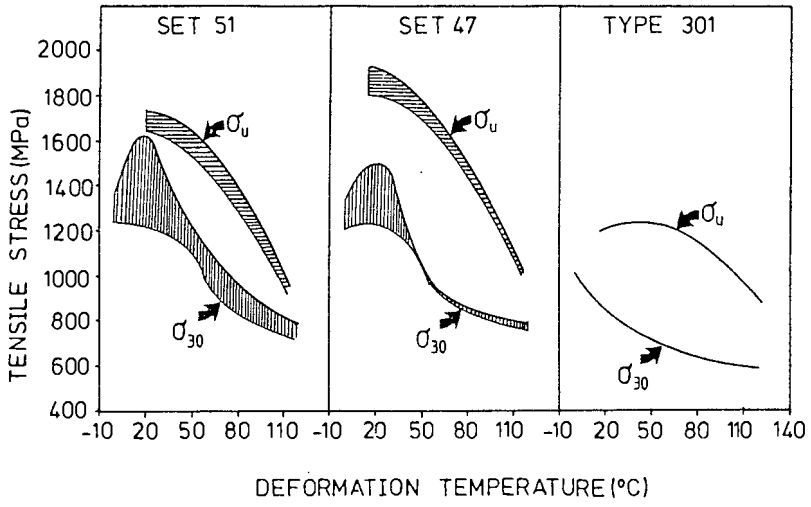

Figure 5.10 Tensile stress at 0.3 strain (σ_{30}) and at maximum uniform strain (σ_u) of sets 51 and 47, and the type 301 alloy, as a function of temperature.

The curves of σ_{30} and PDE_{30} are generally very similar for alloys of sets 51 and 47, as well as the type 301 alloy (compare figures 4.22 and 4.29). It can therefore be inferred, that at 0.3 strain, PDE_{30} is directly proportional to the tensile stress, σ_{30}. In section 5.3.1(b) it was noted that at the maximum uniform strain (e_u), the plastic deformation energy (PDE_u) is directly proportional to e_u. These two observations indicate that in the early stages of deformation (i.e. below 0.3 strain), where relatively little martensite has formed, the deformation energy is determined by the increase in stress. In the stages of deformation between 0.3 strain and e_u however, where martensite is the dominant deformation mode, the deformation energy is now determined by the increase in strain instead.

(b) Variation with nitrogen content

The tensile stress measured at 0.3 strain (σ_{30}), is very similar for sets 51 and 47 at 20, 60 and 120°C, as shown in figure 4.30. In contrast, the tensile stress measured at e_u (σ_u) is similar only at 120°C (figure 4.31). At 20°C for instance, the curve of σ_u versus nitrogen for set 47 is not only higher than the curve of σ_u for set 51, the incline and decline of the former are also greater than that of the latter curve. It is thus not only the uniform strain for set 47 which is

more sensitive to changes in nitrogen (and temperature) than the uniform strain of set 51, but also the tensile stress. At 60°C, the tensile stress measured for set 47 is still greater than that measured for set 51, but the shapes of the two curves have become similar. The peaks observed at 20°C have apparently shifted towards lower nitrogen contents (lower austenite stability) in counteractive response to the increased temperature (higher austenite stability).

5.3.4 Room Temperature Impact Behaviour

The Charpy test was originally introduced to differentiate between steels which failed by brittle cleavage fracture at some specific temperature, and those which failed by ductile dimple fracture, and also to obtain some idea of the ductile-to-brittle transition temperature. If fracture is ductile, as was the case in the present investigation, a considerable amount of energy can be expended due to friction between the specimen ends and the supports against which the specimen is placed. The manner in which a ductile specimen is forced through the gap between the restraining supports, can depend on a number of parameters, and hence the Charpy test becomes qualitative or semi-quantitative, rather than quantitative, in distinguishing between degrees of ductility. The main aim of the impact tests was to determine whether the impact toughness of the experimental alloys was as good as predicted by literature[51], and it was found to be indeed so.

The impact toughness appears to increase with increasing nitrogen content only if the concomitant increase in volume fraction of austenite is significant. It appears that if the nitrogen level is raised above that required to retain around 90% austenite, toughness decreases (figure 4.33). It is of course debatable whether the trend is physically significant, in view of the semi-quantitative nature of the Charpy test, in cases of ductile failure. The high standard deviation of set 47 is attributed to the relatively high oxygen levels contained in the alloys of this set (0.03-0.06%).

CHAPTER 6

SUMMARY AND CONCLUSIONS

6.1 SUMMARY

The study of a range of experimental alloys with the AISI 301 base composition, shows the potential of partially substituting nickel with nitrogen, in an attempt to achieve comparable uniforms strains to that of AISI 301, as well as the limitations involved.

The metastable austenitic stainless steel, AISI 301, is used in stretch forming applications due to its ability to resist plastic instability, by the mechanism of transformation-induced plasticity (TRIP). The effective occurrence of TRIP relies on the gradual and selective formation of martensite at points of incipient necking, counteracting the formation and propagation of microcracks and micronecks. The austenite stability is critical because the TRIP phenomenon is directly affected by it, and an understanding of the effects of changes in alloy composition and temperature on austenite stability is essential in attempting to optimize the TRIP phenomenon in modified compositions.

The three requirements for optimum TRIP to occur are:

(1) The presence of a single-phase austenitic structure at the solution-treatment temperature (i.e. δ-ferrite is absent);

(2) The complete retention of the austenitic structure existing at the solution-treatment temperature, after quenching to room temperature (i.e. M_s is below ambient);

(3) The stability of the austenite phase must facilitate the gradual and selective formation of deformation-induced martensite during straining at the required deformation temperature (usually ambient).

Requirement (1) was satisfied by the experimental alloys, which contained 3.4 - 5.2 wt% nickel and 0.087 - 0.28 wt% nitrogen. In addition, no nitrides were present in any of the experimental alloys. Requirement (2) was satisfied to varying degrees : Alloys bearing 4.7 - 5.2 wt% nickel contained from 84 - 97% retained austenite, and those bearing 3.4 wt% nickel, contained 45 - 63% retained austenite. This study shows that requirement (3) can be satisfied to varying degrees, by maintaining a careful balance between the nitrogen and nickel contents, provided the amount of pre-existing martensite is not too great. Although it is not possible to determine from the study the minimum nickel content required for TRIP to occur in a nitrogen-alloyed

steel, it can be said with confidence that more than 3.4 wt% nickel is needed, otherwise insufficient austenite is retained, and the stability of the austenite which is retained is too low for TRIP to enhance elongation. By keeping within the 4.7 - 5.2 wt% nickel range, it is possible to adjust the nitrogen content, so that a compromise can be reached in attempting to achieve requirement (2) and (3). This study shows that it is not possible to achieve maximum austenite retention without adversely affecting the TRIP behaviour, and the optimum nitrogen range, for which a compromise can be reached was determined. The uniform straining ability of some of the experimental alloys containing 4.7 - 5.2 wt% nickel, compares favourably with the uniform straining ability of the type 301 alloy, due to the optimization of TRIP.

6.2 CONCLUSIONS

(1) The experimental alloys are all fully austenitic at the solution treatment temperature (1050°C) and nitrogen is fully dissolved.

(2) The alloys containing 4.7 - 5.1 wt% nickel (and 0.087 - 0.28 wt% nitrogen) have an austenite stabilizing ability which compares favourably to that of AISI 301. These alloys contain 84 - 97% retained austenite at room temperature. In contrast, only 45 - 63% retained austenite is present in the alloys containing 3.4 wt% nickel (and 0.19 - 0.28 wt% nitrogen).

(3) The TRIP phenomenon can occur effectively under suitable conditions in alloys containing 4.7 - 5.1 wt% nickel. In contrast, alloys containing 3.4 wt% nickel, are not suitable for TRIP, due to the presence of appreciable amounts of pre-existing martensite and the low stability of the retained austenite. The optimum nitrogen content of an alloy bearing 4.7 - 5.1 wt% nickel is 0.14 - 0.16 wt%. In particular, an alloy containing 4.7 wt% nickel and 0.14 wt% nitrogen, has uniform strains at 20, 60 and 120°C which compare favourably with those of AISI 301 at these respective temperatures.

(4) The onset of positive work-hardening generally occurs at lower strains in the experimental alloys than in AISI 301. Furthermore, the maximum work-hardening rate in the experimental alloys is achieved at lower strains than in AISI 301, and the magnitude of their maximum work-hardening rate is also notably greater.

(5) The amount of deformation-induced martensite reaches a maximum around 20°C for some of the experimental alloys while increasing continuously below 20°C for AISI 301. It is thought, that in these particular experimental alloys, local slip becomes less significant with decreasing temperature, and that this together with the presence of some pre-existing

martensite, restricts the formation of martensite below 20°C.

(6) Pronounced serrated tensile flow occurs in the experimental alloys at 60°C, while only very minor serrations were observed in AISI 301. The serration amplitude in the experimental alloys increases with decreasing nitrogen content and increasing strain. The serrations may be due to the formation of martensite in bursts, which occur only at a specific austenite stability, but the exact role of the nitrogen is unclear. The amplitude of serrations can be minimized by careful adjustment of the nitrogen content and/or the deformation temperature.

(7) A marked improvement in tensile strength is achieved after deformation in the experimental alloys for two reasons : The amounts of martensite formed in the experimental alloys containing 4.7 - 5.2 wt% nickel are generally greater than in the type 301 alloy, and the strengthening ability of nitrogen in martensite is considerably greater than in austenite.

(8) The room temperature impact toughnesses of all the experimental alloys compare favourably with other austenitic stainless steels. Although the presence of appreciable amounts of pre-existing martensite lowers toughness, fracture remains ductile.

REFERENCES

1. IRVINE, K.J., LLEWELLYN, D.T. and PICKERING, F.B. (1959). Controlled-transformation stainless steels. *JISI.*, **192**, pp.218-238.

2. PICKERING, F.B. (1979). The metallurgical evolution of stainless steels. *Int.Met.Rev.*, Metals Park, Ohio, pp.1-42.

3. GOLDBERG, A. and HOGE, K. (1974). Effect of strain rate on tension and compression stress-strain behaviour in a TRIP alloy. *Mat. Sci. & Eng.*, **13**, pp.211-222.

4. HUDDLE, F.P. (1955). Nickel conservation with high manganese stainless steels. *Met.Prog.*, **68**, pp.100-103.

5. FRANKS, R., BINDER, W.O. and THOMPSON, J. (1955). Austenitic Cr-Mn-Ni steels containing nitrogen. *Trans.ASM*, **47**, pp.231-266.

6. WHITTENBERGER, E.J., ROSENOW, E.R. and CARNEY, D.J. (1957). Elevated temperature phase relationships in the Cr-Ni-Mn-N system. *Trans.AIME*, **209**, pp.889-895.

7. NIJHAWAN, B.R., GUPTE, P.K., BHATNAGAR, S.S., GUHA, B.K. and DHANJAL, S.S. (1967). Substitute nickel-free austenitic stainless steels. *JISI.*, **205**, pp.292-304.

8. ASHBY, M. and JONES, D. (1980). Engineering materials 1 - An introduction to their properties and applications. Chapter 8: p.79. Pergamon Press, England.

9. Metals Reference Book (1976). 5th edition, ed.C.Smithells, Butterworths, London.

10. PICKERING, F. (1978). Physical metallurgy and the design of steels. Chapter 11: pp.226-268. Applied Science Publishers, London.

11. MARSHALL, P. (1984). Austenitic stainless steels - microstructure and mechanical properties. Elsevier Applied Science Publishers, London & New York.

12. TAMURA, I. (1982). Deformation-induced martensite transformation and transformation-induced plasticity in steels. *Met. Sci.*, **16**, pp.245-253.

13. ANGEL, T. (1954). Formation of martensite in austenitic stainless steels. *JISI.*, **177**(2), pp.165-174.

14. SEETHARAMAN, V. (1984). Deformation and martensitic transformation. *Bull.Mat.Sci.*, **6**(4), pp.703-716.

15. McREYNOLDS, A. (1949). *J.of Appl.Phys.*, **20**, pp.896-907.

16. FAHR, D. (1971). Stress and strain-induced formation of martensite, and its effects on strength and ductility of metastable austenitic stainless steels. *Met. Trans.*, **2**, pp.1883-1892.

17. LENEL, U. and KNOTT, B. (1987). Microstructure-composition relationships and M_S temperatures in Fe-Cr-Mn-N alloys. *Met. Trans.*, **18A**, pp.767-775.

18. LUDWIGSON, D. and BERGER, J. (1969). Plastic behaviour of metastable austenitic stainless steels. *JISI.*, pp.413-419.

19. HONEYCOMBE, R.W.K. (1981). Steels - microstructure and properties. Chapter 11: p.231. Edward Arnold Publishers. ed. E.Arnold, London.

20. GALLAGHER, P.C.J. (1970). The influence of alloying, temperature, and related effects on the stacking fault energy. *Met.Trans.*, **1**, pp.2429-2461.

21. NUTTING, J. (1969). The physical metallurgy of alloy steels. *JISI.*, **207**, pp.872-893.

22. HONEYCOMBE, R.W.K. (1984). The plastic deformation of metals. Chapter 9: p.231. Edward Arnold Publishers. ed. E.Arnold, London.

23. BARCLAY, W. (1965). The mechanism of deformation and work-hardening in AISI type 301 stainless steel. *ASTM Special Technical Publication*, **369**, pp.26-29.

24. HUANG, G., MATLOCK, D. and KRAUSS, G. (1989). Martensite formation, strain rate sensitivity and deformation behaviour of 304 stainless steel sheet. *Met. Trans.*, **20A**, pp.1239-1246.

25. SEETHARAMAN, V. and KRISHNAN, R. (1981). Influence of the martensitic transformation on the deformation behaviour of 316 stainless steel at low temperatues. *J. of Mat. Sci.*, **16**, pp.523-530.

26. MANGANON,P. and THOMAS,G. (1970). The martensite phases in 304 stainless steel. *Met. Trans.*, **1A**, pp.1577-1586.

27. ROSEN, A., JAGO, R. and KJER, T. (1972). Tensile properties of metastable stainless steels. *J. of Mat. Sci.*, **7**, 1972, pp.870-876.

28. LIVITSANOS, C. and THOMSON, P. (1977). The effect of temperature and deformation rate on transformation-dependant ductility of a metastable austenitic stainless steel. *Mat.Sci.Eng.*, **30**, pp.93-98.

29. MAXWELL, P., GOLDBERG, A. and SHYNE, J. (1974). Influence of martensite formed during deformation on the mechanical behaviour of Fe-Ni-C alloys. *Met. Trans.*, **5**, pp.1319-1324.

30. LE CROISEY, F. and PINEAU, A. (1972). Martensitic transformation induced by plastic deformation in the Fe-Ni-Cr-C system. *Met. Trans.*, **3**, pp.387-396.

31. TAMURA, I., MAKI, T. and HATO, H. (1969). On the morphology of strain-induced martensite and the transformation-induced plasticity in Fe-Ni and Fe-Cr-Ni alloys. *J.Japan.Inst.Metals*, **33**, pp.1376-1385.

32. BRESSANELLI, J. and MOSKOWITZ, A. (1966). Effects of strain rate, temperature, and composition on tensile properties of metastable austenitic stainless steels. *Trans.Am.Soc.Metals*, **59**, pp.223-239.

33. FUKASE, Y., EBATO, K., OKUBO, N. and MURAO, S. (1968). On the anomalous behavior of mechanical properties of metastable Cr-Ni austenitic stainless steels around ambient temperature. *Trans.ISIJ.*, **8**(5), pp.311-317.

34. BHANDARKAR, D., ZACKAY, V. and PARKER,E. (1972). Stability and mechanical properties of some metastable austentic steels. *Met. Trans.*, **3**, pp.2619-2630.

35. NEFF, D., MITCHELL, T. and TROIANO, A. (1969). *Trans. Am. Soc. Met.*, **62**, p.858.

36. MANGANON, P. and THOMAS, G. (1970). Structure and properties of thermally-mechanically treated 304 stainless steel. *Met. Trans.*, **1A**, p.1587.

37. MAXWELL, P., GOLDBERG, A. and SHYNE, J. (1974). Stress-assisted and strain-induced martensites in Fe-Ni-C alloys. *Met. Trans.*, **5**, pp.1305-1318.

38. OLSON, G. and COHEN, M. (1976). A general mechanism of martensitic nucleation : FCC→BCC and other martensitic transformations (Part 2). *Met. Trans.*, **7A**, pp.1905-1914.

39. OLSON, G. and COHEN, M. (1976). A general mechanism of martensitic nucleation: Kinetics

of martensitic nucleation (Part 3). *Met. Trans.*, **7A**, pp.915-923.

40. KUMAR, A. and SINGHAL, L. (1988). Effect of temperature and strain rate distribution on martensitic transformation during uniaxial testing of 304 stainless steel. *Met. Trans.*, **19A**, pp.1021-1026.

41. BERGSTRÖM, Y. and ARONSSON, B. (1970). Effects of changes in temperature and strain rate on the "double-n" behaviour of alpha-iron. *Met. Trans.*, **1**, pp.1029-1030.

42. PICKERING, F. (1988). Some beneficial effects of nitrogen in steel. *High nitrogen steels*. eds. J.Foct and A.Hendry, pp.10-31.

43. FRUEHAN, R.J. (1992). Nitrogen control in chromium steels. *SAIMM*, **2**, pp.35-41.

44. KIKUCHI, M., KAJIHARA, M. and FRISK, K. (1988). Solubility of nitrogen in austenitic stainless steels. *High Nitrogen Steels*. eds. J.Foct and A.Hendry, pp.63-74.

45. RAYAPOLU, D. and HENDRY, A. (1988). High nitrogen stainless steel wire. *Mat.Sci.Tech.*, **4**, pp.136-145.

46. UGGOWITZER, P. and HARZENMOSER, M. (1988). Strengthening of austenitic stainless steels by nitrogen. *High Nitrogen Steels*. eds. J.Foct and A.Hendry, pp.174-179.

47. SPEIDEL, M. (1987). High nitrogen steel : austenitic, duplex and martensitic. *Stainless Steels*, pp.247-252.

48. WERNER, E. (1988). Solid solution and grain size hardening of nitrogen-alloyed austenitic steels. *Mat.Sci. and Eng.*, **101** pp.93-98.

49. NORSTROEM, L. (1977). The influence of nitrogen and grain size on the yield stress of 316L austenitic stainless steels. *Met. Sci.*, pp.208-212.

50. GRUJICIC, M., NILSSON, J., OWEN, W. and THORVALDSSON, T. (1988). Basic deformation mechanisms in nitrogen strengthened stable austenitic stainless steels. *High Nitrogen Steels*. eds. J.Foct and A.Hendry, pp.151-158.

51. KENDAL,A., TRUMAN,J. and LOMAX,K. (1988). Properties of AISI 304 and AISI 316 stainless steel with addition of 0.2% nitrogen. *High Nitrogen Steels*. eds. J.Foct and A.Hendry, pp.405-413.

52. COTTRELL, A.H. (1953). Dislocations and plastic flow in crystals. Oxford University Press, London.

53. SUZUKI, H. (1957). Dislocations and mechanical properties of crystals. ed. J.C.Fisher et.al., John Wiley, New York and London, p.361.

54. HONEYCOMBE, R.W.K. (1984). The plastic deformation of metals. Edward Arnold Publishers. Chapter 7: p.175-177. ed.E.Arnold, London.

55. MOTT,N.F. and NABARRO,F.R.N. Report on Conference of the Strength of Solids, Physical Society, London, 1948, p.1

56. MIELITYINEN-TIITTO, K. (1979). Precipitation of Cr_2N in some nitrogen-alloyed austenitic stainless steels. *Acta.Polytechnica Scandinavica*, **141**, pp.62-63.

57. LIVITSANOS, C. and THOMSON, P. (1977). Rapid determination of the deformation-induced martensite in metastable austenitic stainless steels. *J. of Mat. Sci.*, **12**, pp.2209-2213.

58. DICKSON, M.J. (1969). The significance of texture parameters in phase analysis by X-ray diffraction. *J.Appl.Cryst.*, **2**, pp.176-180.

59. HALLIDAY, D. and RESNICK, R. (1981). Fundamentals of Physics, John Wiley & Sons, New York, p.764.

60. JENKINS, R. and DE VRIES, J. An introduction to X-ray Powder Diffractometry, Philips Gloeilampenfabriken, Eindhoven, Holland, pp.14-36

61. ASTM 975-84 (1984). Standard practice for X-ray determination of retained austenite in steel of near random orientation. ASTM Committee E-4 on Metallography (Subcommittee E04.06 on X-ray methods), pp.1050-1057.

62. JATCZAK, C.F., LARSON, J.A. and SHIN, S.W. (1980). Retained austenite and its measurement by X-ray diffraction. Information Manual SP-453 prepared by X-Ray Division of SAE Fatigue Design and Evaluation Committee, Society of Automotive Engineers, Inc., Warrendale, pp.9-27.

63. VAN DER VOORT, G.F. (1984). Metallography : principles and practice. McGraw-Hill, New York, p.234.

64. BENTLEY, A.P. and SMITH, G.C. (1986). Phase transformations of austenitic stainless steels as

a result of cathodic hydrogen charging. *Met.Trans.*, **17A**, pp.1593-1600.

65. FRANK, R.C., BAKER,J.E. and ALTSTETTER, C.J. (1982). A SIMS study of the diffusion and trapping of deuterium in 302 stainless steel. *Met.Trans.*, **13A**, pp.581-583.

66. PERNG, T. and ALTSTETTER, C.J. (1985). Test methods for hydrogen embrittlement-prevention and control. *ASTM symposium*, Los Angeles, CA, May 24-26.

67. WECK, E. and LEISTNER, E. (1983). Metallographic instructions for colour etching by immersion (Part II). *Deutscher Verlag für Schweisstechnik (DVS)*, GmbH-Düsseldorf, pp.3-63.

68. TOMOTA, Y., TANABE, K., KUROKI, K., and TAMURA, I. (1976). Effect of predeformation on the TRIP phenomenon in austenitic Fe-Ni-C alloys. *J.Soc.Mat.Sc.*, Japan, **25**, pp.717-723.

69. RIVLIN, V.G. and RAYNOR, G.V. (1980). Phase equilibria in iron ternary alloys : Critical evaluation of constitution of chromium-iron-nickel system. *Int.Met.Rev.*, **1**, pp.21-38.

70. PHILIBERT, J. and CRUSSARD, C. (1956). *Rev.Metall.*, **53**, p.973.

71. PICKERING, F. (1978). Physical metallurgy and the design of steels. Chapter 10: pp.201-225. Applied Science Publishers, London.

72. KULA, E.B. and DE SISTO, T.S. (1966). Behaviour of metals at cryogenic temperatures. *ASTM Spec.Tech.Publ.*, **387**, Philadelphia, p.3.

73. OLSON, G. and COHEN, M. (1976). Kinetics of strain-induced martensitic nucleation. *Met. Trans.*, **7A**, pp.791-795.

APPENDIX 1

The tables below give the chemical compositions of the alloys the microstructures of which were analyzed, but the alloys were not selected for mechanical testing. The heat numbers supplied by Middelburg Steel and Alloys research laboratory are give in brackets.

	ALLOY			
ELEMENT	3312 (901801)	3211 (901811)	3216 (901821)	3219 (901831)
C	.046	.046	.046	.047
Mn	1.48	1.46	1.44	1.41
Si	.34	.30	.27	.25
V	.07	.07	.07	.07
Cu	.05	.05	.05	.05
Co	.01	.02	.02	.02
Mo	.03	.03	.03	.03
Cr	15.9	15.9	16.0	16.1
Ni	3.28	3.21	3.17	3.15
N	.119	.112	.163	.192

Table 1 Alloys containing 3.2% nickel.

	ALLOY			
ELEMENT	4209 (901851)	4311 (901861)	4213 (901871)	4215 (901881)
C	.091	.093	.092	.092
Mn	1.70	1.69	1.62	1.58
Si	.95	.96	.93	.91
V	.07	.07	.07	.07
Cu	.13	.13	.13	.13
Co	.02	.02	.02	.02
Mo	.02	.02	.02	.02
Cr	16.0	16.2	15.9	16.4
Ni	4.22	4.25	4.16	4.19
N	.088	.109	.129	.148

Table 2 Alloys containing 4.2% nickel.

	ALLOY	
ELEMENT	5110 (901901)	5115 (901921)
C	.084	.084
Mn	1.60	1.50
Si	.64	.60
V	.08	.08
Cu	.08	.08
Co	.02	.02
Mo	.03	.03
Cr	17.4	17.7
Ni	5.13	5.11
N	.101	.163

Table 3 Alloys containing 5.1% nickel.

SCHMID, O. E., and KNUTSEN, R. D. Reducing the nickel content in metastable austenitic stainless steel. *INFACON 6. Proceedings of the 1st International Chromium Steel and Alloys Congress, Cape Town.* Volume 2. Johannesburg, SAIMM, 1992. pp. 151–156.

Reducing the Nickel Content in Metastable Austenitic Stainless Steel

O.E. SCHMID and R.D. KNUTSEN
University of Cape Town, Cape Town, South Africa

The effect of lowering the nickel content, while substituting with nitrogen, on the transformation-induced plasticity (TRIP) behaviour of metastable austenitic stainless steels was investigated. Several experimental alloys, with a range of nickel-to-nitrogen ratios, were compared with an AISI type 301 alloy during tensile deformation between 0 and 120 °C.

Characterization of the tensile-deformation behaviour, as well as an examination of the formation of deformation-induced martensite during elongation, led to the recognition of some similarities between the TRIP behaviour of an alloy containing 5,1 wt per cent nickel and 0,16 wt per cent nitrogen and type 301 alloy. Formation of deformation-induced martensite is optimized at approximately 60 °C for both alloys, giving rise to maximum uniform elongation under these test conditions. However, there are indications that high nitrogen levels can lead to erratic transformation behaviour during deformation conditions, as evidenced by a comparison of work-hardening rate versus strain curves.

Introduction

Considerable work was carried out during the mid 1950's to mid 1960's on the reduction of the nickel content in austenitic stainless steels[1-4]. The primary reason for exploring alternative alloy compositions was, and remains, the relatively high cost of nickel as an alloying element, particularly in types AISI 304 and 316 (which contain 8 to 12 wt per cent). In many instances, a combination of manganese and nitrogen as substitutes has been adopted, and much of this work has led to the development of the AISI 200 series alloys. A comprehensive study by Nijhawan *et al.* has shown that nickel-free Cr–Mn–N steels containing up to 15 wt per cent Mn and 0,6 wt per cent N have properties comparable with AISI 304, and are successful for applications such as household utensils, motor car and railway fittings, hospital ware, and dairy equipment[4]. Manganese, although classed as a very weak delta-ferrite former[3], stabilizes the austenite phase. Nitrogen acts both as a potent austenite former (approximately 20 to 30 times the potency of nickel) and as an austenite stabilizer. It can therefore be expected that various combinations of these elements can have an influence on the stability of austenite and on the overall mechanical properties of a steel.

The present study looked more closely at the consequences of modifying the nickel-to-nitrogen ratios on the stability of austenite, with particular emphasis on the transformation-induced plasticity (TRIP) phenomenon. Metastable austenitic stainless steels of the AISI type 301 are used mostly for products that require moderate strengths, and are produced by stretch forming processes, which rely on the attainment of good ductility. Type 301 alloys nominally contain 6 to 8 wt per cent nickel, and the objective of this paper was to investigate the substitution of a limited amount of nickel content with nitrogen and its effect on the microstructure–property relationships.

Evolution of TRIP steels

Initial research, which eventually led to the development of metastable austenitic stainless steels, was aimed at the production of high-strength stainless steels that could be fabricated with relative ease. The work described here was prompted by the fact that the choice of high-strength stainless steels was limited to cold-worked austenitic or ferritic types, or to martensitic types. These steels, however, presented difficulty where fabrication was concerned, and this led to much interest being shown in the development of controlled-transformation (CT) stainless steels, which have, as an essential feature, a martensite range that occurs below room temperature[5]. Consequently, the steel is austenitic initially and can be fabricated quite readily. A subsequent refrigeration treatment at minus 70 °C will produce transformation to martensite or, alternatively, a heat treatment at 700 °C will precipitate alloy carbides and raise the martensite-transformation range above room temperature so that transformation to martensite will occur. With either treatment, the fabricated steel can be strengthened considerably. The main limitation of these simple CT steels is that accurate control of the martensite transformation is difficult owing to the range of compositions obtained in commercial steel making. Thus, it is difficult to control the M_s temperature owing to the sensitivity of this temperature to alloy composition, particularly regarding interstitial elements such as carbon and nitrogen[6].

In the late 1960's, TRIP steels were developed that differ from CT steels in that essentially no martensite is formed in the latter during straining while, in the former, considerable amounts of austenite can transform to martensite[6,7]. Thus, the TRIP steels achieved in one process what required at least two stages in CT steels. In addition, TRIP steels pro-

duced high strengths coupled with good ductility. It is now well accepted that resistance to local necking during deformation is achieved by the onset of martensite formation during deformation[8-10]. Once a local contraction occurs during deformation, martensite is gradually induced and the increment in strength caused by this martensite is responsible for the increment in applied stress at the necked portion. Thus, the necked region is hardened more by deformation-induced martensite than is the rest of a specimen, so that the incipient necking no longer grows, and further deformation is partitioned to the adjacent region. In addition to the delayed onset of macro-necking, the suppression of the initiation and propagation of microcracks by the formation of deformation-induced martensite has also been considered a major contribution to increased ductility in metastable austenitic steels[9]. A local stress concentration can be relaxed by the formation of martensite, and the initiation of microcracks may be prevented. Furthermore, even if microcracks are initiated, martensite formed at the tips of micro-cracks will relax the stress concentration and suppress their propagation.

In view of the fact that transformation-induced plasticity may be caused by the suppression of necking, and by the suppression of the initiation and propagation of microcracks, the controlled nature of this transformation is important during deformation. The main prerequisite for maximum elongation is that the martensite is constantly formed little by little during deformation. Elongation is much reduced when martensite is formed rapidly during the early stages of deformation or when the total amount of martensite formed during the late stages is small. The former situation arises when the material is deformed just above the M_s temperature, whereas the latter occurs when the material is deformed just below the M_d temperature. Consequently, it has been found that the elongation shows a peak at a certain temperature between the M_s and M_d[9,10].

Experimental Procedure

Six experimental alloys, prepared by Middelburg Steel & Alloys' research laboratory, were selected to provide an alloy composition based on AISI 301 but with a range in the nickel-to-nitrogen ratios. The compositions of the alloys are presented in Tabie I, along with the composition of a type 301 alloy for comparative purposes. Each experimental alloy was cast into a 5 kg ingot (50 mm thick and hot-rolled to plate of 10 mm gauge). A portion of this plate for each alloy was further hot-rolled to a sheet thickness of 4 mm. Flat tensile specimens (gauge length 30 mm, gauge width 7,5 mm, thickness 2 mm) were machined from the 4 mm sheet and were used for X-ray-diffraction (XRD) measurements after various levels of tensile deformation. Hounsfield-type tensile specimens (gauge length 20 mm, diameter 4 mm) were machined from the 10 mm plate for evaluation of their general tensile properties over a range in temperature.

Prior to testing, all the test specimens were ceramic-coated and heat-treated in air at 1050 °C for 30 minutes, followed by oil quenching. The tests were performed using a computer-interfaced Zwick tensile tester, which allowed the data to be captured on computer file. The test set-up incorporated a temperature bath regulated by a Eurotherm controller to within 2 °C. Tensile-fracture tests were performed at 20, 60, and 120 °C, while tests to 0,3 true strain were performed at the same temperatures and also at 0 °C. All the experiments were carried out at an initial strain rate equivalent to 10^{-3} per second.

TABLE I
CHEMICAL COMPOSITION OF THE EXPERIMENTAL ALLOYS AND AISI 301 IN PERCENTAGES BY WEIGHT

Element	A1	A3	A5	A6	D1	D2	301
C	0.084	0.087	0.075	0.071	0.078	0.070	0.029
Mn	1.62	1.61	1.55	1.48	1.51	1.53	1.52
Si	0.65	0.65	0.48	0.44	0.43	0.43	0.44
V	0.08	0.08	0.06	0.06	0.07	0.06	0.05
Cu	0.08	0.08	0.08	0.08	0.06	0.06	0.10
Co	0.02	0.02	0.02	0.02	0.02	0.02	0.03
Mo	0.03	0.03	0.05	0.05	0.05	0.05	0.20
Cr	17.2	17.5	17.9	17.9	17.9	17.9	17.7
Ni	5.12	5.09	5.17	5.03	3.41	3.36	7.48
N	0.087	0.129	0.163	0.276	0.185	0.275	0.074

For XRD phase analysis after deformation, the centre portions of the flat tensile specimens were mounted in resin, mechanically polished to a finish using 1 μm diamond paste, and finally electropolished in a solution containing chromic and glacial acetic acids. Electropolishing was necessary to remove any deformation-induced martensite that may have formed during the mechanical polishing. XRD analysis was performed using Cu Kα-radiation passed through a nickel filter. A step of 0,05° and a counting time of 10 seconds were employed during the direct acquisition of data onto computer file. The martensite–austenite volume fraction was calculated from the integrated area under the (200)α, (211)α, (220)γ, and (311)γ diffraction peaks. The volume fraction was calculated by Dickson's method[11] in order to correct for the error introduced as a result of texture development in either phase.

Experimental Results

After solution heat treatment, the microstructures of the experimental alloys and AISI 301 were examined by light microscopy (Nomarski interference), in order to investigate the presence of delta-ferrite. Ferrite was noted as absent in all instances, and it can therefore be inferred that a single-phase austenitic structure existed at the solution temperature (1050 °C). The XRD analysis of the phase composition of all the alloys after solution heat treatment is presented in Table II, and indicates the stability of the austenite during rapid quenching to ambient. As expected, the percentage retained austenite decreased with decreasing nitrogen content for a particular nickel level, and the overall retained austenite was lower for the low-nickel alloy set (D1, D2).

The true stress at maximum uniform elongation ($\sigma\mu$) and the true uniform strain are plotted in Figures 1 and 2 respectively as a function of test temperature for alloys A1, A3, A5, A6, and type 301. As found by previous workers[8,10], a

TABLE II
RETAINED AUSTENITE CONTENT AT AMBIENT TEMPERATURE (AFTER SOLUTION TREATMENT) FOR THE EXPERIMENTAL ALLOYS AND AISI 301

Alloy	A1	A3	A5	A6	D1	D2	301
Retained austenite, %	70	83	89	91	43	67	98

peak in uniform elongation was detected for type 301 in the vicinity of 60 °C. Alloy A5 also displayed a maximum at 60 °C, whereas the lowest-nitrogen alloy (A1) and the highest-nitrogen alloy (A6) both indicated an increase in uniform elongation up to 120 °C. Alloy A3 had similar elongation at 60 and 120 °C. The tensile strengths of the nitrogen-substituted alloys were consistently higher than that for type 301 at 20 and 60 °C. The strengths generally decreased with increasing temperature (with the exception of A1 and type 301, which have similar strengths at 20 and 60 °C), and the differences in strengths between the set A alloys and type 301 was much reduced at 120 °C.

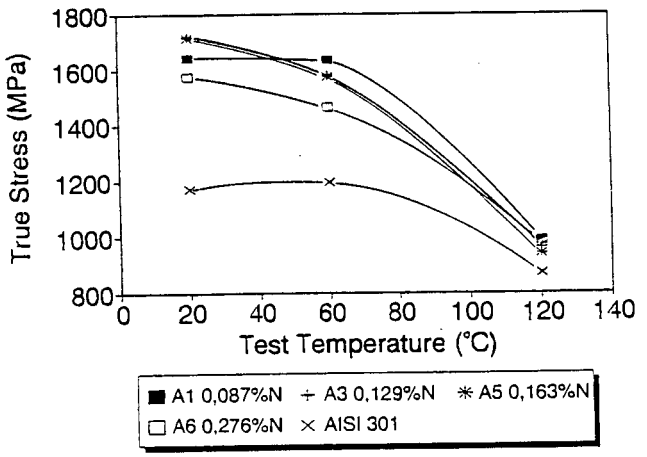

FIGURE 1. True stress at uniform strain (σμ) as a function of temperature (set A alloys and type 301)

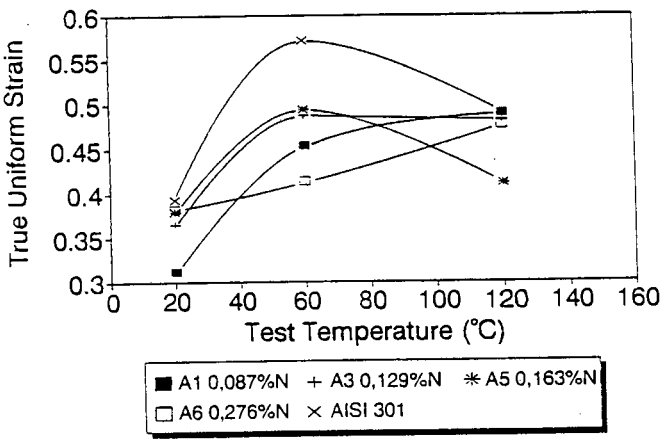

FIGURE 2. True uniform strain as a function of temperature (set A alloys and type 301)

In order to characterize the tensile properties further, the true stress at 0,3 true strain was also plotted as a function of test temperature (including the tests at 0 °C) for the above-mentioned alloys (Figure 3). The difference in stress at 0,3 strain recorded at 20 and 60 °C for set A alloys is much greater than the difference in σμ for these alloys over the same temperature interval. An interesting observation is the anomaly that seems to occur at 0 °C for A1, A3, and A5. In each case, the stress at 0,3 strain is higher during testing at 20 °C than at 0 °C.

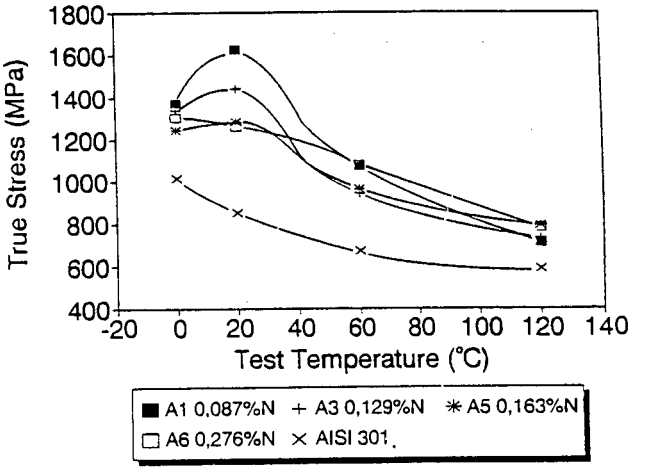

FIGURE 3. True stress at 0,3 strain as a function of temperature for alloys A1, A3, A5, A6, and type 301.

The tensile behaviour of alloys D1 and D2 are characterized by σμ and true uniform strain plotted as a function of test temperature in Figures 4 and 5 respectively. The σμ value for D1 and D2 follows a similar trend to that shown by alloy A1 (Figure 1), but the uniform strain values are very low (Figure 5).

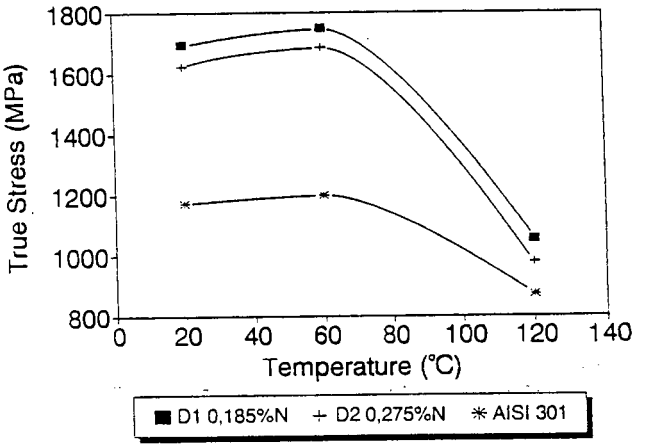

FIGURE 4. True stress at uniform strain (σμ) as a function of temperature (set D alloys and type 301)

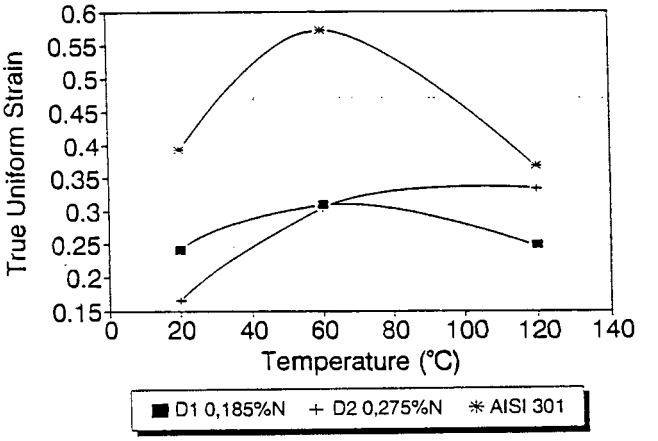

FIGURE 5. True uniform strain as a function of temperature (set D alloys and type 301)

Discussion

Although a fully austenitic microstructure was achieved at the solution treatment temperature (1050 °C) for all the nitrogen-substituted alloys, varying degrees of austenite stability were obtained on rapid cooling to ambient. As far as could be gathered from the literature, TRIP phenomena have been studied mostly on steels whose M_s temperatures were below ambient. Therefore it must be expected that the existence of a two-phase microstructure (austenite and martensite) prior to testing must influence the nature of tensile deformation. Notwithstanding these differences, the TRIP phenomenon should still play a major role in the deformation of the alloys containing low volume fractions of thermally induced martensite (e.g. A3, A5, and A6).

In order to explain the changing tensile behaviour of the set A alloys as a function of temperature, the tendency to form martensite during deformation needs to be investigated. To this end, the total martensite content was measured at 0,3 strain for each test temperature using XRD, and the total deformation-induced martensite (total martensite at 0,3 strain minus martensite prior to testing) was plotted as a function of test temperature (Figure 6). The results for the experimental alloys at 60 and 120 °C appear somewhat spurious in that they have negative values. This can be explained only by the difficulty in measuring the phase ratio in a deformed material due to an increasing amount of noise arising from the strained volume. Nevertheless, it can be stated with a certain degree of confidence that very little, if any, martensite formed during straining of the alloys up to a strain of 0,3 at these temperatures. The values for the type 301 alloy under the same conditions are also included.

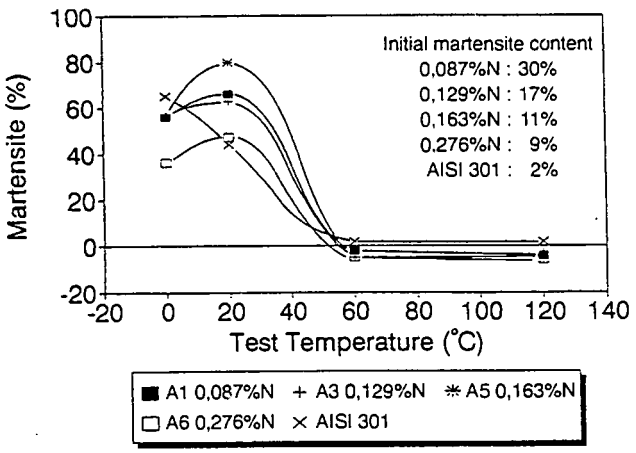

FIGURE 6. Total deformation-induced martensite at 0,3 strain as a function of temperature (set A alloys and type 301)

In addition to these observations, the work-hardening rate (WHR) as a function of true strain is shown for A5 and type 301 at 20 and 60 °C in Figures 7 and 8 respectively. This information will be used in the following paragraphs to explain the tensile behaviour.

As reviewed in the section dealing with the evolution of TRIP steels, maximum elongation is obtained when martensite forms during the latter part of deformation and, in addition, it must form at a controlled rate. The fact that the type 301 alloy has a maximum uniform elongation at approximately 65 °C is consistent with this belief in that negligible

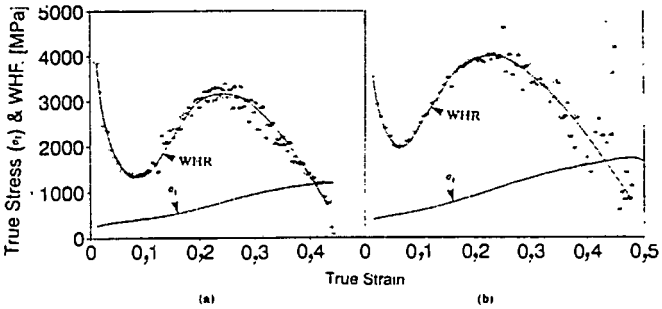

FIGURE 7. (a) Work-hardening rate (WHR) of type 301 as a function of true strain at 20 °C

(b) Work-hardening rate (WHR) of alloy A5 as a function of true strain at 20 °C

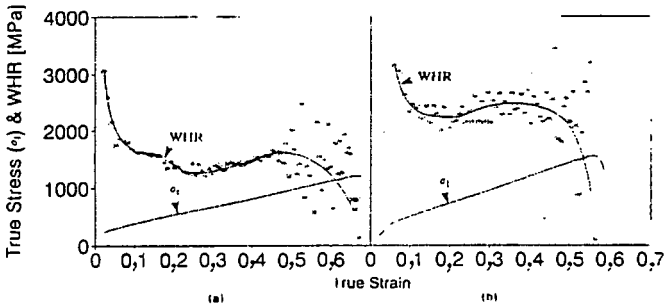

FIGURE 8. (a) Work-hardening rate (WHR) of type 301 as a function of true strain at 60 °C

(b) Work-hardening rate (WHR) of alloy A5 as a function of true strain at 60 °C

amounts of martensite are formed in the initial stages of deformation (Figure 6). At temperatures below the peak value, the martensite forms too rapidly in the early stage of deformation whereas, at the higher temperatures, insufficient martensite forms to enable a considerable contribution to enhanced plasticity and, instead, elongation is provided mostly by deformation of the austenite phase. Alloy A5 follows the same trend in uniform elongation, except that the amount of elongation at the peak temperature is considerably lower. Despite these differences in elongation, the trend observed indicates that the TRIP phenomenon must play a role in alloy A5. This is examined more closely before the remaining set A alloys are dealt with.

Examination of the WHR versus strain curves in Figure 7 indicates similar trends in work-hardening behaviour for the two alloys when tested at 20 °C. In each case, the rise in WHR can be attributed to the gradual formation of martensite during straining, whereas the drop in WHR after the peak value is reached is associated with the more rapid formation of martensite. It has been shown by Tomota *et al.*[12] that, when martensite forms rapidly, the stress relief accompanying the transformation strain can lead to a lowering of overall applied stress. (Martensitic transformation accompanies shear and dilatation, and therefore a certain value of positive transformation strain occurs along the direction of applied stress.) This suggests that the drop in WHR after the peak is reached is at least partly due to dilatation associated with transformation strain. The peak WHR is reached at a strain of approximately 0,22 in the case of alloy A5, and the suggestion that martensite forms rapidly after this point is consistent with the high value of deformation-induced martensite recorded after 0,3 strain (approximately 80 per cent). In the case of type 301, the peak WHR occurs at a similar strain value to that of alloy A5. However, it is

apparent that the rate of martensite formation is not quite as high when compared with the latter alloy, since only 43 per cent martensite has been measured at a strain of 0,3. Nevertheless, it is clear that, for both alloys, martensite forms at a high rate relatively early during straining, and the total uniform elongation attained by each alloy is similar. It can be suggested that the TRIP phenomenon is not prominent in either material during the latter stages of deformation, since the martensite does not form slowly enough to prevent incipient necking.

At 60 °C, the WHR curves for alloy A5 and type 301 demonstrate a behaviour that is more typical of the TRIP phenomenon (Figure 8). In both cases, the peak WHR is delayed to much larger strain values, with this strain value being consistently greater for type 301. The gradual drop in WHR up to a strain of 0,3 is consistent with the deformation of austenite. This is supported by negligible formation of deformation-induced martensite up to this strain value. Above a strain of 0,3, the increase in WHR is due to the favourable formation of martensite, which resists incipient necking. At strains greater than 0,5, Fukase *et al.*[8] have shown that the rate of formation of martensite increases in type 301 at 50 °C. Since their alloy composition was virtually identical to the 301 alloy in the present investigation, it is expected that very much the same behaviour must be occurring at 60 °C, and hence the drop in WHR after a strain of 0,5 can once again be partly explained by the occurrence of transformation strain. It would seem that much the same behaviour is demonstrated by alloy A5, except for the indications that the onset of rapid martensite formation occurs earlier in this alloy. This would explain the lower uniform strain recorded for alloy A5 compared with type 301 during deformation at 60 °C. In addition, the curve for type 301 in Figure 8(a) is relatively smooth up to about 0,45 strain, whereas the corresponding curve for alloy A5 in Figure 8(b) shows a greater amount of scatter. These observations have been produced from several stress–strain curves and would seem to demonstrate a more erratic transformation behaviour in alloy A5, which must be related to some function of the high nitrogen content. Serrations have been identified in the stress–strain curves, and this possibly indicates that martensite forms in bursts over certain strain intervals.

It makes sense that, for reasons similar to those described above, the elongation occurring at 60 °C for alloys A1, A3, and A6 is also improved owing to the favourable formation of martensite during deformation. However, the uniform strain for both A1 and A6 increases further at 120 °C. This can be rationalized more easily for A1 in that, because it has the highest M_s temperature (largest amount of thermally induced martensite at ambient), the peak elongation temperature is expected to be higher. On the other hand, alloy A6, owing to its much greater austenite stability, should not behave like this, and no explanation can be offered for this performance at the moment. The low stability of the austenite in the lower nickel-containing alloys, D1 and D2, is responsible for the low uniform elongation recorded for these alloys. It is expected that the TRIP phenomenon is not significant in these alloys.

The overall strength differences between the nitrogen-substituted alloys and type 301 at room temperature can be attributed to two factors. Firstly, the nitrogen alloys are all being deformed below the M_s temperature (to varying degrees), and it can therefore be expected that a much greater total volume fraction of martensite is present at fracture. The flow stress over any particular strain interval can be related to the amount of martensite present (compare Figures 3 and 6). Secondly, it is well known that nitrogen strengthens both austenite and martensite to a much greater extent than nickel does. The observation of a lower stress and lower martensite fraction at 0 °C than at 20 °C for the set A alloys needs further investigation. It is possible that there is some effect on incubation time due to the refrigeration of a microstructure already containing appreciable amounts of martensite.

Summary

This investigation into the effects of substituting nickel with nitrogen in type 301 alloys on the occurrence of transformation-induced plasticity has given rise to the following conclusions.

(1) There is clearly a careful balance between nickel and nitrogen content that needs to be maintained in order to produce a sufficiently stable microstructure during cooling to ambient. Alloys with poor austenite stability give rise to limited elongation during tensile testing.

(2) An alloy containing 5,1 wt per cent nickel and 0,16 wt per cent nitrogen (A5) compares favourably with the TRIP behaviour shown by the type 301 alloy when tested at 60 °C. The more erratic work-hardening behaviour displayed by the high-nitrogen alloy at this temperature, however, indicates that the formation of martensite during straining is less gradual when compared with type 301.

An exact explanation for the effect of nitrogen on the transformation behaviour during deformation is still not available. Generally, nitrogen-rich alloys follow the same rules in terms of the requirements for optimum enhanced plasticity. However, there are certain anomalies that require further examination.

Acknowledgments

The authors would like to thank Middelburg Steel & Alloys, Transvaal, and the Foundation for Research and Development (FRD), Pretoria, for supporting this work, with special thanks to Mr J Hewitt of Middelburg Steel & Alloys for his interest and encouragement.

References

1. Huddle, F.P (1955). Nickel conservation with high manganese stainless steels. *Met. Prog.*, 68, pp.100-103.
2. Franks, R., Binder, W.O., and Thompson, J. (1955). Austenitic Cr–Mn–Ni steels containing nitrogen. *Trans. ASM*, 47, pp.231-266.
3. Whittenberger, E.J., Rosenow, E.R., and Carney, D.J., (1957). Elevated temperature phase relationships in the Cr–Ni–Mn–N system. *Trans. AIME*, 209, pp.889-895.
4. Nijhawan, B.R., Gupte, P.K., Bhatnagar, S.S., Guha, B.K., and Dhanjal, S.S. (1967). Substitute nickel-free austenitic stainless steels. *JISI*, 205, pp.292-304.
5. Irvine, K.J., Llewellyn, D.T., and Pickering, F.B. (1959). Controlled-transformation stainless steels. *JISI*, 192, pp.218-238.
6. Pickering, F.B. (1979). In *The metallurgical evolution of stainless steels*, ASM, Metals Park, Ohio.

7. Seetharaman, V. (1984). Deformation and martensitic transformation. *Bull. Mat. Sci.*, 6 (4), pp.703-716.
8. Fukase, Y., Ebato, K., Okubo N., and Murao, S. (1968). On the anomalous behavior of mechanical properties of metastable Cr–Ni austenitic stainless steels around ambient temperature. *Trans. ISIJ*, 8(5), pp.311-317.
9. Tamura, I., Maki, T., and Hato, H. (1970). On the morphology of strain-induced martensite and the transformation-induced plasticity in Fe–Ni and Fe–Cr–Ni alloys. *Trans. ISIJ*, 10(3), pp.163-172.
10. Rosen, A., Jago, R., and Kjer, T. (1972). Tensile properties of metastable stainless steels. *J.Mat. Sci.*, 7, pp. 870-876.
11. Dickson, M.J. (1969). The significance of texture parameters in phase analysis by X-ray diffraction. *J. Appl. Cryst.*, 2, pp. 176-180.
12. Tomota, Y., Tanabe, K., Kuroki, K., and Tamura, I. (1977). Effects of predeformation on the TRIP phenomenon in austenitic Fe–C alloys. *Trans. ISIJ*, 17(3), pp. 159-165.